Master's thesis

NTNU
Norwegian University of Science and Technology
Faculty of Engineering
Department of Civil and Environmental Engineering

Saeed Abbasi Hassan Abbadi

Thermal analysis of steel geothermal energy pile foundation

Numerical simulation of heat transfer and fluid flow in annular coaxial energy pile

Master's thesis in Geotechnics and Geohazards
Supervisor: Rao Martand Singh
Co-supervisor: Habibollah Sadeghi
July 2022

NTNU
Norwegian University of
Science and Technology

Saeed Abbasi Hassan Abbadi

Thermal analysis of steel geothermal energy pile foundation

Numerical simulation of heat transfer and fluid flow in annular coaxial energy pile

Master's thesis in Geotechnics and Geohazards
Supervisor: Rao Martand Singh
Co-supervisor: Habibollah Sadeghi
July 2022

Norwegian University of Science and Technology
Faculty of Engineering
Department of Civil and Environmental Engineering

NTNU
Norwegian University of
Science and Technology

Preface

This master thesis was conducted at the department of civil and environmental engineering at the Norwegian University of Science and Technology (NTNU) as a part of a master's degree in geotechnics and geohazards. This thesis is credited with 30 ECTs and spans over 28 weeks in the spring semester of 2022. The thesis is related to the ongoing research of steel energy piles by the Norwegian Geotechnical Institute (NGI). The problem is formulated by numerical simulation using the COMSOL Multiphysics.

Trondheim, 2022-07-31

Saeed Abbasi Hassan Abbadi

Acknowledgment

First and foremost, I wish to thank my beloved wife, Raziyeh, and our son, Karan, who have stood by me through all my struggles, absences, and fits of temper and impatience during my studies.

I want to express my gratitude to Habibollah Sadeghi, Ph.D., for technical and professional help and guidance. He has also been a great motivator and has always taken the time to answer my questions. I also want to thank my supervisor, Dr. Rao Martand Singh, for great help and support throughout the semester.

I also want to express my gratitude for all the external support I received during the project. A special thanks to Sondre Gjengedal at NGI for providing information regarding the case study. Thanks to the Geotechnical lab staff at NTNU for ground investigations of the case study.

Abstract

Geothermal energy has recently been a popular sustainable alternative for heating and cooling buildings. Due to its low power usage, ground heat exchangers employing piles have been recommended as a practical way to reduce initial costs and provide favorable long-term financial returns. In recent years, there has been increased interest in using steel foundation piles as ground heat exchangers. Steel piles are expected to deliver a better thermal conductivity and heat capacity than other energy piles.

The thermal interaction between various components of a steel energy pile and the surrounding soil is presented in this thesis. To better understand the outcomes of the numerical simulations, the analytical relationships between the various physical processes involved in the thermal behavior of a steel pile have been outlined.

The next phase was conducting numerical studies on the thermal performance of experimental research and creating a reliable three-dimensional numerical model that could be used in similar situations. The numerical simulation shows good agreement with the findings of the Saga University experiment.

A similar numerical model was created based on the specifications of a trial piling project in Norway. Through cyclic heat injection in one pile and temperature monitoring in another, the short-term thermal performance of those piles was evaluated. This research demonstrates that short-term (72-hour) heat injection in a steel pile only affects a small area surrounding the pile, and consequently, the temperature fluctuation in the other pile was less evident.

Table of Contents

List of Figures

List of Tables

Nomenclature

Symbols

A	Area [m^2]
b	Inverse of thermal resistance [W/K]
B_q	Pore pressure ratio [-]
c_p	Specific heat at constant pressure [J/kg.K]
C_s	Speed of sound [m/s]
d	Diameter [m]
F_r	Normalized friction ratio [-]
f_s	Sleeve friction [kPa]
g	Gravity acceleration [m/s^2]
h	Convective heat transfer coefficient [$W/m^2.K$]
k	Thermal conductivity [W/m.K]
K	Permeability [m/s]
L	Length [m]
n	Porosity [-]
P	Pressure [kPa]
q	Heat flux [W/m^2]
Q	Heat rate [W]
Q	Volumetric flow rate [m^3/s]
q_t	Corrected cone resistance [kPa]
R	Thermal resistance [K/W]
r	Radius [m]
Re	Reynolds number [-]
T	Temperature [K]
t	Time [s]
U	Internal energy [W]
U	Fluid velocity [m/s]
z	Depth [m]
α	Thermal diffusivity [m^2/s]
α_p	Coefficient of thermal expansion [1/K]
γ	Ratio of specific heats [-]
μ	Dynamic viscosity [kg/m.s]
ρ	Density [kg/m^3]

Abbreviations

BEAR	Bærekraftig Energi fra løsmAsseR
CAD	Computer-Aided Drafting
CPTu	Cone Penetration Test with pore pressure measurement
CXA	Annular CoAxial pile
CXC	Centered CoAxial pile
FEM	Finite Element Method
GEP	Geothermal Energy Pile
GHE	Ground Heat Exchanger
GSHP	Ground Source Heat Pump
HCF	Heat Carrier Fluid
HDPE	High-Density Polyethylene
HDPP	High-Density PolyPropylene
HVAC	Heating, Ventilation, and Air Conditioning
NGI	Norges Geotekniske Institutt
NGU	Norges Geologiske Undersøkelse
NTNU	Norges Teknisk-Naturvitenskapelige Universitet
PE	PolyEthylene
PVC	PolyVinyl Chloride
TRT	Thermal Response Test
REV	Representative Elementary Volume

1 Introduction

1.1 Background

The reduction of fossil fuel consumption has been a subject of discussion on a global scale for many decades, with the large amounts of the total energy consumption of the world coming from resources that are not sustainable. As a consequence of all this, costs for energy have increased; nevertheless, global warming caused by CO_2 emissions is a more significant threat to the environment worldwide. It is a challenge in civil engineering to figure out how to use recently developed technology in civil construction to solve this global problem. Geothermal energy is a potential renewable energy source and has been a research subject for many years. This energy resource would be cost-effective for eventual end-users and contribute to advancing efforts toward a cleaner environment.

Using geothermal energy is characterized by the fact that the temperature of the ground remains reasonably stable beyond a depth of 10 to 15 meters. This temperature is higher than the ambient air temperature in the winter and lower in the summer. During the winter, a geothermal heat pump may transfer the heat in the ground into a building. During the summer, the pump can reverse its operation, collect heat from the building, and inject it into the ground. Therefore, the efficiency of ground-coupled heat pump systems is fundamentally more remarkable than that of air-source heat pump systems. This is because the average ground temperature is a better foundation for heating and cooling throughout winter and summer.

Among different alternatives to ground source heat pumps, energy piles provide cost and energy efficiency by simultaneously serving as structural foundations. Geothermal energy piles are conceived and built to serve two distinct purposes. Piles mainly fulfill the role of typical structural support for buildings, ensuring that the building settlement is within the acceptable range for safety and serviceability. When the ground source heat pump is operating, they also take on the additional responsibility of harvesting heating and cooling energy for the interior space of the building.

1.1.1 Problem formulation

In practice, the structure of energy piles consists of one or more pipes going through the pile and at the bottom, forming a U-turn. The heat carrier fluid enters from one end and leaves the system from the other.

Another novel configuration of energy piles investigated in the present study comes with the idea of bringing the heat carrier fluid as close as possible to the soil to perform efficient heat transfer between the soil and fluid to enhance the energy pile performance. The pile consists of a steel shell and a coaxial pipe. The heat carrier fluid inflows inside the pile from the annulus area and outflows through the middle pipe, or vis versa.

The U-tube configuration of heat exchangers in energy piles has been widely studied in recent years. Many researchers use in-situ experiments, laboratory tests, and numerical simulations to investigate the thermal and mechanical behavior of this configuration or similar configurations. A few years ago, a special physical module for assessing the heat

and fluid transfer in the pipes was developed by COMSOL Multiphysics, which expedited and eased the numerical simulation of the U-tube heat exchangers.

The coaxial configuration of energy piles is not concentrated as extensively as the U-tubes by the researchers. Other than some experimental field studies, the thermal and thermomechanical performance of the coaxial energy piles is not investigated. The main focus of this thesis is to investigate the thermal performance of an annular coaxial energy pile by numerical simulation.

The main goal of the present thesis is to investigate the thermal performance of the BEAR project (Bærekraftig Energi fra løsmAsseR, or Sustainable energy from loose material), which is a part of a larger construction project owned by Malvik municipality, designed to investigate solutions for harvesting energy from surface soil layers as a sustainable and reliable energy source.

1.1.2 Literature survey

Al-Khury (2017) introduced the analytical, semi-analytical, and finite element model for investigating energy piles in his book "Computational modeling of shallow geothermal systems" [1]. This book is the primary reference in expanding the analytical relations governing the heat transfer between soil and the annular coaxial pile in chapter 3.

Jalaluddin et al. (2011) investigated the thermal performance of the coaxial pile and published the results in a paper titled "Experimental study of several types of ground heat exchanger using a steel pile foundation" [2]. Results of this experiment were utilized to verify the numerical model of the present study in chapter 4.

1.2 Objectives

The main objectives of this thesis are

1. Developing the analytical relations between fluid flow and heat transfer in the annular coaxial energy piles.
2. Numerical simulation of the fluid dynamics and heat transfer in coaxial energy piles.
3. Case study of the thermal performance of a pair of coaxial piles in the BEAR project under different application scenarios.

1.3 Approach

COMSOL Multiphysics® is a general-purpose software platform based on a powerful numerical tool for simulating physics-based problems. This thesis uses a 3D numerical model produced in the COMSOL Multiphysics 5.6 by applying fluid flow physics and the heat transfer in porous media modules.

1.4 Limitations

Since field investigations of the thermal behavior of energy piles installed in the BEAR project were not completed when this thesis was written, comparing the field experiments

and numerical simulation of the BEAR project was not feasible. Therefore, the planned scenarios for the field experiments are assumed, and numerical simulations are performed based on them.

1.5 Structure of the report

The thesis contains 6 chapters. The first chapter is the introduction. Chapter 2 contains state of the art related to technical developments of the energy piles. Chapter 3 explains the theory of heat transfer and fluid flow in energy piles, especially in annular coaxial energy piles and heat transfer in the porous media. Chapter 4 establishes a numerical simulation of the thermal performance of a steel pile based on an experimental case study. Chapter 5 contains the field investigations and numerical simulation carried out for the BEAR project. Each simulation and the relevant results are discussed, and the conclusion and recommendations for further work are presented in chapter 6.

2 Literature review

2.1 Introduction

This chapter briefly explains geothermal energy and reviews relevant research on geothermal energy systems in terms of shallow energy piles, their elements, materials and structures, thermo-mechanical behavior, and thermal performance.

2.2 Geothermal energy

Geothermal energy is thermal energy produced around 6000 kilometers beneath the surface in the core of the planet earth. It is renewable because the radiogenic decay of naturally occurring isotopes, particularly those of potassium, uranium, and thorium, continuously generates temperatures hotter than the surface of the sun inside the earth. Up to 5000°C can be found in the core of the earth. This temperature gradually drops from the core as one moves closer to the surface, eventually settling at about 10°C. An extensive renewable energy source is created because of the continual flux of thermal energy from the core to the surface [1] as well as the solar radiation at the ground surface [3].

Geothermal energy, the second most abundant source of heat on the earth after solar energy, is currently accessible and concentrated in underground reservoirs as steam, hot water, and hot rocks. The three relevant technology categories are ground source heat pumps (GSHPs), direct-use applications, and electric power plants. GSHPs utilize the surface ground layers as a heat source and heat sink for cooling and heating buildings. Direct-use applications heat water using geothermally heated water that is already present. Electricity is produced by electric power plants using electric turbines fueled by geysers [4].

2.3 Geothermal energy systems

There are various types of geothermal system classifications. One of the frequently used classifications is based on the depth of the geothermal energy sources. Geothermal systems can be categorized as shallow or deep geothermal, depending on whether they are located at a depth of less than 100 to 150 m or greater [5]. Shallow geothermal systems are designed to work in cold temperatures and low enthalpy. Deep geothermal systems can handle temperatures and enthalpy ranging from mild to high [6].

Geothermal systems are composed of three major components: a heat source, a heat sink, and a heat exchanger (or heat exchangers). Typically, the ground serves as the heat source, and the constructed environment acts as the heat sink, i.e., buildings. On the other hand, the inverse can also occur, where the heat source is the built environment, and the heat sink is the ground (Figure 2.1). As it is called, the heat exchanger transmits the heat from the source to the sink. Heat exchangers have gone through long historical development [7]. Following are some early development examples of their type. Evidence shows that Native Americans used geothermal energy for cooking as far back as 10,000 years ago. According to archaeological evidence, the Greeks and the Romans utilized baths

heated by hot springs in ancient times, and indications of geothermal space heating may be found as far back as the Roman city of Pompeii in the first century CE. Initially, geothermal energy applications were restricted to areas where hot water and steam were readily available [8]. Using the ground as a heat source for electrical power generation, Prince Piero Ginori Conti built the world's first geothermal power plant in Italy in 1904 [6].

One of the most distinguishing characteristics of GSHP systems is utilizing the thermal energy harvested from the ground. It is common to use geothermal energy in shallow geothermal systems directly, which means heating and cooling a structure directly with geothermal energy. Deep geothermal energy can generate electricity, an indirect energy utilization. Aside from devices that circulate a heat carrier fluid (exchanging heat between them), apparatus or instruments that adjust (enhance or lower) the energy input transported between the ground and the target environment are also used in such situations.

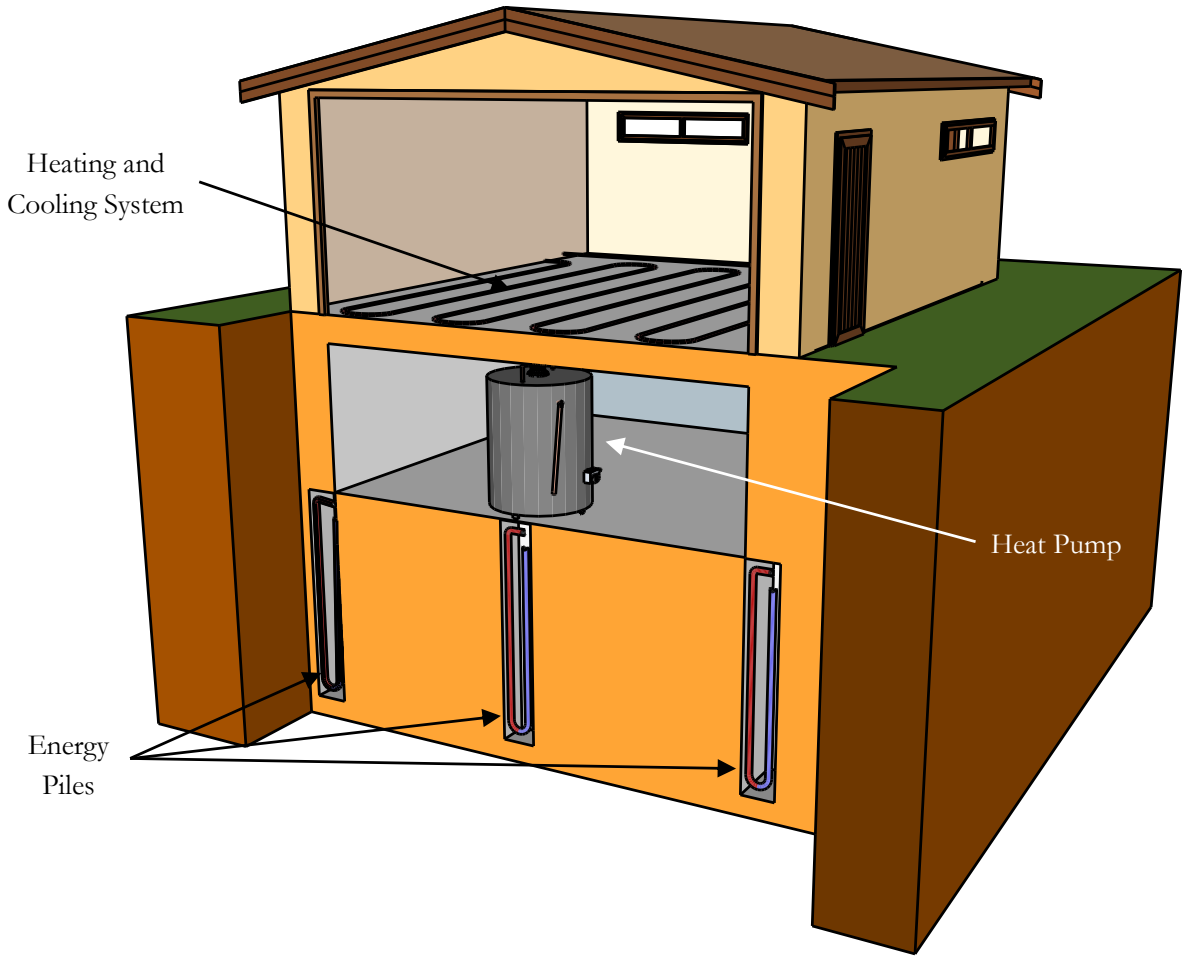

Figure 2.1: Residential heat pump for summer cooling and winter heating

When an indirect use of geothermal energy is not targeted in deep geothermal systems, it is possible to make direct use of geothermal energy. Instead, GSHPs that pump heat from/to the ground and the target environment, devices that compel a heat carrier fluid to flow between the ground and the target environment, are required in this situation, as opposed to the prior scenario. Shallow geothermal systems that operate at temperatures

less than 25°C can provide heat, cooling, and hot water, the temperature available beneath. These systems are environmentally friendly and ideal for small-scale and home use in any geographical area. It is possible to use deep geothermal systems to provide heating, hot water, and electricity while taking advantage of temperatures available underground that is greater than 25°C and up to 200°C because the temperatures required for electrical power generation are generally greater than 175°C [9]. Unlike shallow geothermal systems, which are appropriate for medium to large-scale applications, these systems can be implemented in more specific places than shallow geothermal systems. Shallow geothermal systems can be classified as either closed-loop or open-loop systems [9]. Closed-loop systems use a water-based combination that circulates through sealed pipes to transmit heat from the ground to the superstructure or vice versa, depending on the application. While in open-loop systems, the groundwater is taken from or injected into aquifers through wells and used directly in the heat exchange process [10].

Horizontal ground heat exchangers are the shallowest geothermal system located at a depth of less than 10 m [9]. These systems usually comprise closed polyethylene pipes plowed or excavated horizontally into the ground next to the desired building. A flowing heat carrier fluid in the pipes permits the interchange of heat present in the ground (primarily due to solar radiation), beneficial for heating purposes in residential, agricultural, and aquaculture applications. While achieving energy storage goals by drilling deep geothermal baskets can be used as a more compact system than horizontal and vertical geothermal boreholes, they can be used for the same objectives as horizontal geothermal boreholes. These systems, which usually are buried in the ground at a depth of a few meters, i.e., less than 10 m [11], are composed of closed polyethylene pipes fixed in a spiral geometry through which a heat carrier fluid flows and are typically buried at a depth of several meters. The most significant advantage of horizontal GHEs and geothermal baskets is the application for previously constructed buildings and the no need for deep vertical drilling.

Table 2.1: Characteristics of geothermal systems [11], [6], [9], [12]

system	Depth [m]	Harvested temperature [°C]	Primary circuits	Application	Ecology
Horizontal GHEs Geothermal baskets	<10	<12	Closed-loop	New or renovated single-family houses or small-scale businesses	
Foundation piles, tunnels, walls	<50			Larger buildings	It needs a 20-30% electricity boost
Groundwater wells	<200	<17	Open-loop	Single-residential houses	Emitting 5 tons/yr less CO_2
The array of geothermal boreholes	<100 (500)	<25	Closed-loop	Single-residential houses, Larger buildings	
Mine water energy	<800	<25	Open-loop	Larger private or industrial buildings	It needs electricity for pumping water
Thermal springs	<1000 (3000)	<100	Open-loop	Bathing, local or district heating	
Deep hydrothermal Systems	>3000	<120	Open-loop	Generating electricity, District heating	No CO_2 produced
Petro thermal systems	>5000	<150	Open-loop		

Furthermore, applications in that spiral coils are located in surface water reservoirs adjacent to buildings are also feasible. However, such applications require the reservoirs to be deep enough to avoid conditions detrimental to system operation, such as freezing the reservoir water and the circulating heat carrier fluid in the pipelines. When underground mines are abandoned, the pumps that keep them dry are often switched off, and the mines get filled with water. Geological processes heat this water, and the temperature remains stable year-round. UK coal authorities have calculated that the constantly replenishing water within these mines could potentially be a resource to provide all of the heating requirements for the coalfield areas [13].

Groundwater capture systems use open wells surrounded by groundwater reservoirs (around 200 m deep) [11]. These systems can be used in situations with no hydrological, geological, or environmental constraints. They are primarily employed for heating water

by extracting the thermal energy contained within the underlying water. Singular wells can be utilized for small-family house sizes. Doublet wells are typically required in more significant constructions. It may be necessary to use extraction and injection wells to maintain a balanced underground thermal field, which is required for the performance and, in some circumstances, environmental considerations. Unlike the previous applications, vertical geothermal boreholes (single or an array of boreholes) are made out of closed polyethylene pipes buried vertically in the earth beneath or next to buildings at greater depths than the previous ones (from 100 meters to 500 meters) [11], [12]. A filler material (for example, bentonite) is typically inserted in the borehole to improve the heat exchange between the earth and the pipes; however, some boreholes are just filled with underground water. A heat carrier fluid (HCF) circulating in the pipes provides heat exchange for heating, cooling, storing, and producing hot water in various construction types and environments. Single boreholes provide enough water to supply thermal energy for small residential structures. Borehole fields (an array of several boreholes) are necessary to feed more significant buildings with thermal energy. Higher energy inputs than those transferred through shallower geothermal systems can be attained using vertical geothermal boreholes due to the higher temperature levels of the ground at the specified depths compared to shallower geothermal systems. New geothermal systems, known as energy geostructures, combine the structural support role of any structure in contact with the ground with the heat exchanger role of shallow geothermal systems, resulting in outcomes comparable to or even better than previously described methods.

Thermal springs are often considered part of deep geothermal systems, while they can also be found at shallow depths, a characteristic of shallow geothermal systems. A relatively deep heated groundwater reservoir in the subsurface surrounds open wells in this arrangement, allowing easy access to the water. Thermal energy extracted from subterranean water is primarily utilized for bathing and therapy purposes, and they were historically popular. Open-well hydrothermal systems draw groundwater from depths where the temperature and thermal energy available are high enough to allow for the implementation of large-scale heating applications to be realized (from a depth up to 3000 m) [11], [6]. Although these systems are typically employed in district heating, they can efficiently heat immense industrial or agricultural structures and generate electricity. Like hydrothermal systems, petroleum thermal systems draw groundwater using open wells at a greater depth than hydrothermal systems (from a depth of more than 4 to 5 km). The high temperature and the thermal energy inherent in the water at these depths can be utilized to produce and provide enormous amounts of electrical energy on a large scale [6], [11].

2.4 Shallow geothermal systems

In most locations worldwide, buildings may be heated and cooled using the thermal energy within the shallow soil layers, from 1 m to 200 m [14]. At about 10 to 15 meters below the surface, the seasonal temperature variance at the ground surface is decreased to a practically constant temperature of around 6 to 7 degrees Celsius in Norway [15]. Under this depth, it is known that the temperature rises by an average gradient of 3°C per 100 m of depth [1]. The first 100 meters are sustainable due to the stable thermal interaction between the soil and the air, making them excellent for delivering and storing thermal energy even though the temperature is relatively low [1] (Figure 2.2).

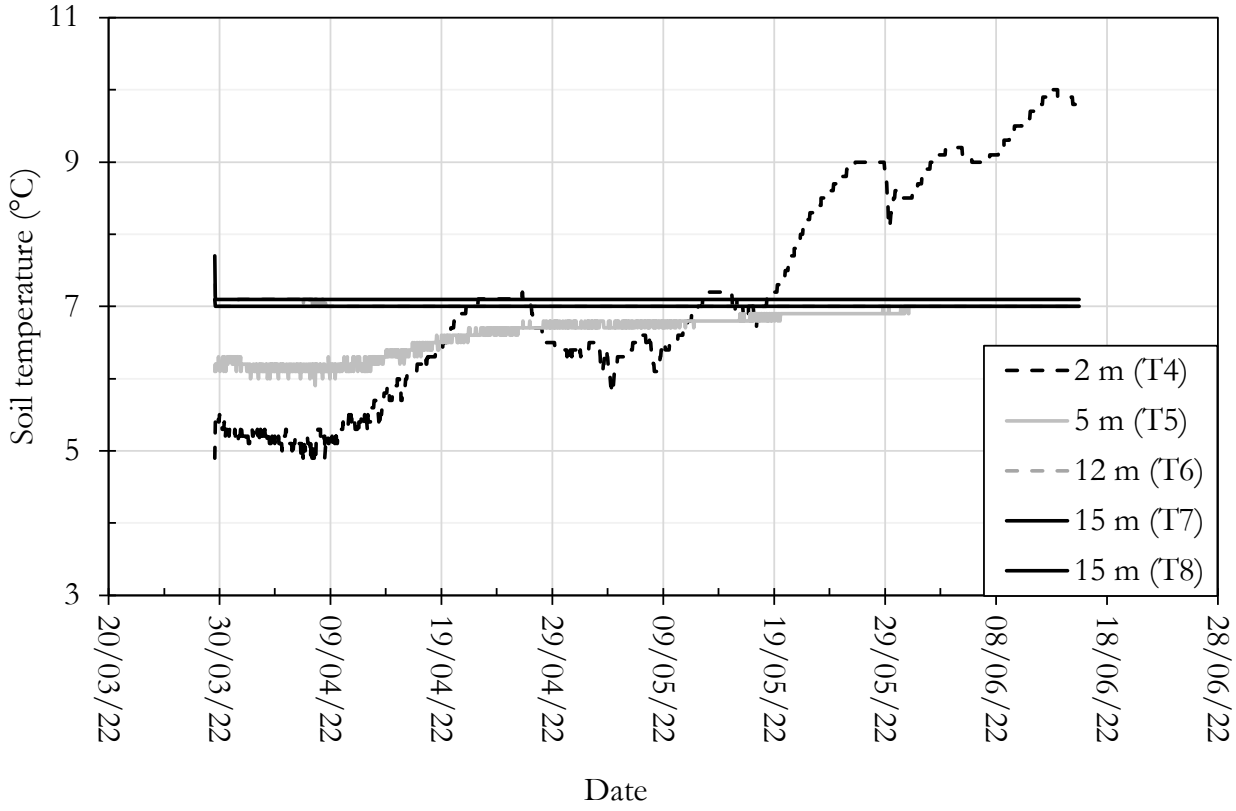

Figure 2.2: Ground temperature variations with depth measured at the BEAR project location near Malvik

More recently, the foundation components of structures are being utilized to capture the ground thermal energy to assist meet the building heating/cooling requirements; these foundations are known as energy or thermo-active foundations. In the 1980s with base slabs, 1984 with piles, 1996 with diaphragm walls, and early 2000 with energy tunnels, Austria and Switzerland pioneered using foundation components to meet building energy needs [14].

Energy Foundations continue to acquire worldwide popularity due to their significant benefits over traditional alternatives. They remove the additional drilling expense and land area needed to install conventional boreholes. In addition, they have a greater cross-section that allows for flexible and diverse pipe arrangement compared to ordinary boreholes of 75–150 mm in diameter, resulting in a significant probability of thermal contact between pipes, making them less favorable [16].

2.5 Materials and technology

Because of its excellent heat conducting characteristic and high thermal storage capacity, mass/reinforced concrete is the most typical material utilized in GEP construction. Similarly, the concrete mixture must correspond to Eurocode 7 specifications for the design of pile foundations [17].

In 1994, Morino and Oka became the first to employ steel piles as heat exchangers due to their high heat conductivity and low thermal resistance. In 1998, two steel piles were used for floor heating and cooling at Hokkaido University in Japan. As of 2002, over 300 buildings

were claimed to have used them for heating and cooling after their successful installation. Nagano claimed that heat energy might be transferred by directly cycling water via steel piles or by equipping steel piles with energy loops. The second option is more economical and needs less maintenance [14].

Installation of main loops of heat exchangers is often accomplished by burying the loops pipe inside the excavated soil for mass concrete pipes or by attaching the loop pipes to reinforcing cages of cast-in-place reinforced concrete piles [18].

Generally, hollow cylindrical precast concrete and steel piles have hollow spaces in the center; after driving the pile into the ground, heat exchanger pipes are installed in the hollow space, and then the hollow space is filled with grout mortar to guarantee thermal contact between the pipes and pile [18].

The pipes may be placed in many configurations within the geothermal energy piles. Single U-shape, double U-shape, triple U-shape, W-shape, spiral or helical shape, direct double-pipe type, and indirect double-pipe type configurations are among the most often reported geometries. These pipes, known as energy loops, are made from High-Density Poly Ethylene/Poly-Propylene (HDPE/HDPP), Polyvinyl-chloride (PVC), and Polybutylene pipes [19]. Careful thought must be used to guarantee that the optimal pipe shape is selected for optimal system performance. Pipes from a single or several piles may be linked in series, parallel, or a mix of the two [6], [20].

The liquid that circulates within the energy loops is called heat carrier fluid (HCF). This liquid is the media for transferring the heat between the ground and the heat pump. The HCF consists of pure water plus some additives such as antifreeze-based solutions. The additive solution can possess up to 40% of the HCF by weight [21].

The performance of shallow geothermal energy systems, especially the geothermal energy piles, is mainly affected by ground heat flow mechanics, mainly through heat conduction and heat convection by the movement of underground water in the porous media. Heat flow mechanics across the pile, groundwater flow rate, initial ground temperature, and soil thermal properties. These factors ensure an effective and cost-efficient geothermal energy pile [14].

2.6 Thermo-mechanical and thermal behavior

The extra settling produced by temperature cycles is a barrier to the safety and serviceability of energy pile foundations from the standpoint of pile foundation design. For geothermal energy piles to become a reality, HVAC engineers must develop heat transfer performance. Some applications, such as the Frankfurt Main Tower and Dock E at Zurich Airport, have already been completed in Europe. However, since the physics are not entirely understood, specific geothermal energy pile applications have been overdesigned for safety concerns. Therefore, experimental and numerical study is still occurring in research labs across the globe [22].

Conventional load transfer techniques, in-situ testing, laboratory testing, and numerical modeling are often used to study the mechanics of geothermal energy piles. In-situ testing gives the circumstances of an actual construction scenario rather than real construction loads and might provide the most accurate data before final construction [23]; nonetheless, the expense of in-situ testing is rather expensive compared to laboratory testing of scaled physical models. Numerous researchers conduct laboratory testing and

numerical modeling to decrease experimental expenditures [24], [25], [26], [22], [27], and [28]. Several kinds of literature studied the mechanical behavior of energy piles exposed to several thermal cycles, which represent seasonal pile temperature fluctuations [29], [30], [31], [32], and [28].

A thermal performance study determines the utilization of geothermal energy piles in commercial buildings. Numerous scholars examined the thermal performance of geothermal energy piles. In geothermal energy piles, the heat exchange function is often performed by installing a water circulation pipe inside the reinforcing cage. Many studies concentrate on the layout of this water circulation pipe to guarantee that thermal exchange rates match thermal performance standards. Similar to the experimental testing of the energy pile performances, numerical simulation provides more details for thermal performance assessments [33], [34], [35], [2], [36], and [37]. Analytical methods for borehole heat exchangers give an idealized scenario for estimating the soil temperature change. Some heat source models collectively describe geothermal heat exchangers: the infinite line source model, the finite line source model, the infinite hollow cylinder model, the infinite solid cylinder model, the spiral line model, and the finite solid cylinder [38], [34], [6], and [1].

3 Geothermal energy piles, physical phenomena

3.1 Introduction

In this chapter, an introduction to physical phenomena related to heat transport is briefly discussed, and the heat transfer in porous media is explained. Then, the focus is placed on mathematical equations governing heat transfer physics of coaxial annular geothermal energy piles, which are the core subject of this thesis.

3.2 Heat transfer, preliminaries

Heat transfer is a thermodynamic term explaining the rate of thermal energy transfer between a system and its surroundings. "Temperature" and "heat flow" are the primary quantities measured in heat transfer. Temperature indicates the quantity of thermal energy in a system, while heat flow describes the movement of thermal energy caused by a temperature difference. The thermal energy is connected to the kinetic energy of the molecules of material since the material shows greater kinetic energy at higher temperatures. There are three main modes of heat transfer: "Conduction", "convection", and "radiation" [1].

3.2.1 Heat transfer by conduction

3.2.1.1 Definition

Conduction is the mechanism that facilitates the direct transfer of heat through a matter caused by the temperature differential between adjacent sections of a domain. It occurs when the temperature of the molecules in a material rises, causing them to vibrate vigorously. The collision of the molecules with neighboring molecules causes them to vibrate, resulting in the transfer of heat energy to adjacent parts of the domain. When two domains are in contact, heat transfers from the warmer to the colder object due to conduction [39].

3.2.1.2 Mechanism

Heat conduction (diffusion) is one of the major mechanisms of thermal energy transfer. According to the second law of thermodynamics, when two objects with different temperatures are brought into thermal contact, thermal energy always flows from the object with the higher temperature to the object with the lower temperature and never in the reverse direction. The two zones exchange heat until they attain thermal equilibrium, a condition where their temperatures become equal. In a control volume same as Figure 3.1, the first law of thermodynamics expresses that:

$$\text{Rate of heat flow in} + \text{rate of energy generation} = \text{rate of heat flow out} + \text{rate of internal energy storage} \quad (3.1)$$

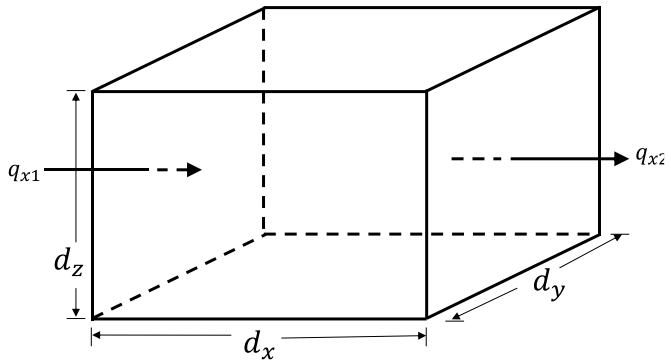

Figure 3.1: A control Volume

Fourier heat conduction equation describes, on a control volume as in Figure 3.1, the heat transfer rate per unit area normal to the direction of heat flow, also known as heat flux. In terms of a single dimension heat flow, the inlet heat flow is defined as Equation (3.2):

$$\mathrm{q_{x1}} = \dot{\mathrm{q}}_{\mathrm{x1}}\mathrm{A} = \underbrace{-\mathrm{k_x}\frac{\partial \mathrm{T}}{\partial \mathrm{x}}}_{\dot{\mathrm{q}}_{\mathrm{x1}}}\underbrace{\mathrm{dydz}}_{\mathrm{A}} \quad (3.2)$$

Where:

$\mathrm{q_{x1}}$: rate of heat flow in $[\mathrm{W}]$

$\dot{\mathrm{q}}_{\mathrm{x1}}$: heat flux $[\mathrm{W/m^2}]$

A: area $[\mathrm{m^2}]$

$\mathrm{k_x}$: thermal conductivity in the x direction $[\mathrm{W/m \cdot K}]$

$\frac{\partial \mathrm{T}}{\partial \mathrm{x}}$: temperature change in the x direction $[\mathrm{K/m}]$

The outlet heat flow $(\mathrm{q_{x2}})$, can be defined as Equation (3.3):

$$\mathrm{q_{x2}} = \mathrm{q_{x1}} + \frac{\partial \mathrm{q_{x1}}}{\partial \mathrm{x}}\mathrm{dx} \quad (3.3)$$

Equation (3.1) for the control volume can be described as:

$$\mathrm{q_1(x,y,z)} + \mathrm{Q(x,y,z)dxdydz} = \mathrm{q_2(x,y,z)} + \frac{\partial \mathrm{U}}{\partial \mathrm{t}} \quad (3.4)$$

Where:

$Q(x,y,z)$: generated heat rate $[W]$

$\frac{\partial U}{\partial t}$: internal energy storage $[W]$

$$\frac{\partial U}{\partial t} = \rho c_p \frac{\partial T}{\partial t} dxdydz \tag{3.5}$$

Where:

ρ: density $[kg/m^3]$

c_p: specific heat at constant pressure $[J/kg \cdot K]$

Equation (3.4) can be rewritten using Equations (3.3) and (3.5):

$$\frac{\partial}{\partial x}\left(k_x \frac{\partial T}{\partial x}\right) + \frac{\partial}{\partial y}\left(k_y \frac{\partial T}{\partial y}\right) + \frac{\partial}{\partial z}\left(k_z \frac{\partial T}{\partial z}\right) + Q(x,y,z) = \rho c_p \frac{\partial T}{\partial t} \tag{3.6}$$

By assuming constant isotropic thermal conductivity $\left(k_x = k_y = k_z = k\right)$ and in the absence of heat generation $(Q(x,y,z) = 0)$ the heat conduction equation can be written as:

$$\nabla^2 T = \frac{1}{\alpha}\frac{\partial T}{\partial t} \tag{3.7}$$

Where:

$\alpha = \frac{k}{\rho c_p}$: thermal diffusivity $[m^2/s]$

∇^2: Laplacian operator

Laplacian operator in the cartesian coordinate system is described as:

$$\nabla^2 = \frac{\partial^2}{\partial x^2} + \frac{\partial^2}{\partial y^2} + \frac{\partial^2}{\partial z^2} \tag{3.8}$$

Laplacian operator in the cylindrical coordinate system is given by:

$$\nabla^2 = \frac{\partial^2}{\partial r^2} + \frac{1}{r}\frac{\partial}{\partial r} + \frac{1}{r^2}\frac{\partial^2}{\partial \emptyset^2} + \frac{\partial^2}{\partial z^2} \tag{3.9}$$

3.2.2 Heat transfer by convection

3.2.2.1 Definition

Convection refers to the kind of heat transfer that happens exclusively in fluids and involves the actual movement of materials. The term fluid refers to any material whose molecules flow easily from one location to another, including liquids and gases. It occurs either naturally or forcibly. Gravity plays a significant role in natural convection, such that the hotter portion expands when a material is heated from below. As a result of buoyancy, the hotter domain rises because it is less dense, while the colder substance replaces it by sinking at the bottom owing to its high density. When the colder substance becomes hot, it rises, and the process repeats. When heated by convection, the molecules of material scatter and move apart. By any physical means, such as a pump, the material is forced to rise when convection is accomplished with force [39].

3.2.2.2 Mechanism

Heat convection is a main heat transfer mechanism fundamentally related to fluid flow. Heat convection is the result of simultaneous heat diffusion (on a microscopic scale, heat convection is caused by thermal diffusion, which is the transmission of energy through vibrations at the molecular level inside the fluid), and heat advection (on a macroscopic size, it is caused by the bulk motion of the liquid, which carries heat from one area to another along the direction of its movement). For a one-dimensional situation, the convective heat flux (heat flow rate per unit area normal to the direction of heat flow) is defined as:

$$\dot{q}_{x1} = \underbrace{-k_x \frac{\partial T}{\partial x}}_{\text{diffusion}} + \underbrace{\rho c_p u T}_{\text{advection}} \tag{3.10}$$

Where:

u: fluid velocity in the x direction $[m/s]$

Content of Equation (3.1) is valid here, and the three-dimensional heat conduction-convection can be obtained as:

$$\nabla \cdot (k \nabla T) + \nabla\left(\rho c_p U T\right) + Q(x, y, z) = \rho c_p \frac{\partial T}{\partial t} \tag{3.11}$$

Where:

U: Fluid flow velocity vector $([u, v, w])$ $[m/s]$

∇: Nabla operator

Nabla operator in the cartesian coordinate system is described as:

$$\nabla = \frac{\partial}{\partial x} + \frac{\partial}{\partial y} + \frac{\partial}{\partial z} \tag{3.12}$$

Nabla operator in the cylindrical coordinate system is given by:

$$\nabla = \frac{\partial}{\partial r} + \frac{1}{r}\frac{\partial}{\partial \emptyset} + \frac{\partial}{\partial z} \tag{3.13}$$

3.2.3 Radiation definition

Radiation is the heat transmission process that does not need a material-filled medium. It refers to the wavelike flow of heat, which does not need molecules to travel. The objects do not need to be in direct contact to transfer heat. In addition, surface features such as color, surface orientation, etc., significantly impact radiation. This method transfers energy using electromagnetic waves, also known as radiant energy. In general, hot things radiate thermal energy to their surroundings. Radiant energy can pass across a vacuum domain from its source to its surrounds. The finest example of radiation is the solar energy we get from the sun at a distance of millions of kilometers from the earth [39].

Heat flow in a typical shallow geothermal system is a mixture of heat conduction and convection. In such a system, heat radiation plays no significant function. Hence it will not be discussed in this thesis.

3.3 Heat transfer in porous media

A porous media is a multiphase material consisting of a porous substance containing particles with varying thermodynamic characteristics, such as densities and thermal conductivities.

Typical soil mass, for instance, comprises solid, liquid, and air phases, as shown in Figure 3.2. While the solid particles make up the skeleton of the material, also known as the solid matrix, the water and the air are contained in the pores (voids) of the material. In the context of shallow geothermal systems, the soil mass around borehole heat exchangers and the grouting material are typical examples of porous materials.

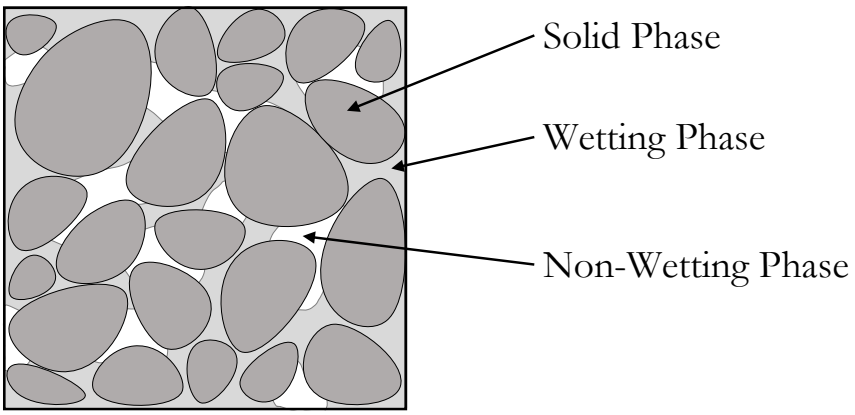

Figure 3.2: Sample of a multiphase medium

Transport in porous media is a broad topic that has lured interest and attention as a research topic. In this study area, the balance and field equations are derived from classical continuum mechanics, but the focus is on the contribution and interaction of the individual element. Modeling multiphase materials requires a precise mathematical description of the thermodynamic processes occurring at the interfaces between the components. Currently, no theory effectively explains the connection between microscopic elements and their macroscopic consequences. However, significant modeling ideas have been established.

"The averaging theory" allows for a more physically scaling up microscopic values to their corresponding macroscopic equivalents. This method describes multiphase processes both physically and thermodynamically. In this method, macroscopic quantities are derived from formal local volume averaging of microscopic values. The standard interpretation fully accounts for the interfacial effects, including the potential of mass, momentum, and energy exchange between the elements. This method often states constitutive connections based on entropy inequality. The process of averaging is carried out from a Representative Elementary Volume (REV), which is much bigger than the individual component volumes but significantly lower than the volume of the physical system (Figure 3.2). In the averaging theory, REV is supposed to be space- and time-invariant; hence, this technique is invalid for heterogeneous materials.

When evaluating shallow geothermal energy piles, the temperature gradient at the microscopic (pore) level is smaller than that at the macroscopic (REV) level, and both are much less than that at the megascopic (physical system) level. That is to say:

$$\Delta T_{micro} < \Delta T_{REV} \ll \Delta T_{system} \tag{3.14}$$

This implies that the local temperature gradient between the phases is slight; hence, it is reasonable to assume that the solid and fluid phases within a sample basic volume are in local thermal equilibrium. This indicates that the average temperatures of both phases are similar:

$$T_{solid} = T_{fluid} = T \tag{3.15}$$

By applying the condition of Equation (3.15) to the general three-dimensional heat conduction–convection Equation (3.11) and omitting the convective term of the solid phase (considering that solid particles lack any advection) and ignoring the heat energy generated inside the system, the system macroscopic field heat transfer equation or the heat transfer equation in the porous media can be obtained, as follows:

$$\left(\rho c_p\right)_{eff}\frac{\partial T}{\partial t}+\nabla\cdot k_{eff}\cdot\nabla T+\left(\rho c_p\right)_{fluid}U_{fluid}\nabla T=0 \tag{3.16}$$

Where:

$\left(\rho c_p\right)_{eff}$: local averaged effective heat capacity of the porous medium

$k_{eff}\equiv k_{solid}+k_{fluid}$: local averaged effective thermal conductivity of the porous medium

U_{fluid}: fluid velocity, which can be described by the simplified Darcy's law as:

$$U_{fluid}=-\frac{\mathbf{K}}{\mu_{fluid}}\cdot\left(\frac{\partial P}{\partial z}-\rho_{fluid}g\right) \tag{3.17}$$

Where:

$\mathbf{K}$: generalized permeability of the porous medium $\left(\mathbf{K}_x=\mathbf{K}_y=\mathbf{K}_z=\mathbf{K}\right)$ $[m/s]$

μ_{fluid}: dynamic viscosity $[kg/m\cdot s]$

$\frac{\partial P}{\partial z}$: pressure gradient $[Pa/m]$

ρ_{fluid}: fluid density $[kg/m^3]$

g: gravity acceleration $[m/s^2]$

The effective heat capacity $\left(\left(\rho c_p\right)_{eff}\right)$, can be calculated by a simple volume averaging:

$$\left(\rho c_p\right)_{eff}=n\left(\rho c_p\right)_{fluid}+(1-n)\left(\rho c_p\right)_{solid} \tag{3.18}$$

Where:

n: porosity of the porous medium

Calculating the effective thermal conductivity of porous media characterizing energy geostructures is more complex, and several mathematical expressions have already been provided [6]. However, similar to the effective heat capacity, a simple volume average will suffice for shallow geothermal systems when the temperature gradient is negligible:

$$k_{eff} = nk_{fluid} + (1 - n)k_{solid} \quad (3.19)$$

3.4 Heat transfer in geothermal energy piles

The heat transfer method in a geothermal energy pile is relatively complex since it includes both convection and conduction processes in a medium with multiple parts. This medium comprises inflow and outflow pipes, bentonite-cement grout, circulating fluid, typically water with 20–25% anti-freezing coolant, and a steel casing in the case of the present study. Due to the different thermal characteristics of these materials, the mechanism of heat transfer in each component of the borehole heat exchanger varies significantly from the others. The shape of the relevant components and their thermal interactions are also vital factors that affect the process of heat transfer in a borehole heat exchanger. Each component interacts directly with at least one other component and has indirect contact with others. Due to this very complex heat transfer mechanism, several models with varying degrees of complexity have been presented in the research literature. This study aims to give a mathematical model for hollow steel piles.

3.4.1 Thermal resistance

Thermal resistance, often known as heat resistance, is the capacity of the material to bear the heat. It is the reciprocal of heat conductivity. This feature is essential in several engineering applications since it is utilized to improve the energy efficiency of an object or device. Especially for heat exchanger design, accurate thermal resistance estimation is crucial. Several approaches have been developed for this purpose, and they may generally be divided into three categories: experimental, analytical or numerical, and thermal circuit [1].

According to Fourier's law, the rate of heat conduction across a homogeneous domain is proportional to the cross-sectional area of the domain and the temperature differential across borders along the heat flow channel (Figure 3.3).

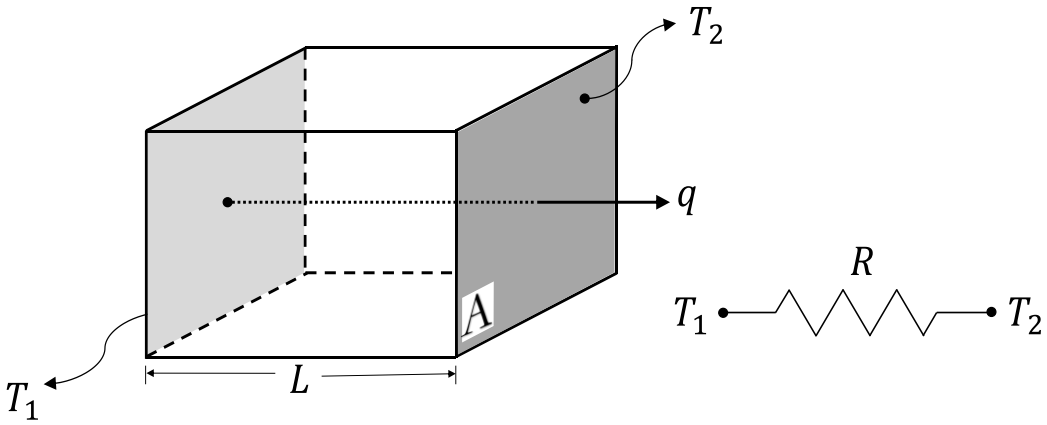

Figure 3.3: Thermal circuit related to a control volume

Fourier law may be stated as:

$$q = -\frac{(T_2 - T_1)}{R} \tag{3.20}$$

Where:

q: rate of heat flow in $[W]$

R: thermal resistance $[K/W]$

3.4.1.1 Conductive thermal resistance

Considering Equation (3.20) and comparing it to Equation (3.2) for a one-dimensional steady-state heat flow in a homogeneous control volume such as Figure 3.3, while T_1 and T_2 are kept constant, will reflect the conductive thermal resistance as:

$$R = \frac{L}{k \cdot A} \tag{3.21}$$

Take into account a single-layer cylindrical pipe with the following dimensions: length L, inner radius r_1, outside radius r_2 and thermal conductivity k. The temperatures of the inner and outer surfaces are kept at T_1 and T_2 respectively, as in Figure 3.4:

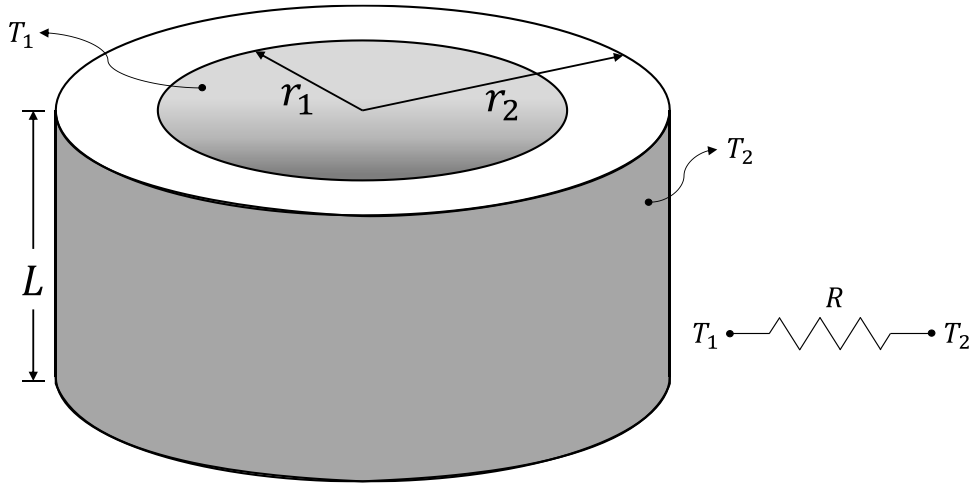

Figure 3.4: Thermal circuit of heat conduction in a single-layer cylindrical pipe

In this scenario, a cylindrical-based coordinate system may be used to characterize the steady-state heat conduction as:

$$q = -\frac{2\pi Lk}{\ln\left(\frac{r_2}{r_1}\right)}(T_2 - T_1) \tag{3.22}$$

Therefore, the thermal resistance can be explained by:

$$R = \frac{\ln\left(\frac{r_2}{r_1}\right)}{2\pi Lk} \tag{3.23}$$

3.4.1.2 Convective thermal resistance

Convective thermal resistance must be considered when heat flow results from heat advection processes. Heat convection at the boundary between a conductive surface and its surrounding convective fluid may be described using Newton's law of cooling:

$$q = -h(T_2 - T_1) \tag{3.24}$$

Where:

h: convective heat transfer coefficient $[W/m^2 \cdot K]$

Consider a single-layer cylindrical pipe with constant thermal conductivity and uniform inner and outer surface temperatures, T_1 and T_2, respectively. Figure 3.5 shows that the pipe has dimensions of L, r_1, and r_2 and transports a fluid with a temperature of T_f. Energy must be conserved by keeping the rate of heat transfer in the conductive and convective parts equal.

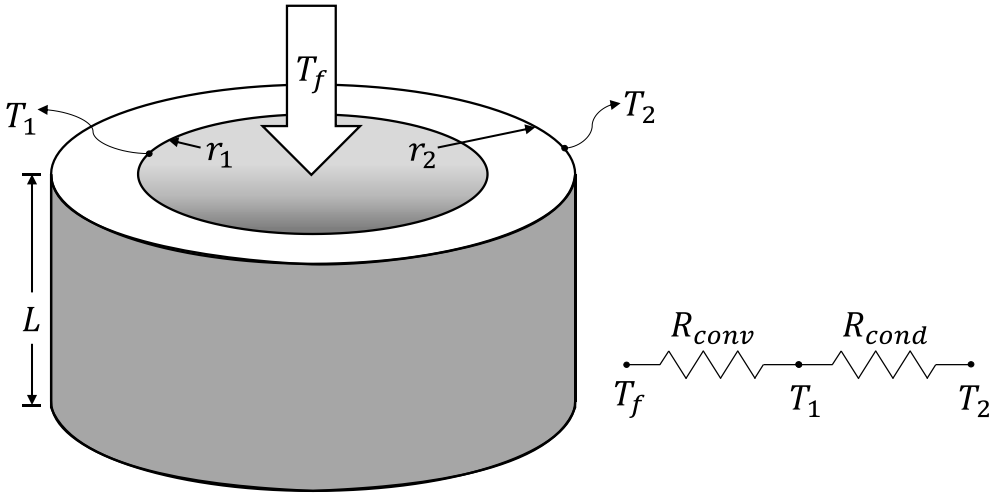

Figure 3.5: Thermal circuit of heat transfer of a single-layer cylindrical pipe (control volume)

$$R_{tot} = R_{conv} + R_{cond} = \frac{1}{2\pi r_1 Lh} + \frac{\ln\left(\frac{r_2}{r_1}\right)}{2\pi Lk} \tag{3.25}$$

The thermal resistance is characterized in the literature by the overall heat transfer coefficient [40]:

$$b = \frac{1}{A \cdot R_{tot}} \tag{3.26}$$

Where b is the inverse of the sum of the thermal resistances, and A is often expressed by the outer surface area (here $A = 2\pi r_2 L$). Thus, the thermal resistance may be represented as:

$$b = \frac{1}{\left(\frac{r_2}{r_1 \cdot h}\right) + \left(\frac{r_2}{k}\right) \cdot \ln\left(\frac{r_2}{r_1}\right)} \tag{3.27}$$

Therefore, the overall heat transfer can be expressed as:

$$Q = -b(T_2 - T_f) \tag{3.28}$$

3.4.2 Heat transfer in coaxial energy piles

In practice, there are different types of geothermal energy piles, which are different in the configuration of heat exchanging components. Coaxial steel geothermal energy piles are the focus of the present thesis. Coaxial GEPs consist of concentric pipes. These sorts of GEPs have two main configurations, which are called annular (CXA) or centered (CXC) [41], depending on the location of the HCF inflow location. In the CXA, the central pipe is the outlet path, and the annular space is the inflow path, while in the CXC, the central tube is the inflow path and the annular space is the outflow.

Since the CXA steel energy pile (Figure 3.6) is the aim of this study, hereafter, the mathematical heat transfer relations of only this type will be discussed in detail. Cylindrical bodies might be considered to generate heat. These bodies may be modeled as long, solid cylinders with uniform heat energy production per unit of Q. To keep the surface temperature at a constant value equal to T under steady-state circumstances, the rate of heat generation inside the cylinder must match the rate of heat convection from the surface of the cylinder to the surrounding fluid. Considering the slenderness of the GEPs, as discussed before, the three-dimensional heat conduction–convection Equation (3.11) can be written as:

$$k\frac{\partial^2 T}{\partial z^2} + \rho c_p u \frac{\partial T}{\partial z} - \rho c_p \frac{\partial T}{\partial t} = -Q_z \tag{3.29}$$

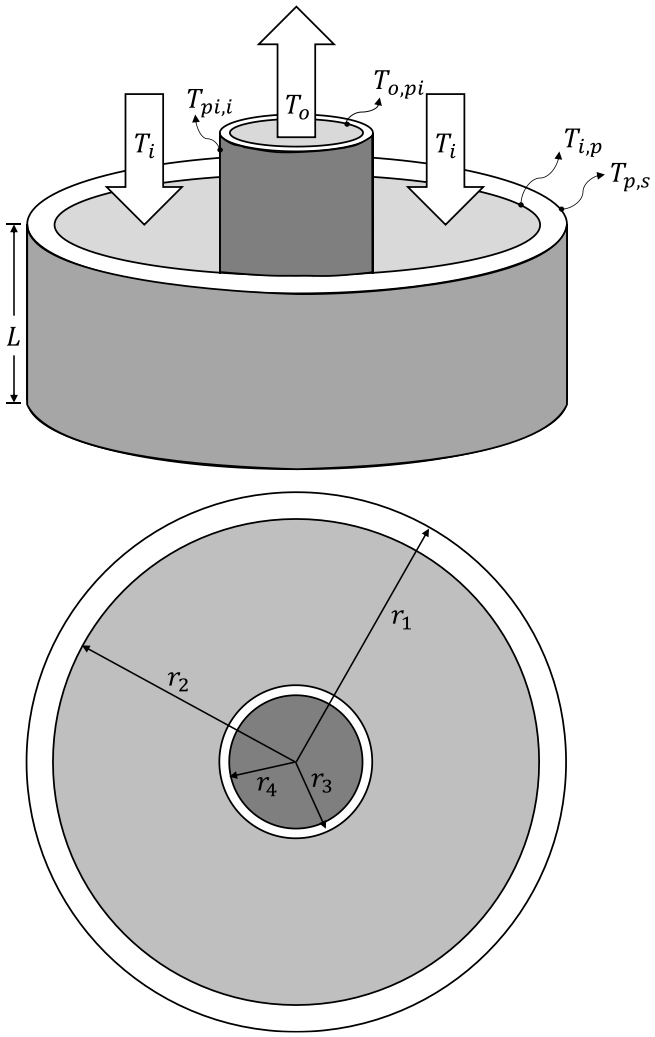

Figure 3.6: schematic of the CXA

Temperature distribution in a CXA geothermal energy pile can be schematically shown in Figure 3.7. In this illustration, two different scenarios have been considered; in the upper graph, it has been assumed that the inflow temperature is higher than the soil temperature ($T_i > T_{s,\infty}$), and in the lower graph, the opposite has been assumed ($T_i < T_{s,\infty}$).

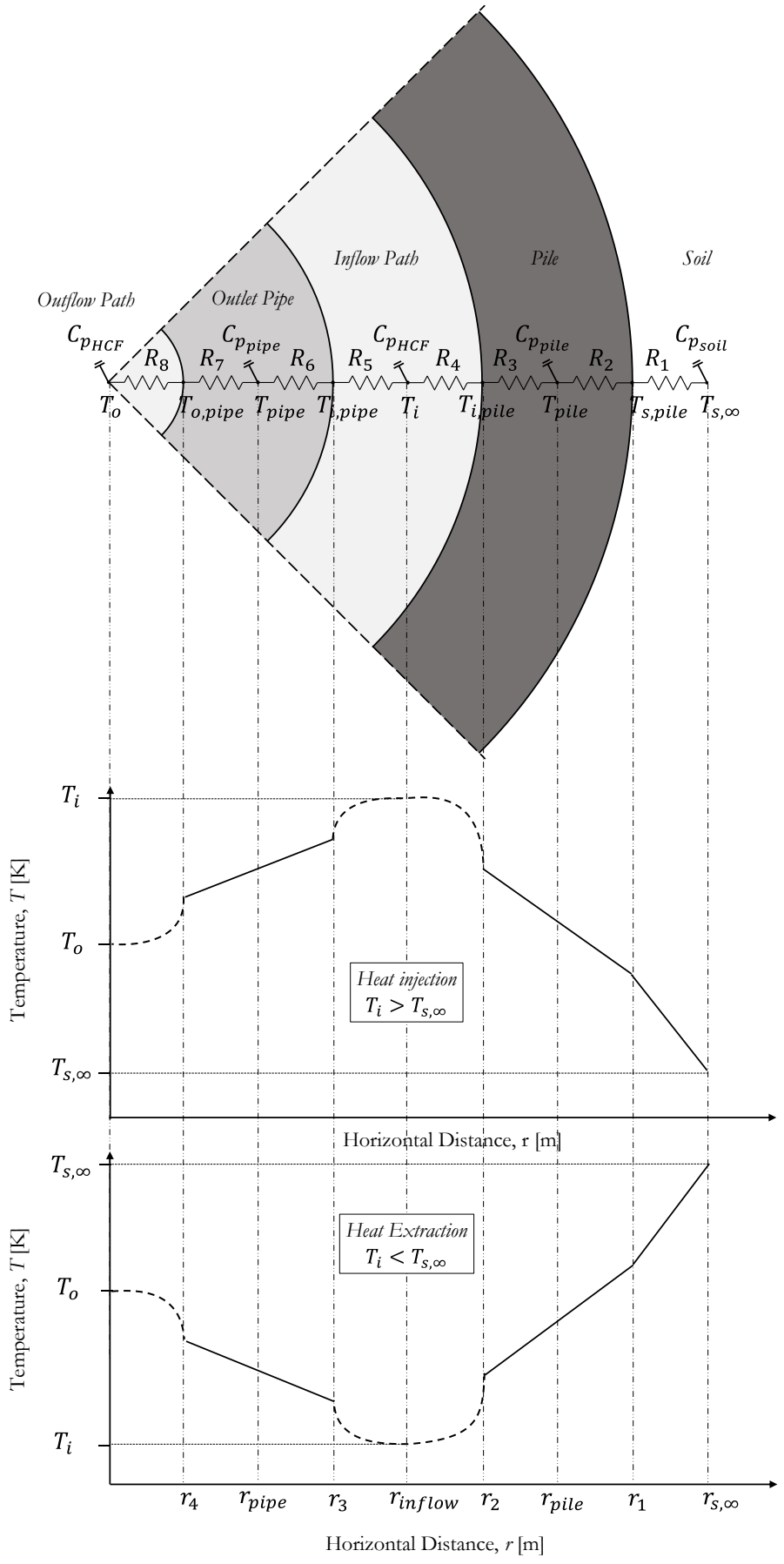

Figure 3.7: Idealization of CXA energy pile and related temperature distribution

Thermal resistances in Figure 3.7 can be written as follows:

$$R_1 = \frac{\ln\left(\frac{r_{s,\infty}}{r_1}\right)}{2\pi L k_{soil}} \tag{3.30}$$

$$R_{pile} = R_2 + R_3 = \frac{\ln\left(\frac{r_1}{r_{pile}}\right)}{2\pi L k_{pile}} + \frac{\ln\left(\frac{r_{pile}}{r_2}\right)}{2\pi L k_{pile}} = \frac{\ln\left(\frac{r_1}{r_2}\right)}{2\pi L k_{pile}} \tag{3.31}$$

$$R_4 = \frac{1}{2\pi r_2 L h_{HCF_i,pile}} \tag{3.32}$$

$$R_5 = \frac{1}{2\pi r_3 L h_{HCF_i,pipe}} \tag{3.33}$$

$$R_{pipe} = R_6 + R_7 = \frac{\ln\left(\frac{r_3}{r_{pipe}}\right)}{2\pi L k_{pipe}} + \frac{\ln\left(\frac{r_{pipe}}{r_4}\right)}{2\pi L k_{pipe}} = \frac{\ln\left(\frac{r_3}{r_4}\right)}{2\pi L k_{pipe}} \tag{3.34}$$

$$R_8 = \frac{1}{2\pi r_4 L h_{HCF_o,pipe}} \tag{3.35}$$

In Equations (3.30) to (3.35):

$r_{s,\infty}$ is an assumptive dimension showing the radial distance from the pile center that the soil temperature is not disturbed due to the pile thermal performance. The soil radius can vary between r_1 and $r_{s,\infty}$ Moreover, the soil resistance and eventually the soil temperature can be calculated for that specific radius.

r_{pile} and r_{pipe} assumptive dimensions representing pile and pipe are also eliminated in the equations.

The convective heat transfer coefficient, h, highly depends on the fluid characteristics, surface temperature, surface roughness, and fluid flow type (laminar or turbulent) [40]. Therefore, the convective heat transfer coefficient has been mentioned explicitly for the related surface, whether for the contact surface of inflow HCF and pile, inflow HCF and the pipe, or the outflow HCF and pipe. It should be emphasized that each surface has different temperatures and roughness.

In heat transfer equations, the heat capacity (c_p) of each component acts as the capacitor in electrical circuits and stores a part of the transferred heat energy to increase the temperature of that component.

One dimensional solution for heat transfer with internal energy generation in a CXA geothermal energy pile, as shown in Figure 3.6, with the temperature distribution as shown in Figure 3.7, can be written as:

For the soil:

$$k_{soil}\frac{\partial^2 T_s}{\partial z^2} - \left(\rho c_p\right)_{soil}\frac{\partial T_s}{\partial t} = \frac{T_{s,\infty} - T_i}{2\pi L r_{s,\infty} \times (R_1 + R_2 + R_3 + R_4)} \tag{3.36}$$

For the pile:

$$k_{pile}\frac{\partial^2 T_p}{\partial z^2}-\left(\rho c_p\right)_{pile}\frac{\partial T_p}{\partial t}=\frac{T_{s,\infty}-T_i}{2\pi L r_{s,\infty}\times\left(R_1+R_2+R_3+R_4\right)} \tag{3.37}$$

For the inflow path:

$$\begin{aligned}k_{HCF}\frac{\partial^2 T_i}{\partial z^2}+\left(\rho c_p u_i\right)_{HCF}\frac{\partial T_i}{\partial z}-\left(\rho c_p\right)_{HCF}\frac{\partial T_i}{\partial t}\\ =\frac{T_i-T_o}{2\pi L r_{s,\infty}\times\left(R_5+R_6+R_7+R_8\right)}+\frac{T_{s,\infty}-T_i}{2\pi L r_{s,\infty}\times\left(R_1+R_2+R_3+R_4\right)}\end{aligned} \tag{3.38}$$

For the pipe:

$$k_{pipe}\frac{\partial^2 T_{pi}}{\partial z^2}-\left(\rho c_p\right)_{pipe}\frac{\partial T_{pi}}{\partial t}=\frac{T_i-T_o}{2\pi L r_{s,\infty}\times\left(R_5+R_6+R_7+R_8\right)} \tag{3.39}$$

For the outflow path:

$$k_{HCF}\frac{\partial^2 T_o}{\partial z^2}+\left(\rho c_p u_o\right)_{HCF}\frac{\partial T_o}{\partial z}-\left(\rho c_p\right)_{HCF}\frac{\partial T_o}{\partial t}=\frac{T_i-T_o}{2\pi L r_{s,\infty}\times\left(R_5+R_6+R_7+R_8\right)} \tag{3.40}$$

Where:

r_α: radial distance of the α component from the CXA centerline $[m]$

k_α: thermal conductivity of the α component $[W/m\cdot K]$

T_α: temperature of the α component $[K]$

t: time $[s]$

z: depth $[m]$

$T_{\alpha,\beta}$: temperature of the interface of α and β components $[K]$

$\left(\rho c_p\right)_\alpha$: density multiplied by the heat capacity of the α component $[J/m^3\cdot K]$

$u_{i/o}$: inflow/outflow velocity of the HCF velocity $[m/s]$

h_α: convective heat transfer coefficient of the HCF when contacting with the solid surface of the α component $[W/m^2\cdot K]$

4 Annular coaxial steel geo-energy pile numerical modeling

4.1 Introduction

This chapter explains a reliable numerical model for predicting the thermal performance of a coaxial energy pile and the related fluid dynamics and heat transfer aspects of such steel piles based on an actual case study. The characteristics of the case study have been described first, followed by clarification of the various steps leading up to the final model. Finally, a comparison of the numerical simulation results with those obtained from field investigations is presented, accompanied by a short discussion on the lessons learned during the numerical simulation.

4.2 Finite element model

The finite element method (FEM) is a powerful numerical method to solve various partial differential equations. It is especially well suited for solving initial and boundary value problems in engineering applications, considering complex initial and boundary conditions and geometries. Partitioning a continuum of space and time into a group of discrete components, expressed by elements and nodes, is the essential characteristic of the finite element approach. Numerous other numerical methods, notably the finite difference method, have this characteristic. The finite difference approach can be used to solve issues involving heat and fluid flow. However, the finite element approach was mainly used to solve transient and steady-state problems involving advective-diffusive transport. Later, it became an essential tool for simulating a diverse set of thermo-hydro-mechanical issues in geosciences. This slightly delayed use of the finite element approach to solving flow issues was not due to individual preferences. Instead, due to the natural inability of the FEM to solve differential equations involving convection-dominated phenomena [1].

COMSOL Multiphysics® is a general-purpose software platform and powerful numerical tool for simulating physics-based problems. It is possible to cope with coupled or multi-physical phenomena using COMSOL Multiphysics. Some of the applications of COMSOL interfaces and tools are for electrical, mechanical, and fluid flow. Models of COMSOL Multiphysics simulations can be visualized using CAD and COMSOL built-in kernels. COMSOL Multiphysics assembles and solves models using finite element analysis, the finite volume method, the boundary element method, and particle tracing methods; nevertheless, the finite element approach is the primary focus of COMSOL Multiphysics. Numerous forms of finite elements are accessible, and the program automatically generates ultimately linked aspects at the moment of solution. The COMSOL is also notable for its versatility. If the model requires additional physical effect, it is enough to include it. If one of the input values of the model needs a mathematical formula, it is possible to apply it. Using capabilities such as parameterized geometry, interactive meshing, and custom solver sequences, it can swiftly adjust to changes in requirements over time. The adaptable nature of the COMSOL environment helps additional analysis by making it simple to build up and execute conditional scenarios.

4.3 Description of Saga University experiment

Saga University (2011) conducted an experimental study on multiple types of ground heat exchangers (GHEs) installed in a steel piling foundation [2]. They installed double-tube, U-tube, and multi-tube GHEs, and their performances were analyzed. The so-called double tube is the coaxial steel pile, which is also the focus of this thesis and will be explored in this chapter.

The three varieties of above mentioned GHEs were tested experimentally in the cooling mode under identical settings. Evaluated are the depth-dependent temperature distributions of the ground and GHE tube walls, the heat exchange rates over 24 hours of continuous operation at flow rates of 2, 4, and 8 [lit/min], and the impact of increasing the flow rate.

The foundation piles (steel pipes) were installed up to a depth of 20 meters and utilized as GHEs. Figure 4.1 illustrates the schematic illustration of the double tube (CXA) and the thermocouple placements for measuring the ground and tube wall temperatures. As the inlet tube of the GHE, a stainless-steel pipe with an outer diameter of 139.8 [mm] is used, and a polyvinyl chloride pipe with an outer diameter of 48 [mm] is installed within the stainless-steel pipe as the output tube. Table 4.1 displays the characteristics of the components.

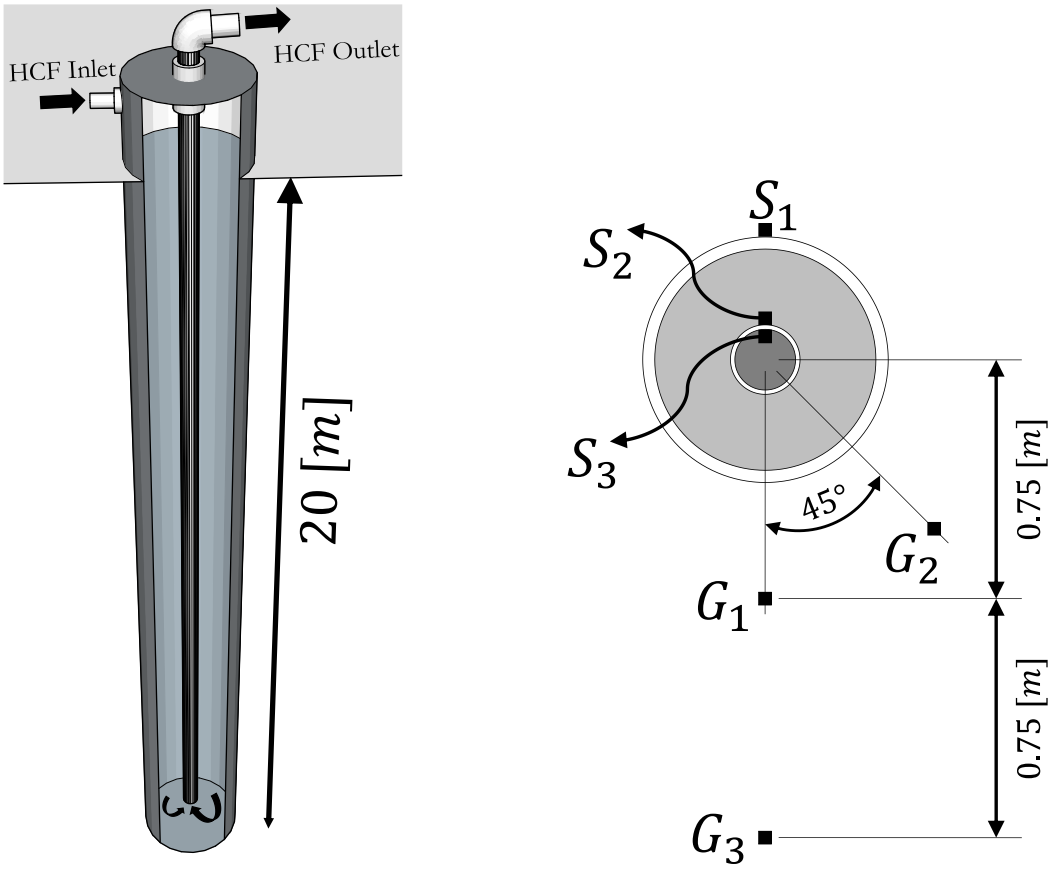

The schematic diagram of the pile

Cross-section of the pile and position of thermocouples

Figure 4.1: The Layout of the pile and position of the thermocouples

Table 4.1: Characteristics of the GEP components [2]

	Parameter	Value	Unit
Inlet pipe stainless steel (SUS304)	Length	20	[m]
	Outer diameter, $(d_{o,pile})$	0.1398	[m]
	Inner diameter, $(d_{i,pile})$	0.1298	[m]
	Thermal conductivity, $(k_{stainless})$	13.8	$[W/m \cdot K]$
Outlet pipe polyvinyl chloride (PVC)	Outer diameter, $(d_{o,pipe})$	0.048	[m]
	Inner diameter, $(d_{i,Pipe})$	0.040	[m]
	Thermal conductivity, (k_{PVC})	0.15	$[W/m \cdot K]$

The local ground temperatures were measured at a point far enough from the installation position of the trial piles in a way that the GHEs did not influence the ground temperature through the tests (Figure 4.2). It is evident in this graph that only a few meters from the ground surface layers are affected by ambient air temperature variation. In depths deeper than 5 meters, the temperature is stable year-round.

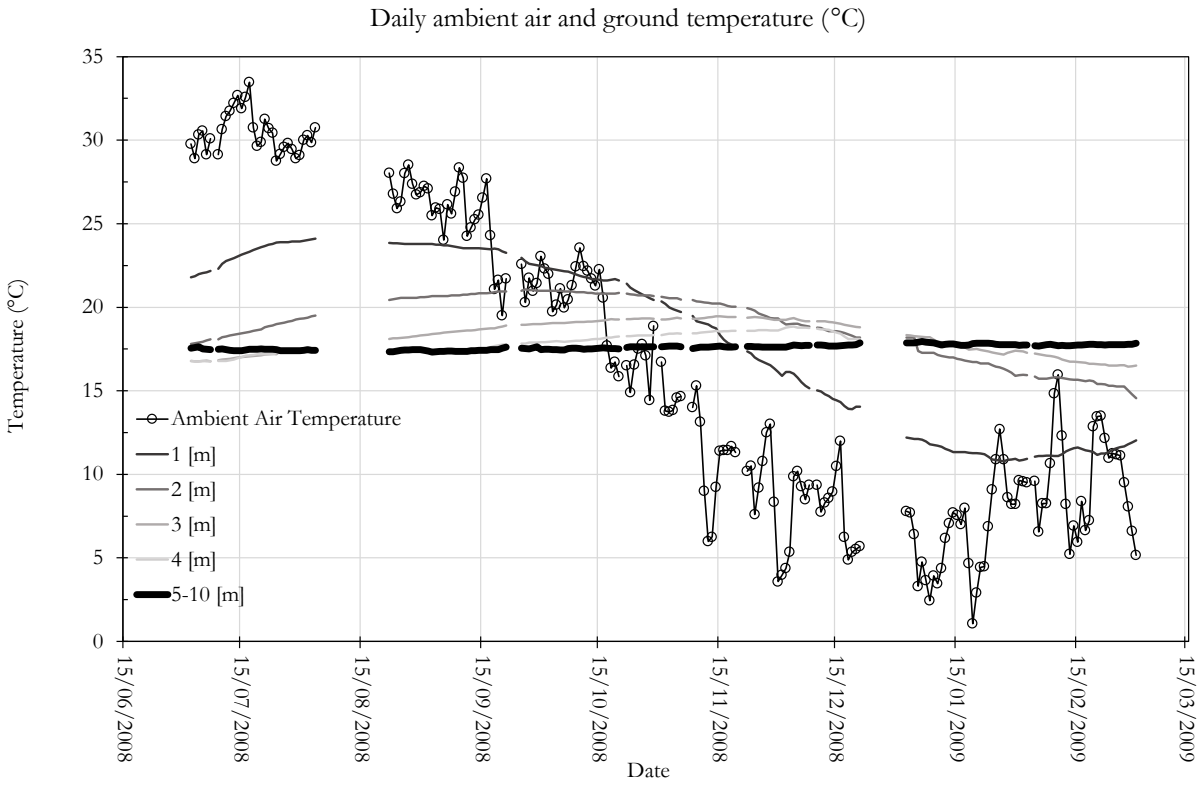

Figure 4.2: Ambient and ground temperature variation at the test location (reproduced from [2])

At three places to a depth of 25 [m], the temperature distributions of the ground were monitored at fixed depth intervals using T-type thermocouples (G_1, G_2, and G_3). Temperature change before and after the test is not significant. This slight difference can be due to either the short test period compared to other similar tests (72 hours in TRT) or higher heat capacity and higher volume of water in this type of energy pile. The study at the Saga university did not investigate the HCF flow rate effect on the ground temperature variation.

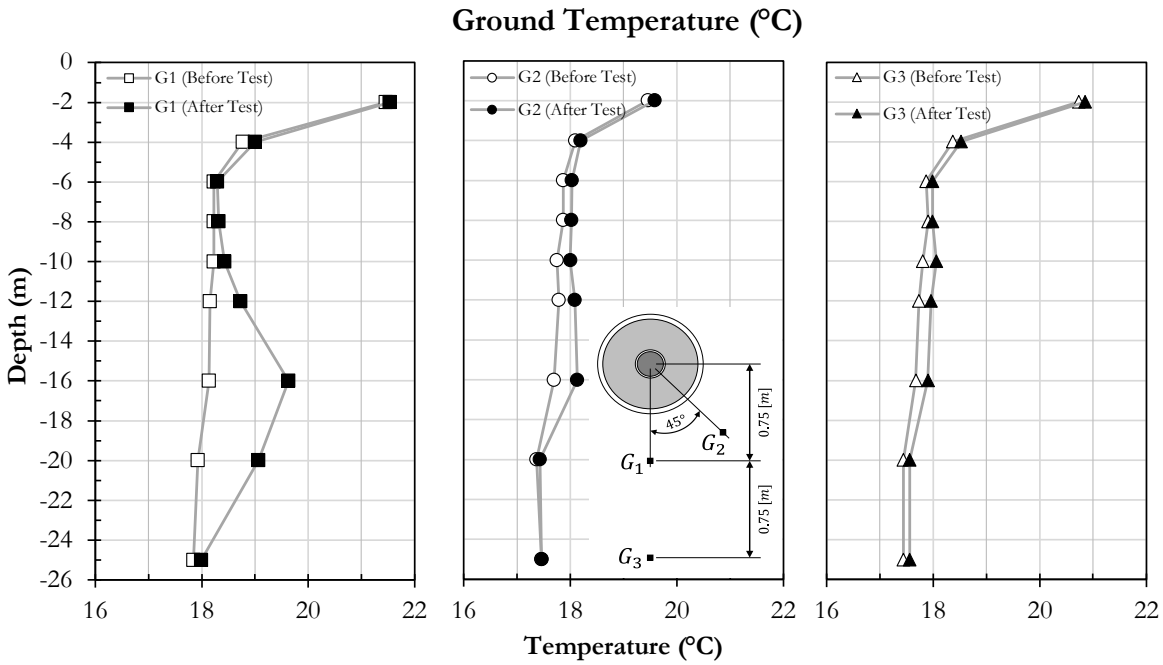

Figure 4.3: Ground temperature measured in the vicinity of the test pile before and after the test (reproduced from [2])

Temperatures on the outside surface of the input tube decrease steadily with depth. This implies that heat is lost to the ground via the inlet tube, resulting in a steady decrease in water temperature. The temperatures on the inner side of the outlet tube are lower than those on the outer side, and the temperature of the outlet tube rises gradually as it approaches the exit. This shows a heat exchange between the inflow and outflow of water, decreasing the effectiveness of GHE. At the G_1 location, the ground temperature around the double-tube GHE rose at depths of 16 and 20 meters. This can be attributed to underground water at these places and flows around the pile to the northwest-bound G_1 location. Flowing underground water may boost the heat transfer rate of the GHE. The ambient air temperature regulates the temperature from the surface up to 4 meters.

The wall temperatures of the GHE tube were measured up to a depth of 20 meters. Temperatures of the inflow and outflow streams are monitored on the inner and outer sides of the outlet tube. The temperature profiles at the end of the test, after 24 hours, are plotted in Figure 4.4. S_1 is showing the location of the thermocouples installed on the outer wall of the pile, S_2 and S_3 are the location of the thermocouples installed along the pile length on the outer and inner walls of the outlet pipe, respectively.

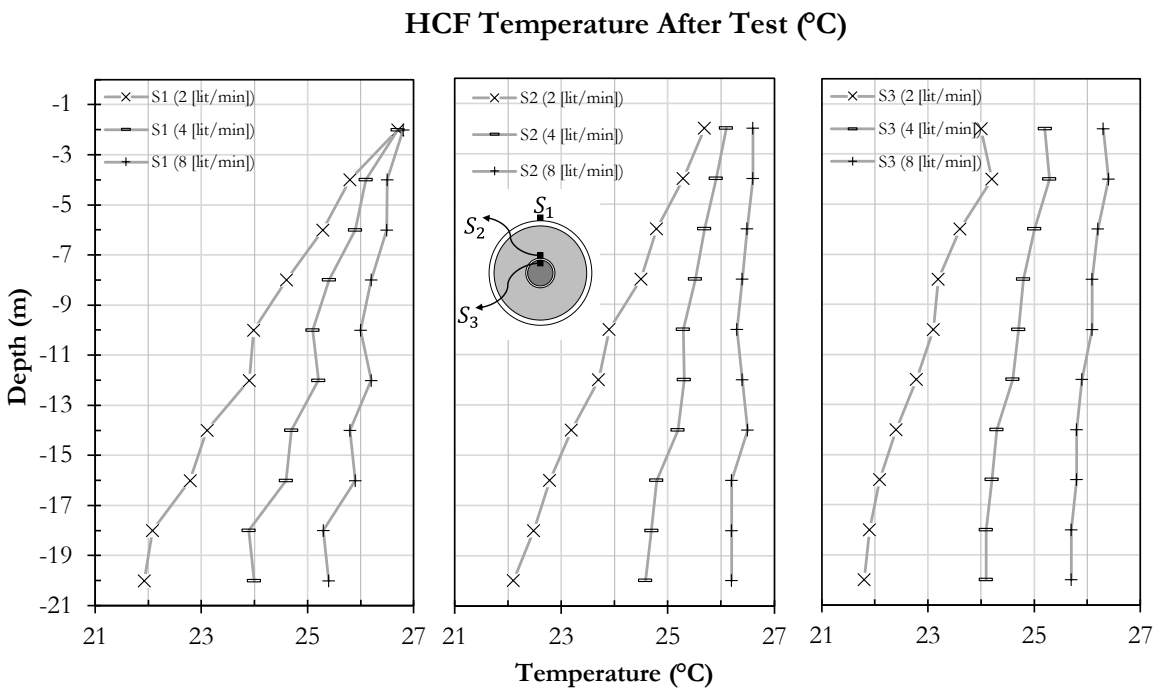

Figure 4.4: Temperature measured on the walls of the pile at the end of the test (reproduced from [2])

The experiment was conducted continuously for 24 hours. In Table 4.2, the experimental conditions are presented. In the GHEs, water circulated, and the input temperature was maintained at 27 [°C].

Table 4.2: Experimental conditions

Date	Flow rate [lit/min]	Average of the ambient air temperature [℃]
05/10/2008	2	20.3
29/09/2008	4	19.5
20/10/2008	8	14.1

The stated Reynolds values for the double-tube GHE range from 331 to 1323. Periodically, the temperature distributions of the ground and GHE tube walls by the depth, inlet, and outlet of the circulating water were recorded. In addition, the ambient air temperature was measured regularly, and the average temperature over 24 hours is shown in Table 4.2. Due to the inlet water temperature setting, the influence of daily fluctuations in ambient temperature did not substantially alter the heat exchange rate in this experiment because the test duration is limited, the average daily ambient temperature is considered, and the stable ground temperature is not affected by ambient over one day. While seasonal changes affect the ground near the surface. The accuracy of the temperature measurement was 0.2 [°C].

The soil in the location of the test consists of Ariake clay from the depth of 0 to 15 [m], sand and sandy clay from 15 to 20 [m]. Soil properties in this study were estimated using the values of similar soil types, as shown in Table 4.3.

Table 4.3: Soil properties measured at 293 [K]

			Clay	Sand	Sandy Clay
Parameter	Density, ρ_{soil}	$[kg/m^3]$	1700	1510	1960
	Specific heat, $C_{p_{soil}}$	$[J/kg \cdot K]$	1800	1100	1200
	Conductivity, K_{soil}	$[W/m \cdot K]$	1.2	1.1	2.1
	Thermal diffusivity, α_{soil}	$[mm^2/s]$	0.39	0.68	0.93
	Water Content, w_{soil}	[%]	27.7	7.90	21.6

The inflow and outflow water temperatures of the GHE were monitored for 24 hours of continuous operation. As the flow rate increases, the temperature differential between the inlet and outlet reduces. The inflow and outflow temperatures of circulated water during the test period are shown in Figure 4.5.

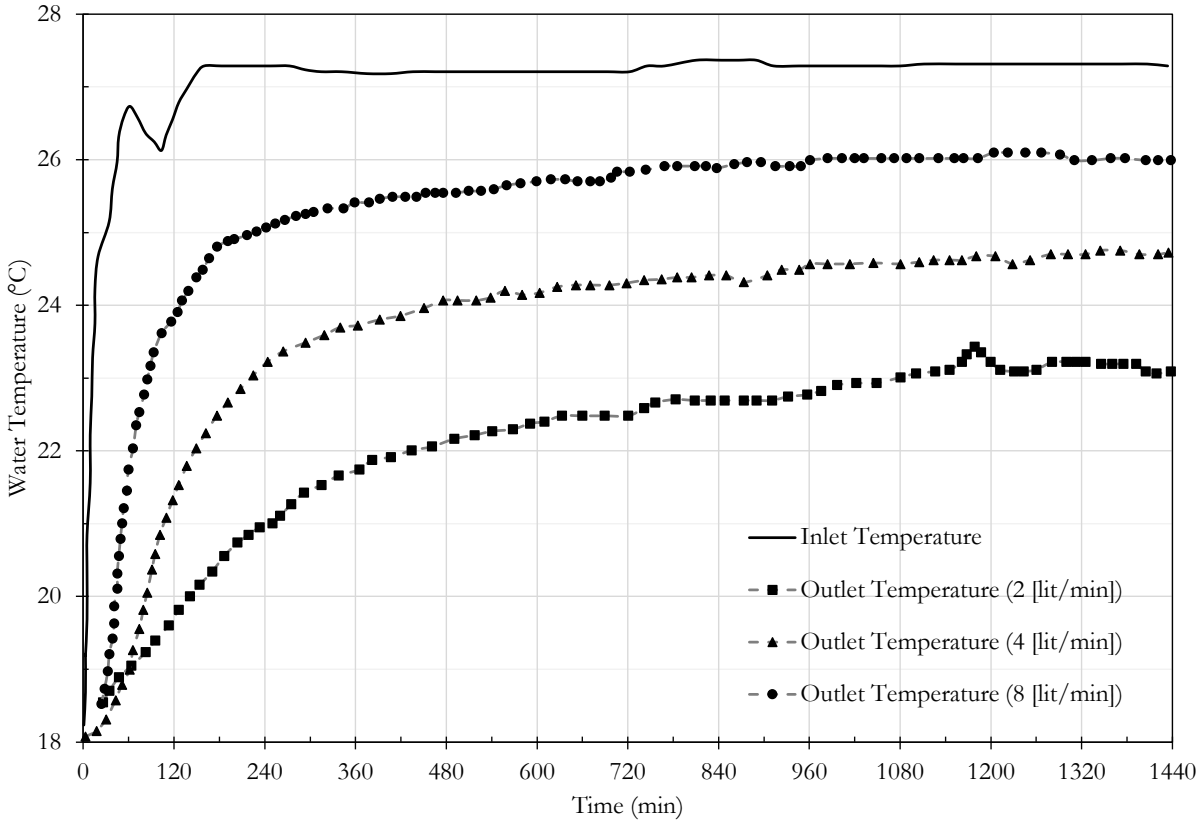

Figure 4.5: Temperature at inlet and outlet continuously measured during the test (reproduced from [2])

4.4 Numerical modeling of the Saga University project

4.4.1 Geometry

To investigate the thermal performance of a steel energy pile filled with water, a 3D numerical model is established using the COMSOL Multiphysics 5.6, and the results are verified using the data from the Saga University project Experiments. The model geometry consists of a cylindrical soil domain, pile and PVC outlet pipe, and water circulating inside the pile.

Table 4.4 reflects the values used in building the model geometry, while the COMSOL Multiphysics enables the user to introduce all variables as parameters that can be modified in any modeling step.

Figure 4.6 illustrates the model that includes a steel pile at the center, surrounded by the cylindrical soil domain with a diameter of 20 meters and a height of 30 meters (equal to the length of the pile plus 10 meters of thermal margin to the bottom boundary). The dimensions are chosen in a way to ensure that the far-field boundary conditions do not have an adverse effect on the simulation results.

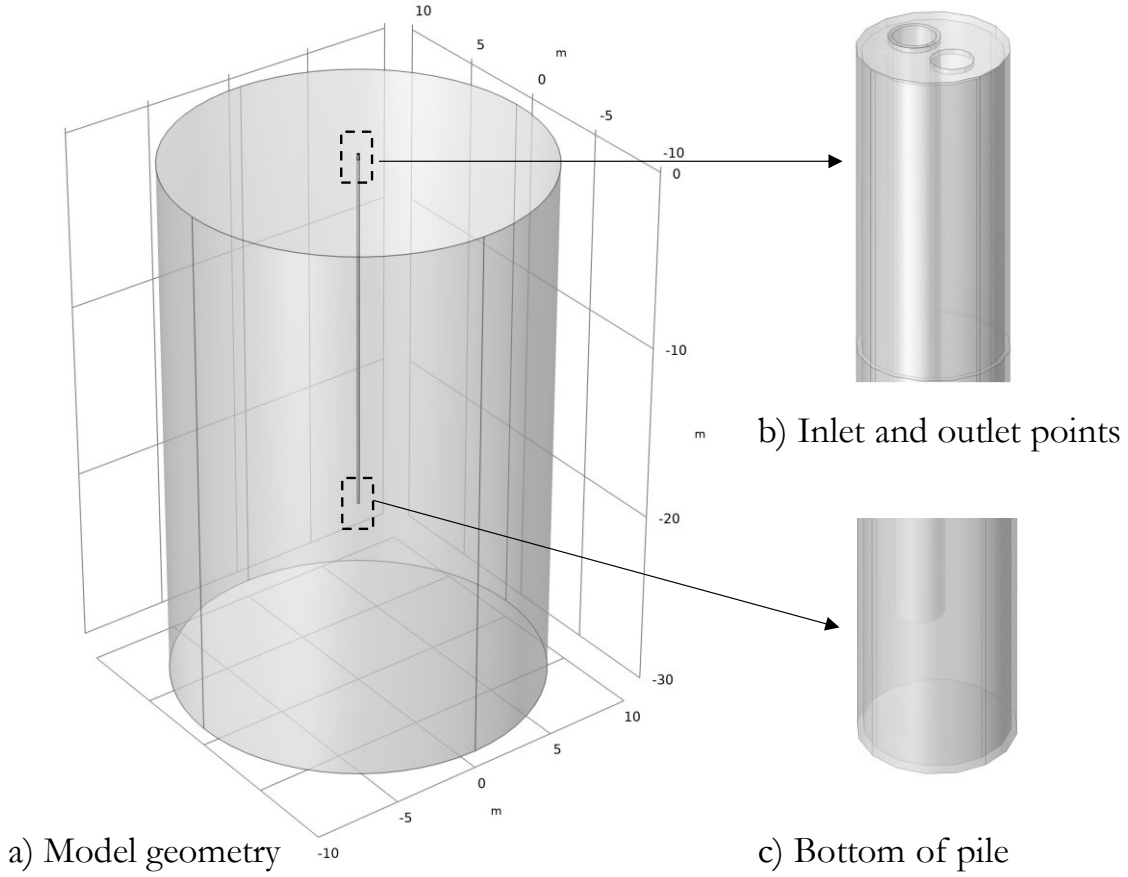

Figure 4.6: 3D FEM model geometry

Table 4.4: 3D FEM model geometry values

Description	Value
Pile length	20 [m]
Soil cylinder diameter	20 [m]
Soil cylinder height	30 [m]
Steel pile outer diameter	0.1398 [m]
Steel pile inner diameter	0.1298 [m]
PVC pipe outer diameter	0.048 [m]
PVC pipe inner diameter	0.040 [m]
Pile extrusion from the ground	0.30 [m]
End distance between PVC pipe inlet and steel pile bottom plug	0.10 [m]
The thickness of the steel pile bottom plug and top cap	0.005 [m]

As shown in Figure 4.6 b, the inlet and outlet points are not positioned similar to the experiment configuration, as shown in Figure 4.1, where the inlet pipe is situated at the side wall of the pile, and the outlet pipe is simply in the center of the pile. Many approaches for creating the model geometry were considered when designing this pile, such as adopting symmetry, placing the entrance on the side wall, or modeling the pile tube using 2D shell elements (Figure 4.7). In some cases, details of the primary geometries did not affect the results but only prevented the simulation from converging. In some cases, the numerical simulation outcomes did not match the experimental results but gradually improved to produce the final geometry.

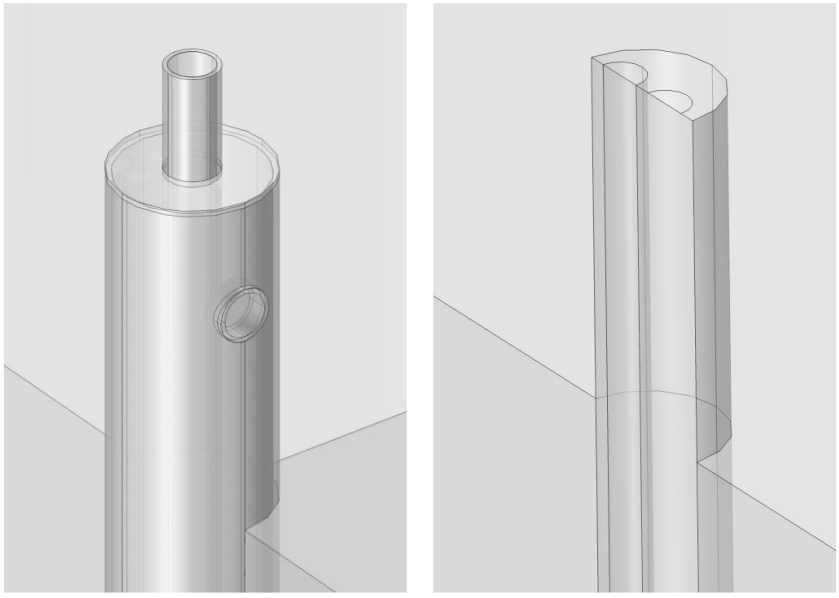

Figure 4.7: Different approaches in building the geometry: Inlet point on the side wall (left), 2D shell with symmetry (right)

4.4.2 Material properties

A Material node is used to represent each material in the COMSOL simulations. Each material has a set of physical characteristics that define it, along with values or functions (for temperature-dependent characteristics, for example).

All the materials used in the simulations are homogenous and isotropic. The materials that make up the ground and energy geostructures contain pores filled with fluid, and the thermophysical properties of the fluid and solid phases are considered according to Equations (3.18) and (3.19).

4.4.2.1 Soil

Table 4.3 shows the soil properties at the test location. The layering of the soil at the site of the test consists of Ariake clay from the depth of 0 to 15 $[\mathrm{m}]$, sand and sandy clay from 15 to 20 $[\mathrm{m}]$. Since the exact boundaries of sand and sandy clay for the depths of 15 to 20 meters and the underground flow regime at the test location were not defined in the experiment results, the soil in the numerical modeling was assumed to be fully saturated clay with the input values presented in Table 4.5.

Table 4.5: Soil characteristics used in numerical modeling

Parameter	Value	Unit	Reference
Density, (ρ_{soil})	1700	$[\mathrm{kg/m^3}]$	
Heat capacity at constant pressure, $\left(C_{p_{soil}}\right)$	1800	$[\mathrm{J/kg \cdot K}]$	[2]
Thermal conductivity, (k_{soil})	1.2	$[\mathrm{W/m \cdot K}]$	
The ratio of specific heats, (γ_{soil})	1	$[-]$	
Porosity, (ε_{soil})	50	$[\%]$	[42]

4.4.2.2 Heat carrier fluid (HCF)

The HCF in this numerical modeling is considered pure water with temperature-dependent properties, as shown in Table 4.6. These parameters are available in the built-in material library of COMSOL Multiphysics.

Table 4.6: Water characteristics used in numerical modeling [43]

Parameter	Unit	Value
Density, (ρ_{water})	$[kg/m^3]$	For $273.15 < T \leq 293.15$: $6.3 \times 10^{-5}T^3 - 6.04 \times 10^{-2}T^2 + 18.9T - 950.7$ For $293.15 < T \leq 373.15$: $1.03 \times 10^{-5}T^3 - 1.34 \times 10^{-2}T^2 + 4.97T + 432.26$
Heat capacity at constant pressure, $\left(C_{p_{water}}\right)$	$[J/kg \cdot K]$	For $273.15 < T < 553.75$: $12010.1 - 80.4T + 0.3T^2 - 5.4 \times 10^{-4}T^3 + 3.6 \times 10^{-7}T^4$
Thermal conductivity, (k_{water})	$[W/m \cdot K]$	For $273.15 < T < 553.75$: $-0.87 + 8.9 \times 10^{-3}T - 1.6 \times 10^{-5}T^2 + 7.97 \times 10^{-9}T^3$
Dynamic viscosity, (μ_{water})	$[Pa \cdot s]$	For $273.15 < T < 413.15$: $1.4 - 0.02T + 1.4 \times 10^{-4}T^2 - 4.6 \times 10^{-7}T^3 + 8.9 \times 10^{4}T^4 - 9.1 \times 10^{-13}T^5 + 3.8 \times 10^{-16}T^6$
The ratio of specific heats, (γ_{water})	$[-]$	$1 + \left(\frac{T}{C_{p_{water}(T)}}\right) \times \left(\alpha_{P_{water}}(T) \times c_{s_{water}}(T)\right)^2$
Coefficient of thermal expansion, $(\alpha_{P_{water}})$	$[1/K]$	$-\left(\frac{1}{\rho_{water}(T)}\right) \times \left(\frac{d\rho_{water}(T)}{dT}\right)$
Speed of sound, $(c_{s_{water}})$	$[m/s]$	From Figure 4.8

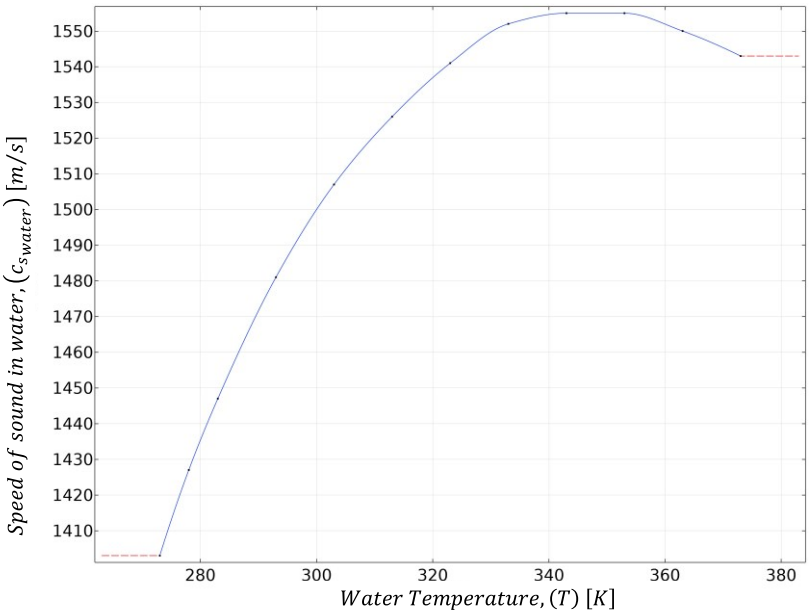

Figure 4.8: Sound speed inside water [43]

4.4.2.3 Steel

Stainless steel SUS304, often known as the Japanese designation for SS304 or AISI 304 in American references, comprises the pile body material. SUS304 offers outstanding warm workability for bending and stamping, good heat and corrosion resistance, low-temperature strength, processability, and mechanical qualities [44]. Table 4.7 illustrates the thermal properties of SUS304 used in numerical modeling.

Table 4.7: Table 4.8: Stainless steel characteristics used in numerical modeling

Parameter	Value	Unit	Reference
Density, (ρ_{steel})	7950	$[kg/m^3]$	[44]
Heat capacity at constant pressure, $\left(C_{p_{steel}}\right)$	510	$[J/kg \cdot K]$	
Thermal conductivity, (k_{steel})	13.8	$[W/m \cdot K]$	[2]
The ratio of specific heats, (γ_{steel})	1	$[-]$	

4.4.2.4 Polyvinyl chloride (PVC)

Polyvinyl chloride (PVC) pipe has been used as the outflow path and material property according to Table 4.9, adopted for the numerical modeling.

Table 4.9: PVC characteristics used in numerical modeling

Parameter	Value	Unit	Reference
Density, (ρ_{PVC})	1760	$[kg/m^3]$	[45]
Heat capacity at constant pressure, $\left(C_{p_{PVC}}\right)$	921	$[J/kg \cdot K]$	
Thermal conductivity, (k_{PVC})	0.15	$[W/m \cdot K]$	[2]
The ratio of specific heats, (γ_{PVC})	1	$[-]$	

4.5 Physics and boundary conditions of the model

The nature of the physics which must be dealt with in solving the thermal performance of coaxial steel pile can be divided into two main parts. The **time-dependent** heat transfer problem in the volumetric domains, the **transient** fluid flow, and forced convection problems along the pile axis. Pure conductive heat transport is predicted in the solid part such as steel pile and PVC pipe domains; heat conduction and convection in the porous media such as surrounding soil and the fluid flow and heat transfer problem regarding the HCF domain.

4.5.1 Heat transfer in porous media

To simulate heat transport through conduction, convection, (and radiation) in porous media, COMSOL Multiphysics provided the heat transfer in porous media interface, which may be found under the Heat Transfer module.

On all domains, a porous medium model is automatically active. There is also the full capability to add more domain types, such as solid domains under the same heat transfer in porous media module. The convection-diffusion equation, with thermodynamic properties averaging models to consider solid matrix and fluid characteristics, corresponds to the temperature equation described in porous media domains. When the temperatures within the porous matrix and the fluid are in balance, this equation stands true.

The heat transfer phenomena in the coaxial steel energy pile combine heat transfer in the soil as the heat transfer in porous medium, heat transfer in the pile and pipe as the heat transfer in solid media, and the HCF as the heat transfer in fluid phase (Figure 4.9).

Figure 4.9: Heat transfer interface and boundary conditions used in the present study in COMSOL

4.5.1.1 Boundary conditions

One of the essential boundary conditions is the inflow temperature. Therefore, an upstream temperature profile, similar to the experimental temperature profile, has been introduced to the model using the built-in interpolation function and the discrete values of several points taken from the original data set (the inlet temperature line in Figure 4.5).

A nonlocal integration coupling over the boundary surface must be defined to evaluate the outflow temperature at the outlet point of the PVC pipe. The integration operator ($\mathrm{intop1(T)}$) must be divided over the boundary surface area using the ($\mathrm{intop1(1)}$) operator. To monitor, save, and later visualize the temperature development during the simulation, a global variable probe should be defined to store the real-time values obtained from the integration operator.

To estimate temperature variations in each node, boundary conditions are employed to specify the behavior of the numerical model during runtime.

In heat transfer applications, boundary conditions can be classified into three categories [2]:

- The prescribed temperature at a point or along a boundary surface (Dirichlet, essential)
- Prescribed heat flux at a point or along a boundary surface (Neumann, natural)
- A linear combination of prescribed temperature and heat flux at a point or along a boundary surface (Cauchy, mixed)

Equation (4.1) shows Newton's law of cooling, a well-known Cauchy or mixed thermal boundary condition.

$$q = h(T_{ext} - T) \quad (4.1)$$

Where:

q: boundary convective heat flux $[W/m^2]$

h: convection heat transfer coefficient $[W/m^2 \cdot K]$

T_{ext}: external temperature $[W/m^2]$

T: temperature of the domain at the outer interface $[W/m^2]$

The lateral and bottom of the model can be assumed to have prescribed temperature (Dirichlet) conditions. The Dirichlet condition should be applied only when the initial temperature profile of the ground is prescribed [46].

The top boundary of the model can have one of the following conditions:

- Fixed temperature (Dirichlet, essential) ($T = T_{air}$)
- Insulated (Neumann, natural) ($T = T_{ext} \rightarrow q = 0$)
- Heat flux (Cauchy, mixed)

In general, keeping the ground surface temperature constant will cause artificial effects on the energy pile performance. The best two options are either insulated or Cauchy. If the energy pile is supposed to be utilized under a building structure, the top boundary condition can be assumed as "Insulated".

The "heat flux" boundary conditions can be assumed either by assuming fixed heat flux value ($q = q_0$) or variable value depending on soil surface temperature (T) at each stage of simulation by defining the convection heat transfer coefficient (h). The convection heat transfer depends on the fluid (air) thermophysical properties and fluid velocity (air velocity at the ground surface). Therefore it can be broken into two components [6]:

$$h = h_n + h_f \quad (4.2)$$

Where:

h_n: natural convection coefficient portion $[W/m^2 \cdot K]$

h_f: forced convection coefficient portion $[W/m^2 \cdot K]$

There are several equations for determining the natural convection coefficient (h_n) based on airflow across surfaces (Table 4.10).

Table 4.10: Natural convection coefficient estimations

h_n $[W/m^2 \cdot K]$	Reference
1 to 3	[47]
2 to 4	[48]
2.5	[49]

For calculating the forced convection coefficient (h_f) with airflow across the surfaces, many expressions are also available [2], [6], [50]. However, for airflow velocity of less than 5 (m/s) a linear relationship between the average airflow velocity and the forced convection coefficient is sufficient (Figure 4.10) [6].

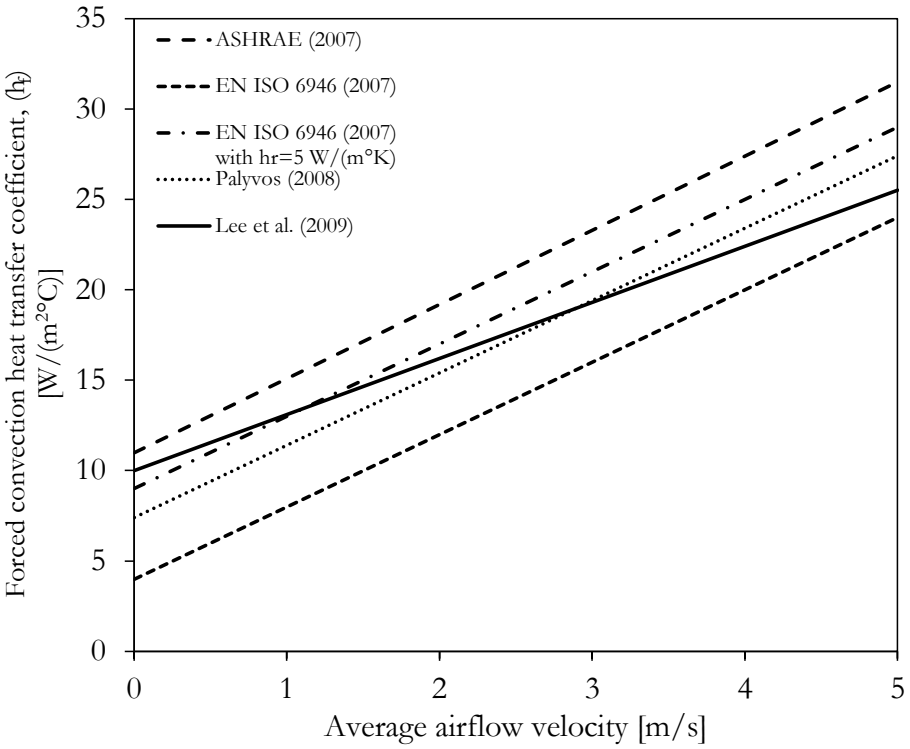

Figure 4.10: Comparison of correlations for forced convective heat transfer coefficient (Reproduced from [50]**)**

According to Table 4.10 and Figure 4.10, the value of the convective heat transfer coefficient is expected to be in the range of 5 to 16 $[W/m^2 \cdot K]$**.**Since no information is available regarding the average airflow velocity during the Saga university experiment, other methods should be used to evaluate the convective heat transfer coefficient (h). Table 4.11 shows some empirical correlations derived from greenhouse trials. Different coefficients of free convection and turbulent flow equations are used to fit these models.

Table 4.11: Empirical equations for convective heat transfer between the soil surface and air [51]

$h\ [W/m\hat{}2 \cdot K]$	Conditions
$3.40\Delta T^{0.33}$	Screened greenhouse
$10.0\Delta T^{0.33}$	Bare soil
$1.86\Delta T^{0.33}$	Large-scale greenhouse
$5.20\Delta T^{0.33}$	Heated floor surface

Table 4.12 shows the convective heat coefficient derived from the "Bare soil" equation for the numerical simulation.

Table 4.12: Convective heat transfer coefficients and external temperatures applied in the simulation

Flow rate (lit/min)	Date	$T_{air}\ [°C]$	$h = 10.0\Delta T^{0.33}\ [W/m^2 \cdot K]$
2	05/10/2008	20.3	13.16
4	29/09/2008	19.5	11.43
8	20/10/2008	14.1	15.67

At the top surface boundary, the extrusion of the pile is in contact with the ambient air and has a heat flux between steel and air; some literature suggested a value of 25.32 $[W/m^2 \cdot K]$ as the convective heat transfer coefficient between steel and air [52], the same value was used in the present study.

4.5.1.2 Continuity

While creating a geometry by assembling different parts, where there is a need to connect parts at the interfaces (soil-pile, pipe-water, and pile-water), a pairing option is available in the COMSOL Multiphysics. By default, pairs are created automatically when forming an assembly at the final stage. There are two types of pairs: (a) identity pairs and (b) contact pairs.

Identity pairs connect overlapping boundaries in different connecting parts of an assembly to specify two selections of boundaries that overlap but belong to different parts of an assembly.

Then assign a boundary condition to connect the physics nodes in the two parts in a physics interface. To ensure a continuous transfer of heat among different parts of the model, a boundary condition called "continuity" must be assigned on contacting surfaces of different assembly parts. Continuity prescribes that the temperature field is continuous across the identity pairs, where the boundaries match.

4.5.2 Fluid flow

Fluid flow or mass transfer inside the pile and outlet pipe is the movement of generic particles due to different hydraulic heads.

The flow condition (laminar or turbulent) is crucial to convection mass transport phenomena. Laminar flow and turbulent flow are the two primary regimes of convection mass transfer. Laminar flow is a type of mass transfer when the effective pathways of the average fluid motion and the pathways of the individual particles match. The pathways of the individual particles that make up the fluid in motion are random in turbulent flow and therefore do not match the effective pathways of the average fluid motion [6].

Reynolds number is often used to distinguish between laminar and turbulent flows. For fluid flow in a pipe or a tube, the Reynolds number is as presented in Equation (4.3).

$$\mathrm{Re} = \frac{\rho Q D_H}{\mu A} \tag{4.3}$$

Where:

ρ: fluid density $[\mathrm{kg/m^3}]$

Q: volumetric flow rate $[\mathrm{m^3/s}]$

D_H: hydraulic diameter $[\mathrm{m}]$

μ: dynamic viscosity $[\mathrm{m/kg \cdot s}]$

A: pipe area $[\mathrm{m^2}]$

Typically, the following classification is used to distinguish the flow regime inside the pipes:

$$\begin{aligned} &\mathrm{Re} < 2300 \quad \text{laminar} \\ &2300 < \mathrm{Re} < 4000 \quad \text{transient} \\ &\mathrm{Re} > 4000 \quad \text{turbulent} \end{aligned} \tag{4.4}$$

Table 4.13 shows the Reynolds number for the coaxial energy pile of the study. The flow condition for the three tested flow rates can be assumed as laminar.

Table 4.13: Reynolds number calculated from different scenarios

Flow rate [lit/min]	Calculated from the annular area	As suggested in the experiment	calculated from the steel pile
2	281	331	381
4	562	662	761
8	1124	1323	1522

The Laminar Flow interface in COMSOL Multiphysics (Figure 4.11) is used to calculate the velocity and pressure fields for the flow of a single-phase fluid in the laminar flow regime. The laminar flow interface accommodates incompressible flow, weakly compressible flow (temperature affects density but not pressure), and compressible flow at low Mach numbers (typically less than 0.3). It also facilitates the movement of non-Newtonian fluids. The Navier–Stokes equations for conservation of momentum and the continuity equation for conservation of mass are solved using the Laminar Flow interface. The Laminar Flow interface is applicable for both stationery and time-dependent analysis. As these flows tend to become fundamentally unstable in the high Reynolds number zone, time-dependent research should be used.

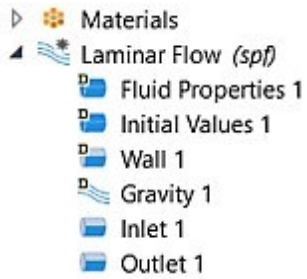

Figure 4.11: Laminar flow interface and boundary conditions used in the present study in COMSOL

4.5.2.1 Boundary conditions

The HCF flowing inside the pile system is considered a Newtonian fluid. In COMSOL, the gravity feature should be activated while dealing with CFD and Heat transfer in fluid modules.

The default boundary condition for solid walls is "No-slip". A non-slip wall is one in which the fluid velocity relative to the wall velocity is zero. Since the walls of the pile and the outlet pipe are fixed, the translation velocity of the walls should be equal to zero.

To obtain a numerically well-posed problem, it is advisable to consider the Outlet conditions as well as the inlet. Conditions at the inlet are defined as "fully developed flow", with the volumetric flow rate equal to 2, 4, and 8 [lit/min].

The outlet pressure may be set if velocity is defined at the inlet. Specifying the velocity vector at both the inlet and outlet may induce convergence errors. Therefore, the outlet boundary condition is equal to 200 [kPa], resembling the pressure tank in standard pumping systems.

4.5.3 Multiphysics

Fluid flows having variable temperatures are referred to as non-isothermal flows. The material characteristics of a fluid, such as density and viscosity, alter in response to a change in temperature. These changes may, in some instances, be significant enough to affect the flow field. Changes in the flow field also impact the temperature field since the fluid carries heat. This mutual connection between fluid flow and heat transfer is standard in heat exchangers like energy piles [53].

Since the HCF in this simulation is considered an incompressible fluid, the "Boussinesq approximation" option must be activated to evaluate the HCF at the reference temperature and reference pressure.

4.6 Results and discussions

To investigate the thermal performance of a pile similar to the experimental study of the coaxial pile at Saga University, a 3D numerical model using the COMSOL Multiphysics 5.6 has been established. In that experimental investigation, water was injected inside the coaxial pile with volumetric flow rates equal to 2, 4, and 8 [lit/min] for 24 hours. In the numerical simulation using COMSOL Multiphysics 5.6, the same scenarios with a similar inflow temperature have been adopted, and the outflow temperatures have been monitored. Figure 4.12 demonstrates the experimental and numerical simulation results.

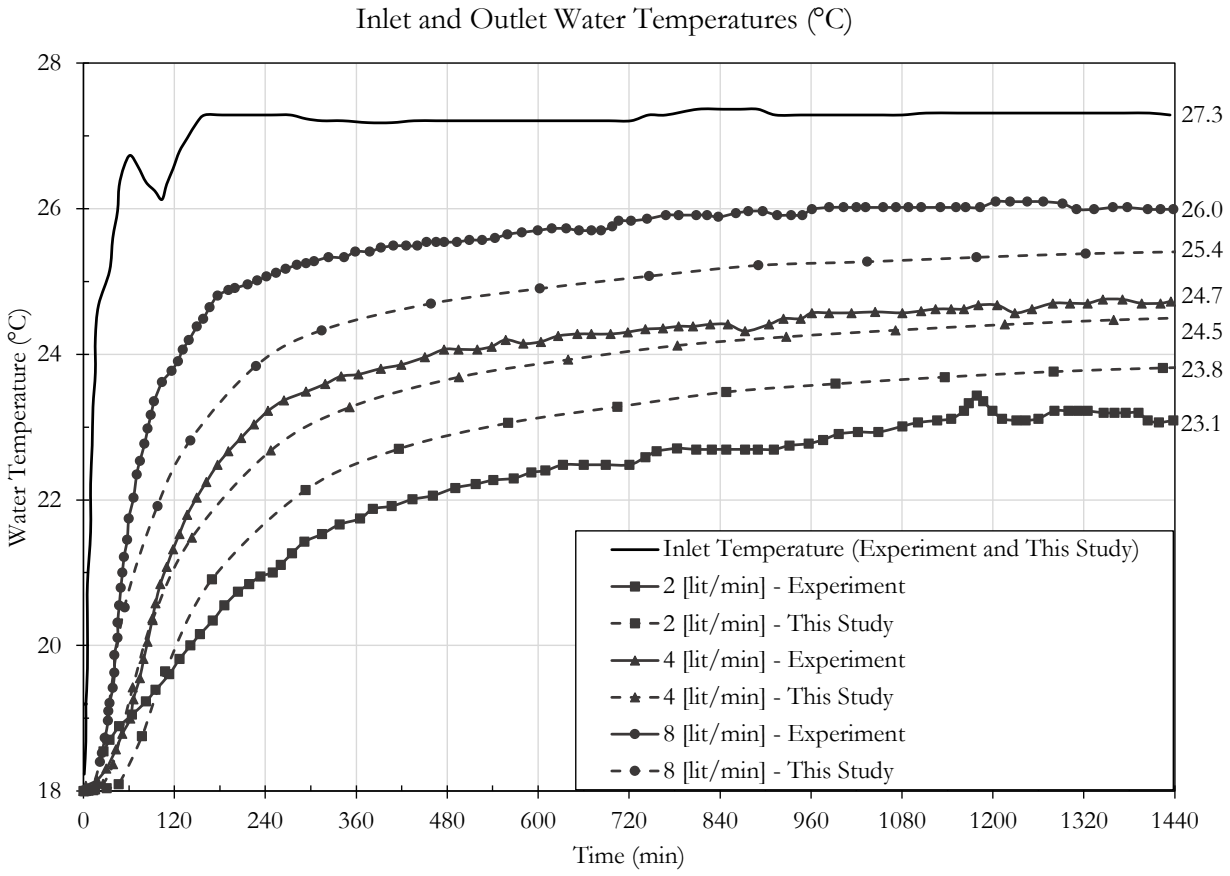

Figure 4.12: Inlet and outlet temperatures

At the inlet point, water was injected with an almost constant temperature of 27 [°C]. Table 4.14 shows the final temperatures of the experimental tests and numerical simulation.

Table 4.14: Comparison between the experimental results and numerical simulation

Inflow rate	Outflow temperature [℃]		Difference	
[□lit/min]	Experiment	Numerical	[℃]	[%]
2	23.1	23.8	-0.7	-3.03
4	24.7	24.5	+0.2	+0.81
8	26.0	25.4	+0.6	+2.31

As shown in Figure 4-12, the numerical simulation results show a good agreement with the observed results of the Saga university experiments.

Table 4.14 reveals that the difference between the outcome of the numerical simulation matches the data from the site investigation with accuracy enough to expand the application of the same numerical model to future studies for similar piles.

Figure 4.13 shows the HCF velocity profile on a longitudinal cross-section of the pile while the volumetric flow rate was equal to 2 [lit/min]. As was expected, the velocity at the inlet is partly disturbed. It reaches a smooth flow after less than a meter inside the pile. However, the depth through which the velocity field of the HCF looks like a jet depends on the inlet velocity. The velocity of the HCF on the walls of the pile and the outlet pipe is zero, as its condition in the simulation has been defined as the "No-slip" flow over the solid walls. Outflow velocity is higher than inflow due to the outlet PVC pipe's smaller dimension than the inlet steel pile. Figure 4.14 shows the velocity streamlines of the HCF inside the pile at the inlet and at the bottom part of the pile, where the fluid enters the outlet PVC pipe.

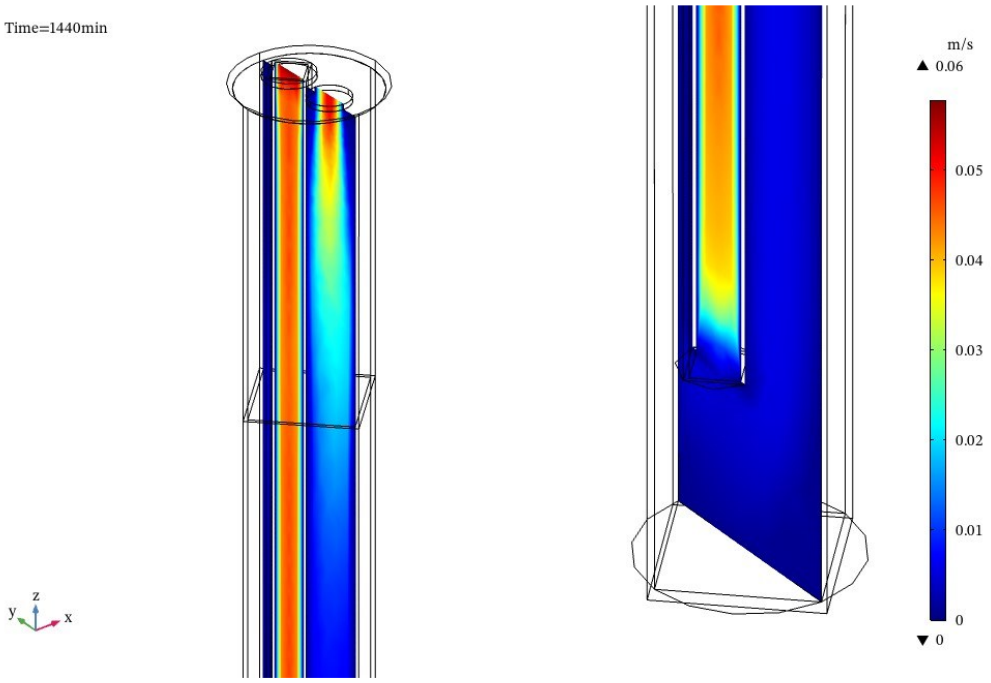

Figure 4.13: cross-section of the HCF velocity at the entrance (left) and bottom of the pile (right)

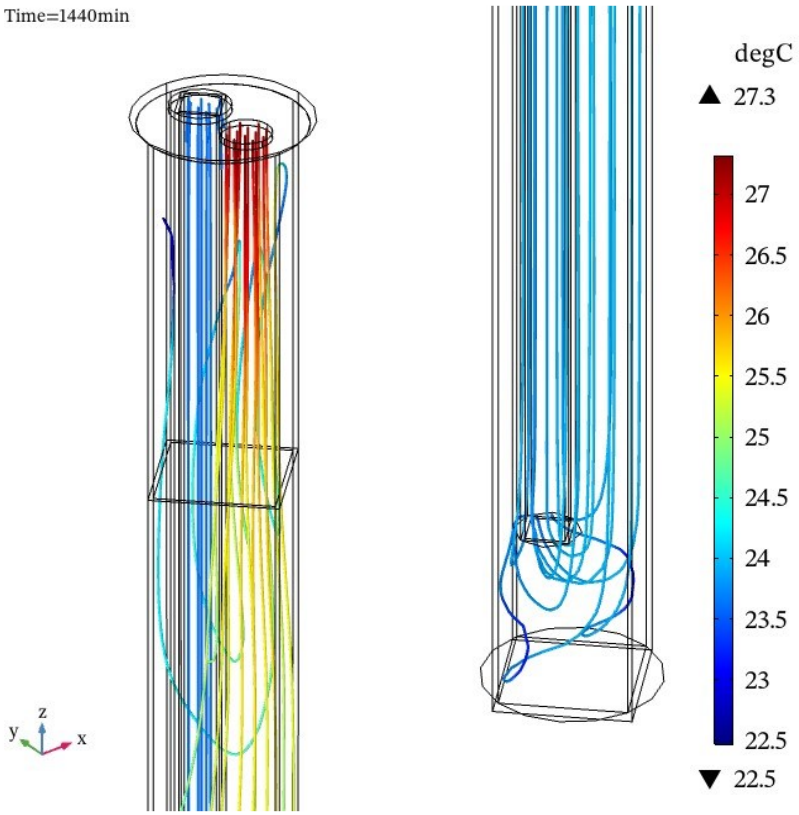

Figure 4.14: Velocity streamlines at the entrance (left) and the bottom of the pile (right)

Figure 4.15 shows the isothermal heat contours in the ground and the pile after 24 hours. This diagram shows the heat distribution pattern in the model.

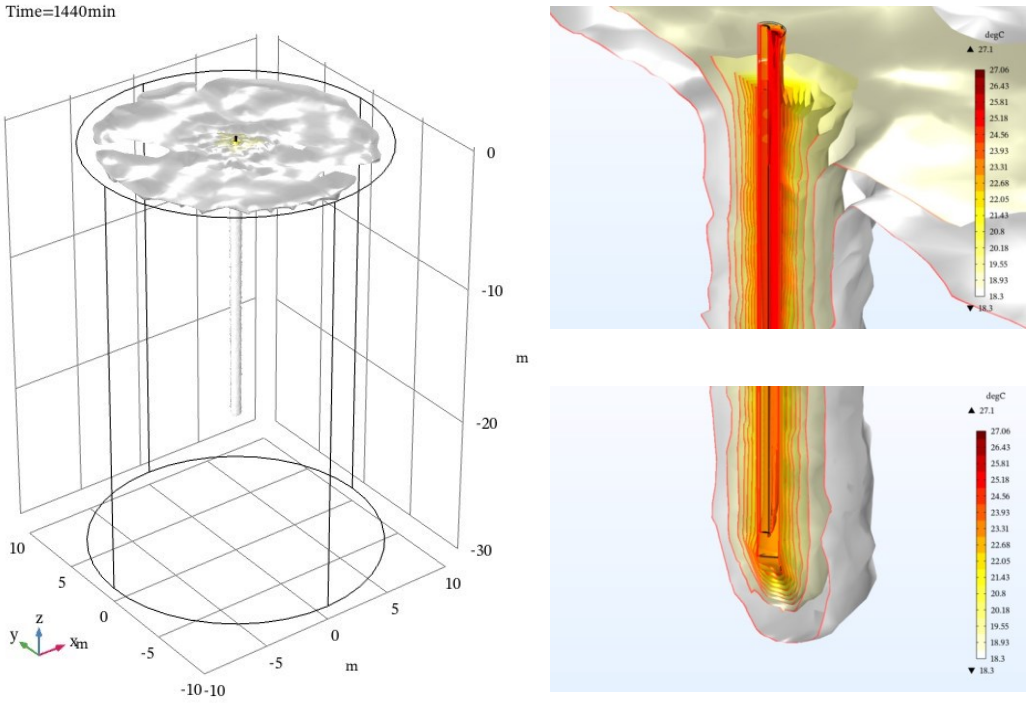

Figure 4.15: Isothermal contours after 24 hours in the model (left), at the ground surface (right upper), and bottom of the pile (right lower)

Figure 4.16 shows the isothermal heat contours, which explain the thermal flows in the model from the start to the end at different time steps.

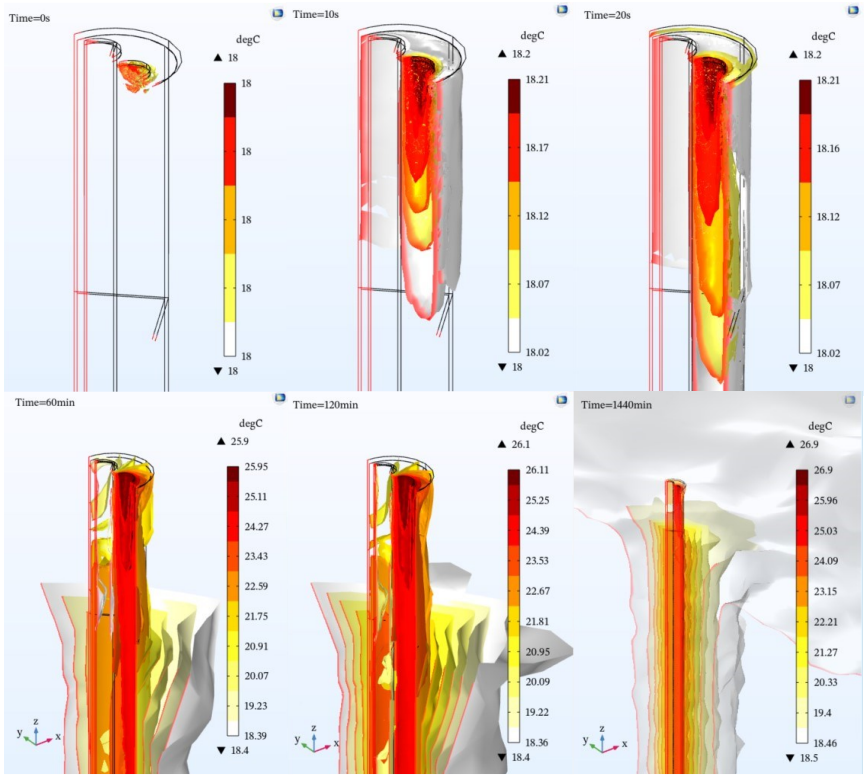

Figure 4.16: Isothermal contours in the model in different time steps from the beginning to the end of the simulation

Figure 4.17 shows the temperature distribution at the ground surface and a depth of 20 meters at the last stage of the test. Due to the 24 hours of pile performance, the thermally affected zone has a radial distance smaller than 0.3 m. This distance relies on the soil, pile, fluid material properties, temperature difference between the inlet and outlet, and inlet velocity.

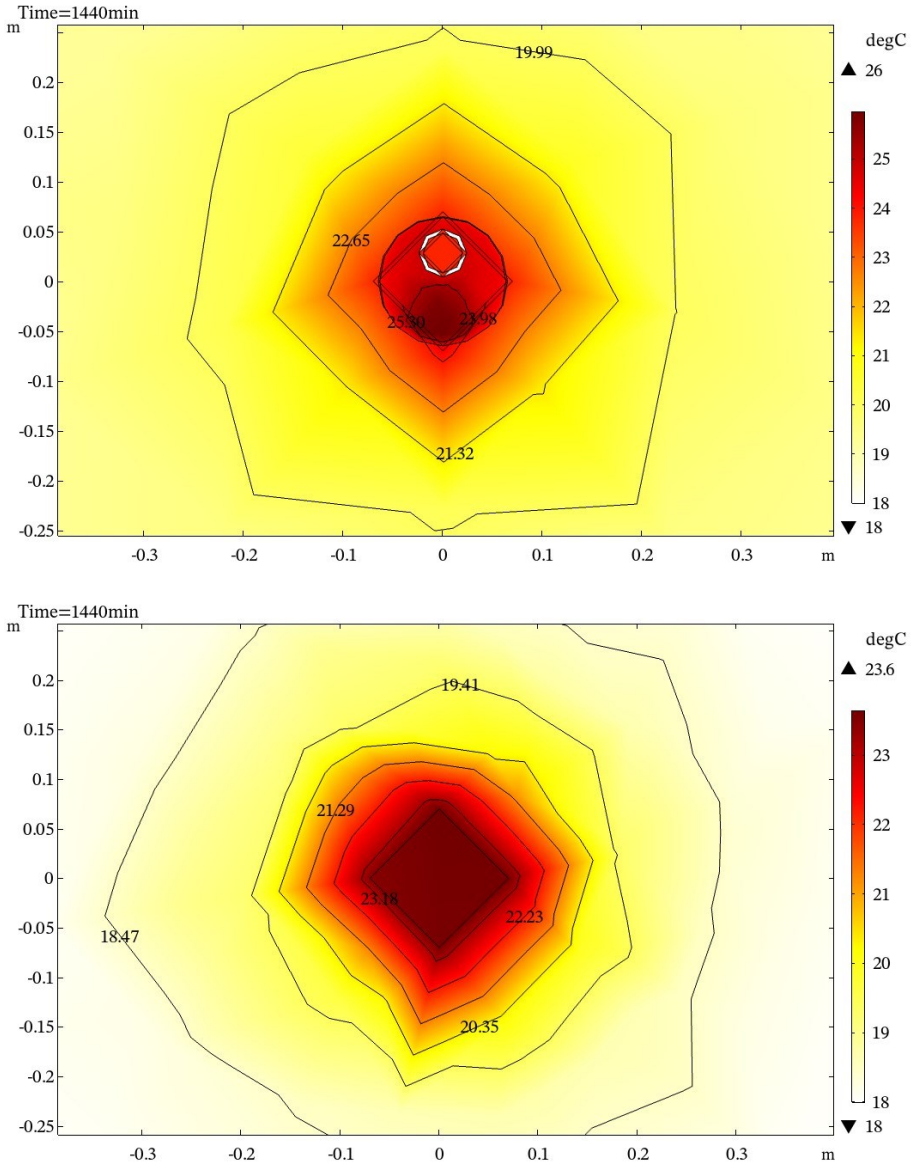

Figure 4.17: Temperature distribution at Ground surface (upper) and a depth of 20 meters (lower) after 24 hours

To evaluate the heat exchange rate of the coaxial energy pile per meter of the pile, the inlet and outlet temperatures of the HCF were monitored at different flow rates. The heat exchange rate can be calculated from Equation (5.1).

$$\overline{Q} = \frac{\dot{m} c_p \Delta T}{L} \qquad (4.5)$$

Where:

$\bar{Q}$: heat exchange rate per meter of the pile [W/m]

$\dot{m}$: gravimetric flow rate [kg/s]

c_p: specific heat of water [J/kg · ℃]

ΔT: the temperature difference between inlet and outlet of HCF [℃]

L: the pile length [m]

The heat exchange rate per meter of the pile for 24 hours of operation in the Saga experiment and the present numerical simulation are compared in Figure 4.18 to Figure 4.20. After certain hours of operation, the heat exchange from the circulation HCF to the soil raises the ground temperature around the pile, and then the heat exchange rate decreases gradually and remains stable.

It should be noted that the temperature difference between the inlet and the outlet is relatively high due to the considerable amount of water stored in this type of energy pile, which is in thermal equilibrium with the surrounding soil. This means that a considerable amount of heat is required to increase the temperature of the water inside the pile due to the specific heat capacity of the water. This is an important finding because it shows that such piles can be used as thermal storage tanks under buildings.

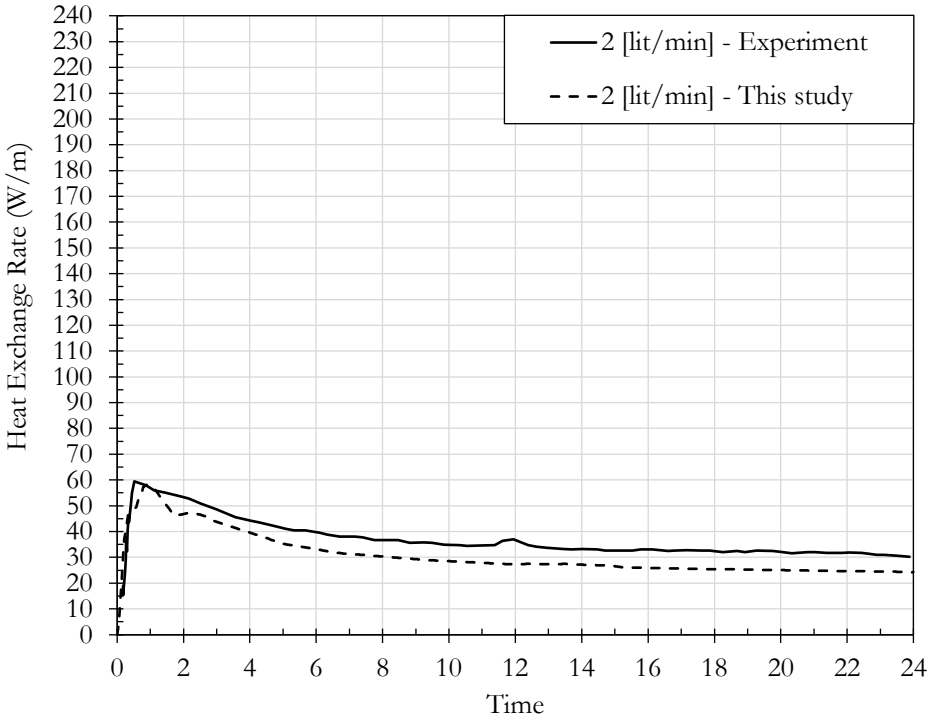

Figure 4.18: comparison of the heat exchange rate (2 [lit/min])

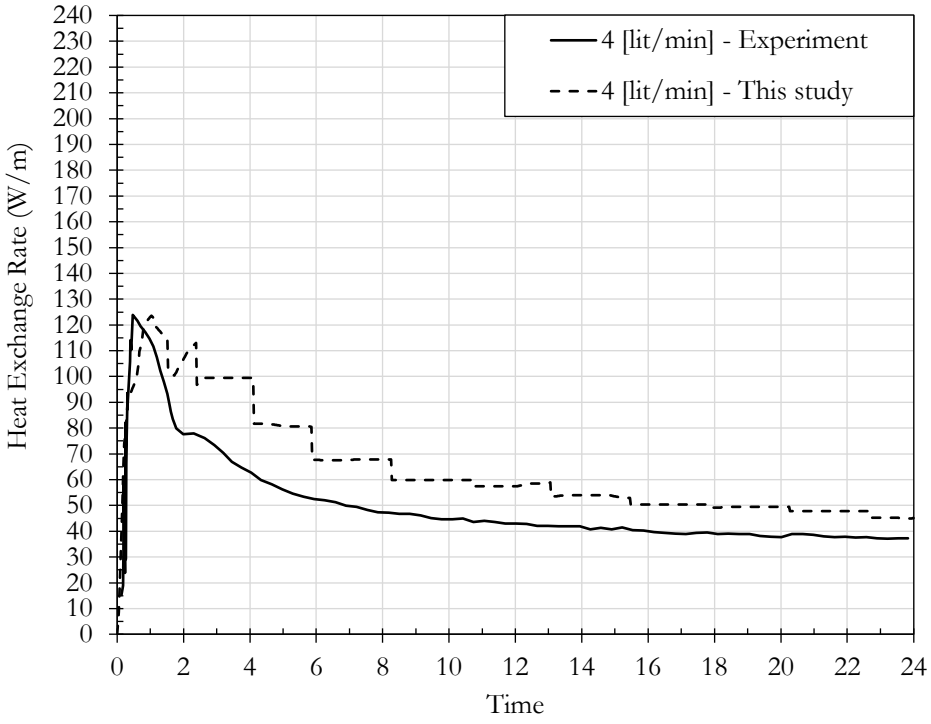

Figure 4.19: comparison of the heat exchange rate (4 [lit/min])

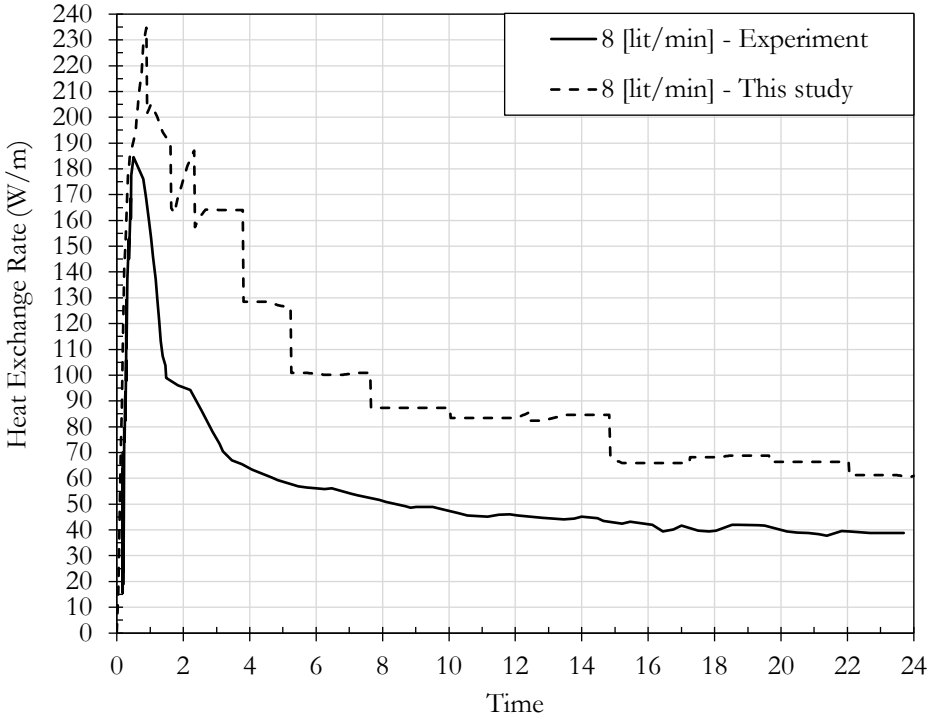

Figure 4.20: comparison of the heat exchange rate (8 [lit/min])

4.7 Lessons learned during the numerical simulation

Numerical simulation of the Saga university experiment, which investigated coaxial annular steel energy pile, comes with several challenges that made us change the modeling strategies several times and struggle with the simulation at the initial phases of the present study. However, the final structure of the model is due to successfully overcoming these challenges. The novelty of this study is the numerical simulation of the fluid flow and heat transfer in the solid and liquid parts of the model. Most research has focused on solid energy structures with HCF passing through plastic pipes. However, in the present study, the energy pile is filled with water and may act as thermal storage.

Additionally, in the previous numerical simulations, the COMSOL "pipe flow module" made it easier for users to analyze such heat exchangers. In comparison, the regulating physics and boundary conditions of the coaxial steel pile have previously been given less thought and consideration. This is the main novelty of the present numerical simulation.

4.7.1 Fluid flow caused instabilities

Having initial conditions inconsistent with the loads and boundary conditions is a typical error, which stops the numerical simulation when building time-dependent simulations, usually with fluid flow modeling.

For example, in this energy pile case, at the inlet, the velocity of the fluid is introduced, and at the outlet, the pressure has been defined as boundary conditions, while the initial values inside the pile are left to their default values, i.e., zero velocity and pressure. This inconsistency between initial values at the inlet and other elements inside the pile in time-dependent solves leads to non-convergence errors. There are two intelligent methods to overcome this error. First, initializing the time-dependent study with a stationary study; second, ramping up the initial conditions over time. However, the first approach is proven effective in almost any similar CFD simulation.

The former solution corresponds to the actual test conditions better than the later one. In the first solution, the test is simulated as the HCF water pump starts circulating the fluid inside the system, and after reaching a steady state, the heat is introduced to the system. While in the second solution, heated fluid is introduced to the system, and the velocity of the liquid is increased from zero to the final value over time, which does not represent the actual conditions of the test.

4.7.2 Heat transfer modules

As pointed out before, the nature of the physics which has to be dealt with in solving the thermal performance of coaxial steel pile is pure conductive heat transport in the solid part such as steel pile and PVC pipe domains; heat conduction and convection in the porous media such as surrounding soil; and the fluid flow and heat transfer problem regarding the HCF domain.

Even though in COMSOL Multiphysics, independent heat transfer modules are available for investigating these heat transfer phenomena separately, it is impossible to combine all these heat transfer modules in one complex system.

To solve this problem, the COMSOL has provided another possibility to assign all the model parts in the heat and mass transfer in the porous media module and define each part separately as the solid or the fluid parts.

4.7.3 Stabilization

When numerically solving transport phenomena driven by convection-dominated transport problems, such as the numerical simulation of the coaxial pile, where the fluid flow is supposed to be considered, the approach can lead to numerical instabilities or oscillation in the results. These instabilities are mainly due to the convective velocity vector, the diffusion coefficient, and the mesh size. The consistent stabilization option in COMSOL efficiently solves the problem with less computational effort and time, which is active in flow-related physics by default. Figure 4.21 shows the numerical simulation results with normal-sized and finer-sized mesh.

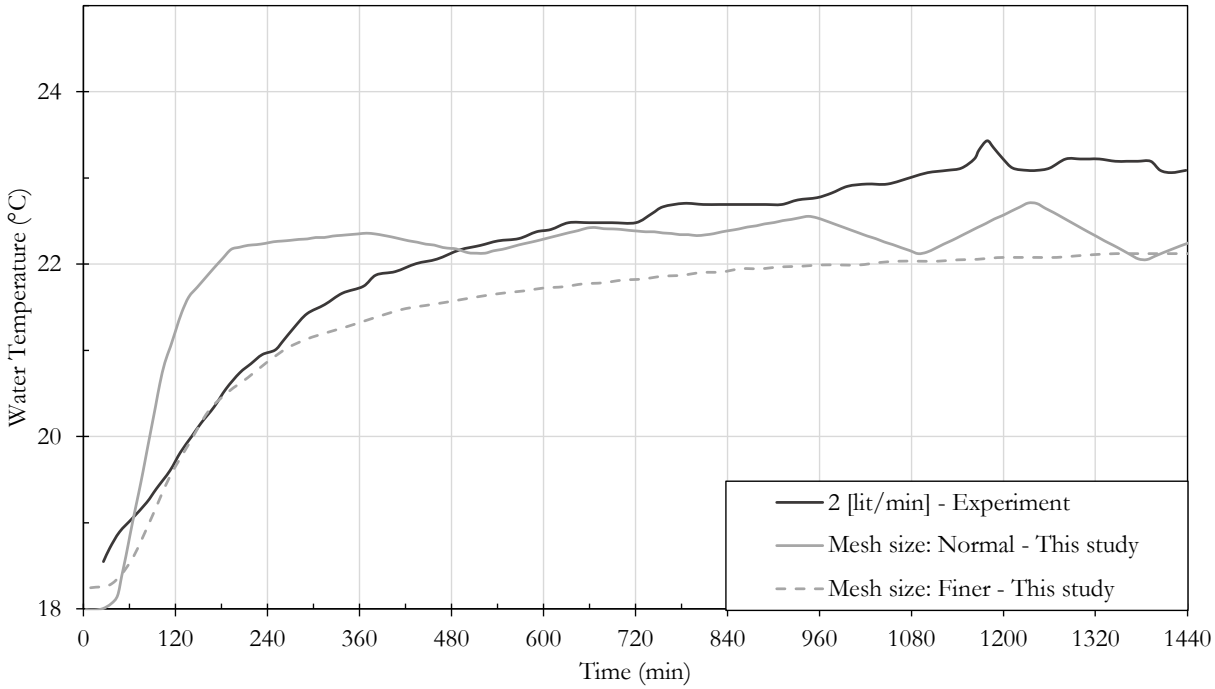

Figure 4.21: Effect of mesh size on the stability of results

4.7.4 HCF temperature-dependent characteristics

As mentioned, the HCF in this numerical modeling is considered pure water with temperature-dependent properties. Since thermal and physical properties of water change slightly with the temperature, ignoring these slight variations will considerably affect the results. Figure 4.22 shows numerical simulation results of the coaxial energy pile with a flow rate of 2 [lit/min]. In one study, the physical and thermal characteristics of the inflow water are considered constant (temperature independent) for the inflow temperature equal to the properties at 27 [℃]. In the other study, these properties were assumed to be temperature-dependent during the test period (the fluid temperature varies between 18 and 27 [℃]).

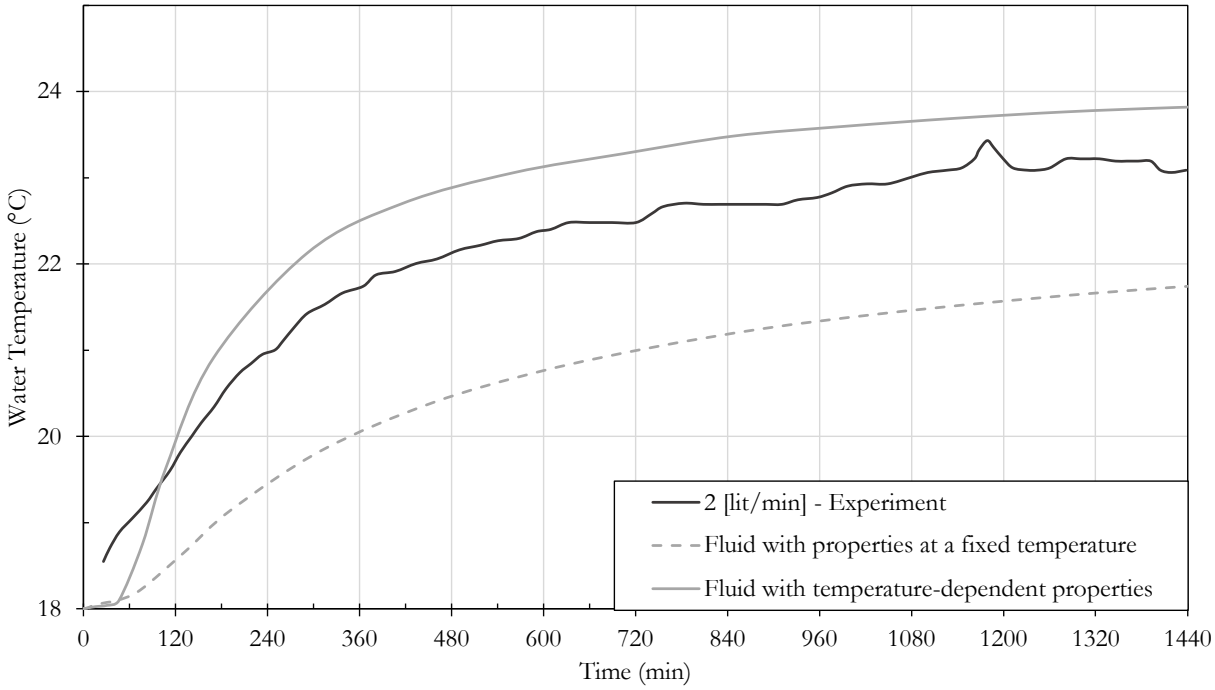

Figure 4.22: Temperature dependency of the fluid and its effect on the results

5 Thermal analysis of the BEAR project

5.1 Introduction

The Norwegian Geotechnical Institute (NGI) is the project leader of the BEAR project (Bærekraftig Energi fra løsmAsseR, or Sustainable energy from loose material). This project is part of a larger construction project owned by Malvik municipality. The primary goal of the BEAR project is to design solutions for harvesting energy from surface soil layers as a sustainable and reliable energy source utilizing steel energy piles. The aerial image of the project location is shown in Figure 5.1.

Figure 5.1: Aerial photo of the BEAR project location [54]

In December 2021, two steel hollow cylindrical piles were installed in the field. Piles configurations are shown in Figure 5.2, and the characteristics are listed in Table 5.1.

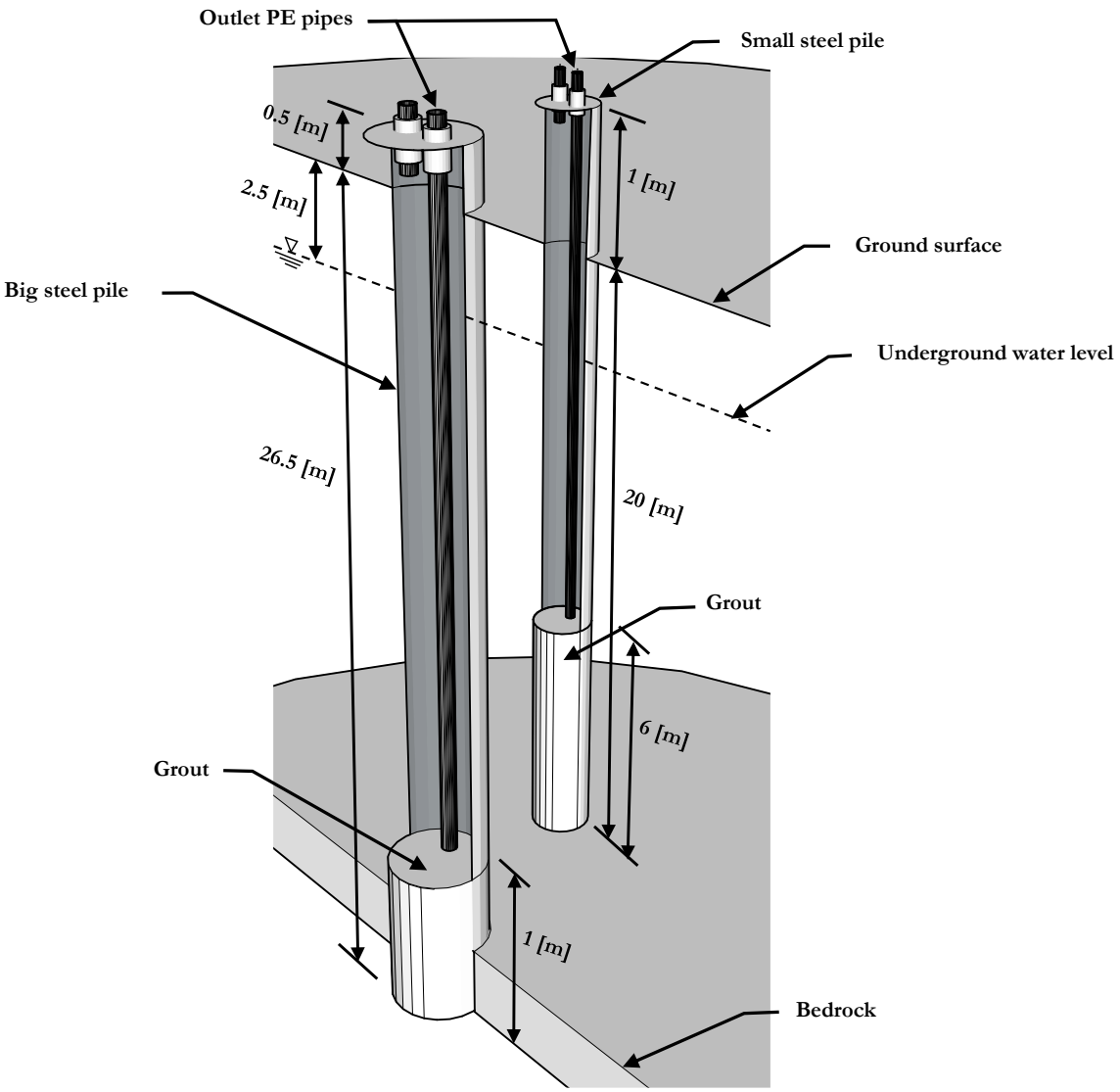

Figure 5.2: Configuration of the steel piles in the BEAR project

The big pile is an end-bearing type with an outer diameter of 0.323 [m] and a length of 27 [m], 0.5 [m] penetrating into the bedrock and protruding 0.5 [m] out of the ground. The bottom of the big pile is filled with a 1-[m]-thick plug of cement grout. The small pile is a friction pile with an outside diameter of 0.139 [m] and a total length of 21 [m], 20 meters of which are buried in the earth, and 1 [m] extrude out the ground surface. The small pile is plugged with a 6-[m]-thick cement grout at the bottom. Both piles are 4 mm thick steel cylinders.

An outlet polyethylene (PE) pipe is used in the suggested configuration for both piles.

Table 5.1: Characteristics of the GEPs in the BEAR project

Parameter	Value	Unit
Small Pile, S355J2H		
Buried length	20	[m]
Length	21	[m]
Outer diameter, (d_o)	0.139	[m]
Inner diameter, $(d_{i,pile})$	0.131	[m]
Bottom plug, cement grout		
Length	6	[m]
Big Pile, S355J2H		
Buried length	26.5	[m]
Length	27	[m]
Outer diameter, (d_o)	0.323	[m]
Inner diameter, $(d_{i,pile})$	0.315	[m]
Bottom plug, cement grout		
Length	1	[m]
Outlet Pipe, polyethylene (PE100)		
Outer diameter, $(d_{o,pipe})$	0.048	[m]
Inner diameter, $(d_{i,Pipe})$	0.040	[m]

5.2 Soil Layering

A total sounding and CPTu field investigation were conducted close to the coaxial piles in March 2022. Pore water pressure measurements as the complementary data obtained from piezometers at depths -10, -18, and -22 [m] from the ground surface.

5.2.1 Pore pressure measurement

The pore pressure measurement results and the values used in this investigation to interpret CPTu data are presented in Figure 5.3 and Table 5.2. It should be noted that the installed piezometer at -22 [m] shows errors after the first few readings and before reaching to steady state; therefore, its measurements are not considered in the interpretations. Based on the measured pore pressure at depths -10 and -18, the underground water table level was estimated at the depth of -2.5 [m].

Table 5.2: Pore pressure measurements

Depth [m]	Average measured pore pressure [kPa]	Expected Hydrostatic Pressure (10 kPa/m) [kPa]	The pressure used in the interpretation [kPa]
-2.5	Extrapolation	0	0
-10	100.3	75	100
-18	207.5	155	208
-22	148.9	195	261

As mentioned above, the piezometer at the depth of -22 stopped working before reaching the steady state pore pressure measurements. So, the measured value at that depth has not been considered in the interpretation, and the pore pressure profile was built based on extrapolation of the piezometer recordings at depths -10 and -18 [m].

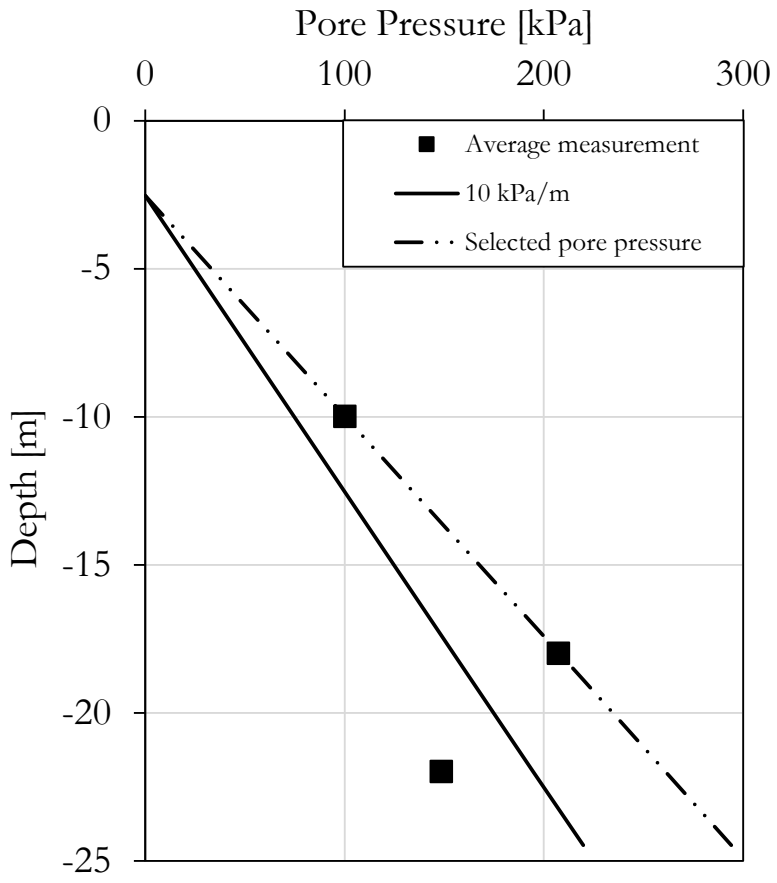

Figure 5.3: Pore pressure measurements [kPa]

5.2.2 Total sounding and CPTu recordings

In the conventional geotechnical practice in Norway, a total sounding is often used to initiate an in-situ soil investigation scheme [55]. The primary purpose of total sounding is to determine the soil layers and the bedrock location, as well as to detect stiff layers that might damage the CPTu probe. It offers a foundation for planning additional in-situ studies,

including CPTu (cone penetration test with pore pressure measurement), soil sampling, and pore pressure measurements [56].

The CPTu data might serve as a reference to the sort of soil behavior. The CPTu data consistently measure the in-situ behavior of aggregates in the vicinity of the probe. Using the obtained CPTu values, one can calculate the preliminary undrained shear strength using two different methods. The first approach is based on cone resistance and considers the theory of undrained bearing capacity, whereas the second approach is based on the excess pore pressure and therefore considers the theory of undrained expanding cavity [57].

The total sounding measurements were performed at 2 [m] far from the CPTu recording, and since the total sounding recordings showed a stiff layer at a depth of -24.5 [m], the CPTu measurements carried out up to level -24 [m].

Figure 5.4 shows the results of CPTu and total sounding main parameters recordings. For the determination of stratification, one first must plot the results of the calculated corrected cone resistance (q_t), the pore pressure (u_2) and the sleeve friction (f_s) with the depth.

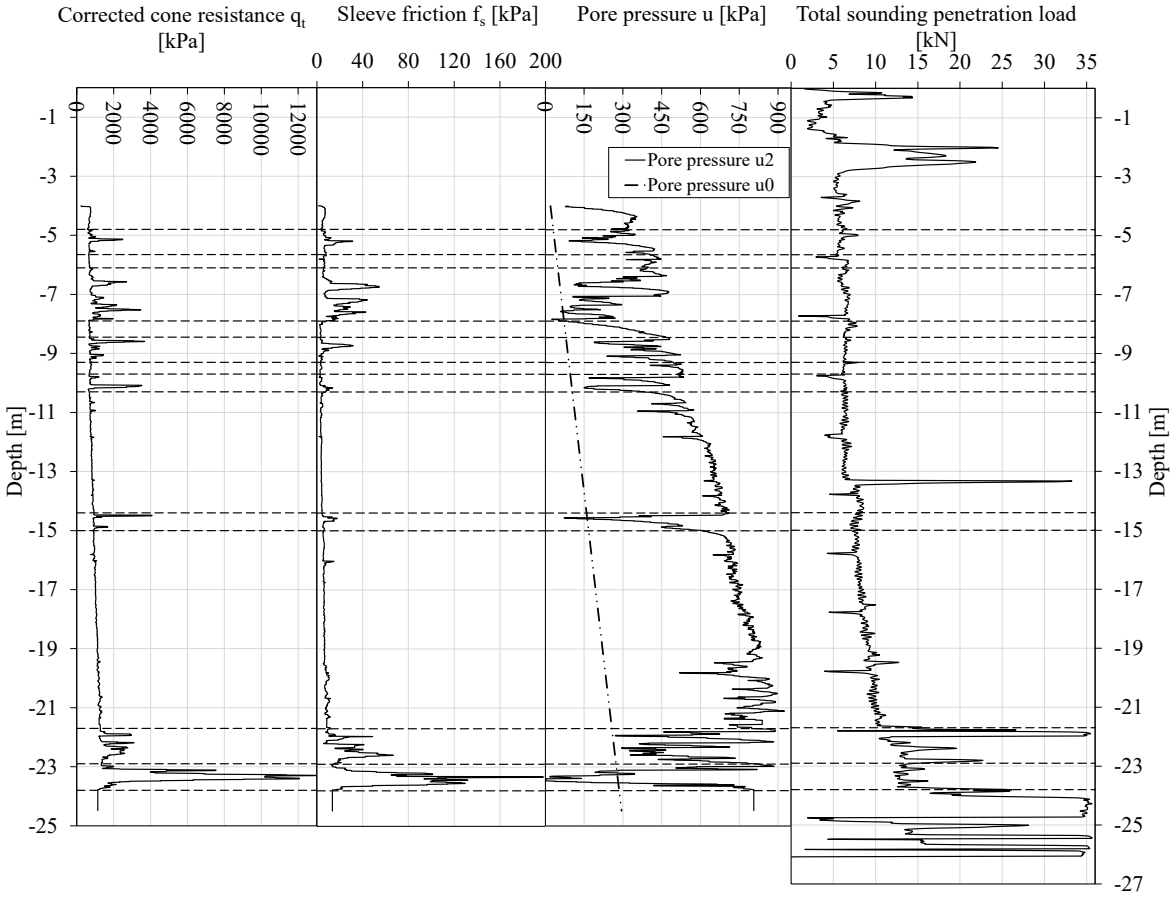

Figure 5.4: Combination of CPTu main parameters and total sounding recordings

5.2.3 Soil and rock type

The CPTu data was used to estimate the soil type using Robertson charts (2011) [58]. Results are shown in Figure 5.5 to Figure 5.8, and the soil stratification is as stated in Table 5.3.

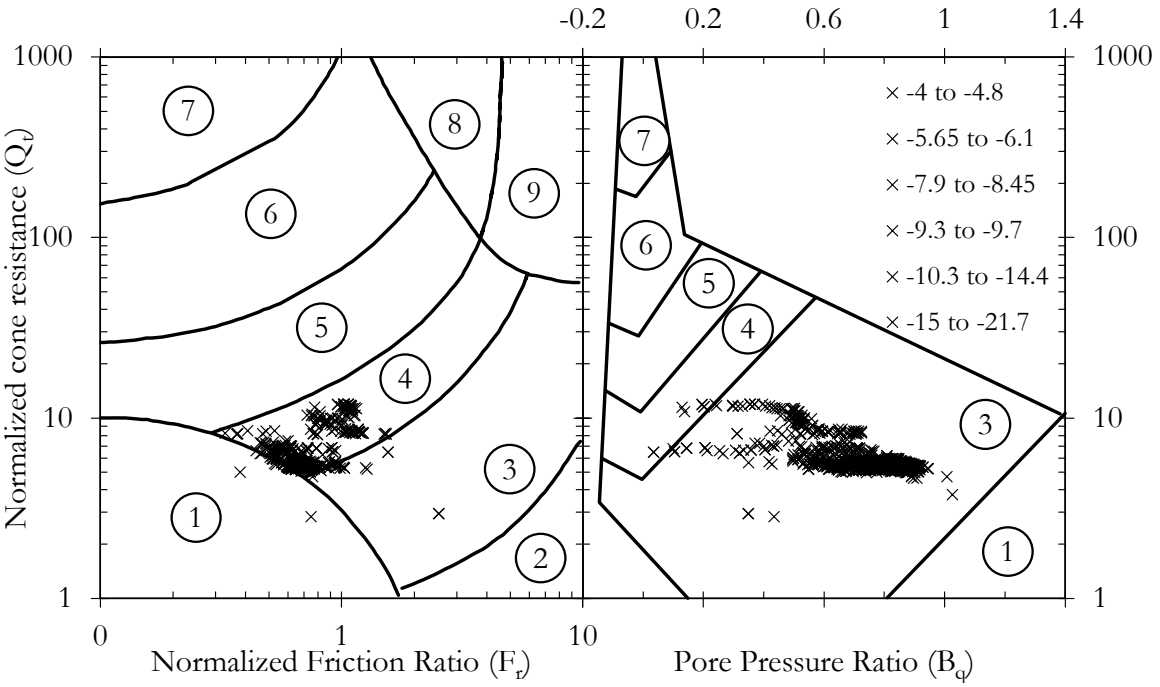

Figure 5.5: CPTu Data for Clays – Clay to silty clay layers presented on the Robertson chart

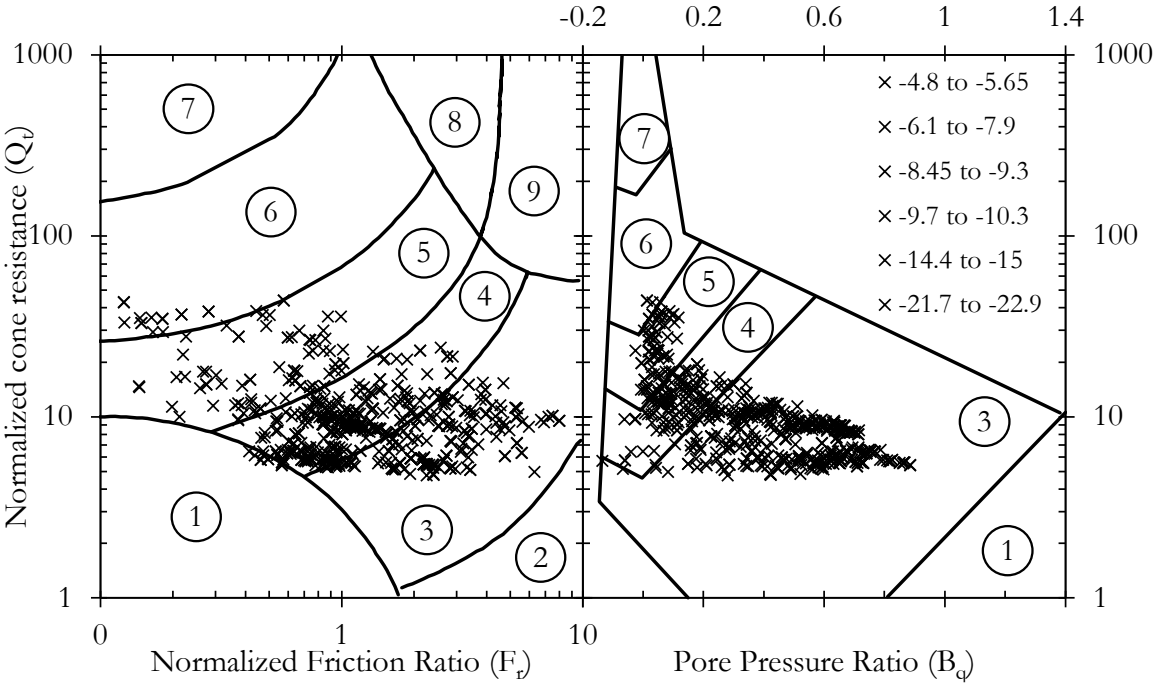

Figure 5.6: CPTu Data for Mixture of Clay, Silt, and Sand layers presented on the Robertson chart

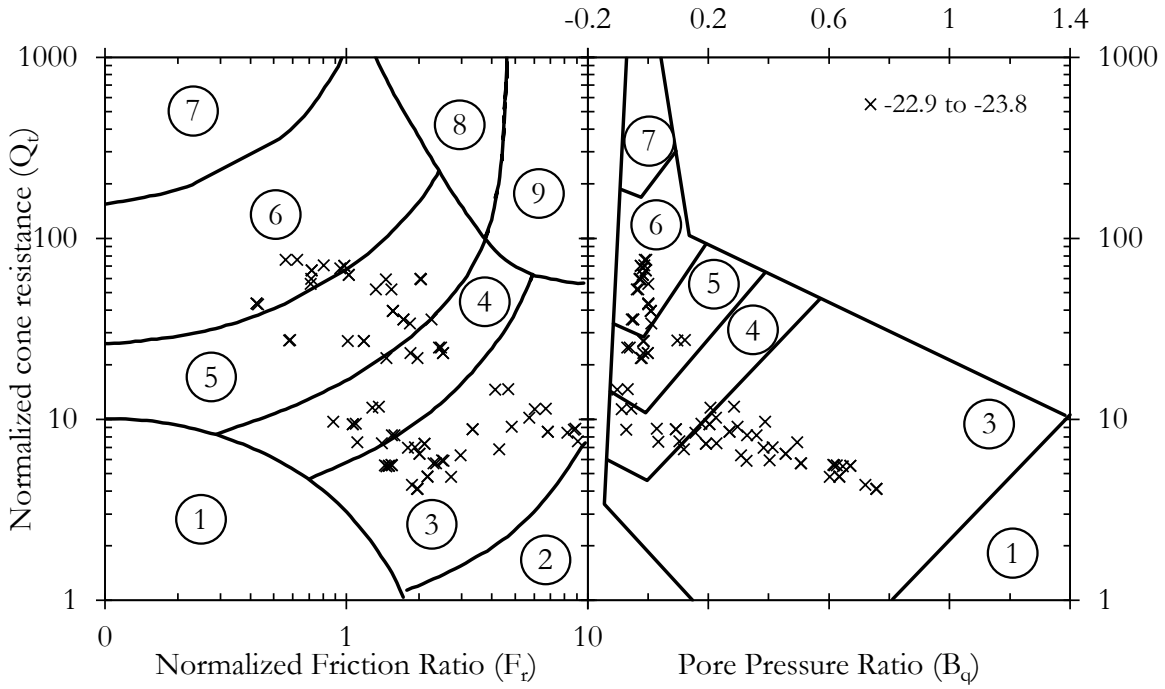

Figure 5.7: CPTu Data for Silty sand to Sand silty layer presented on the Robertson chart

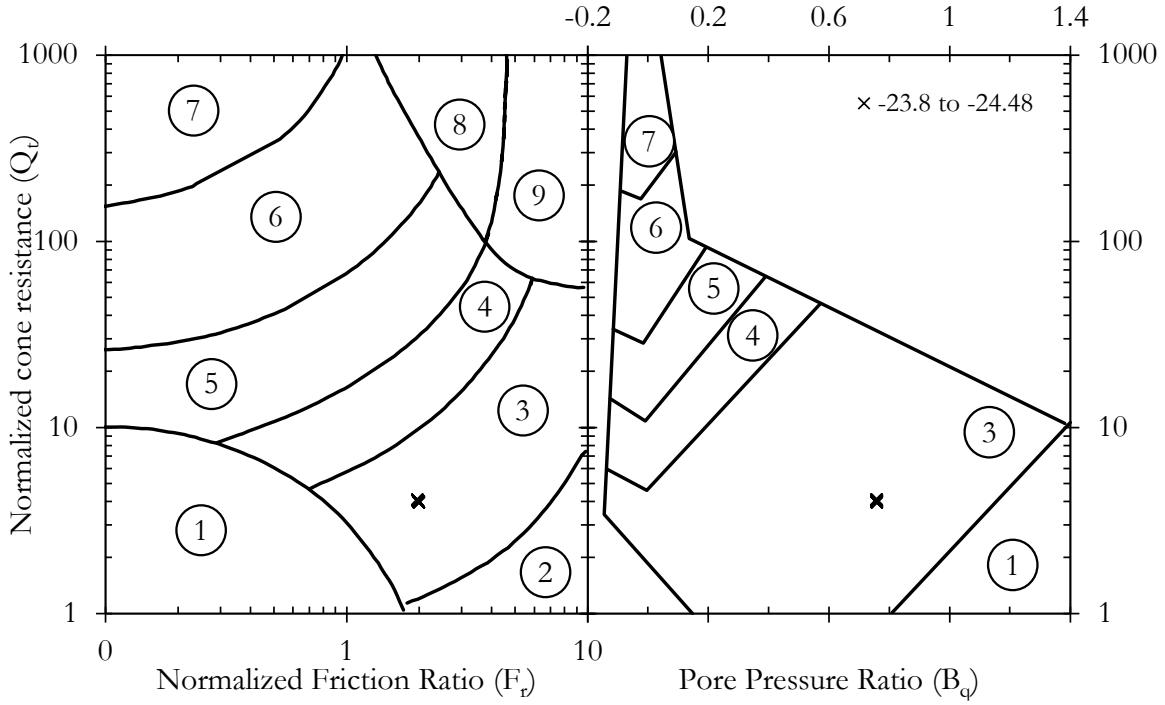

Figure 5.8: CPTu Data for Sensitive soil, Fine-grained layer presented on the Robertson chart

Table 5.3: Soil stratification based on field data

Depth [m]		Thickness [m]	Soil type zone classification		Zone description based on Robertson chart	Reference
From	to		$Q_t - F_r$ Zone	$Q_t - B_q$ Zone		
0	-2	2.00	-	-	Organic Soil	Drilling Report
-2	-3	1.00	-	-	A mixture of Clay, Silt, and Sand	Total Sounding
-3	-4.8	1.80	3-4	3	Clays – Clay to silty clay	CPTu
-4.8	-5.65	0.85	4 (3 - 5)	3 (4-5)	A mixture of Clay, Silt, and Sand	CPTu
-5.65	-6.1	0.45	3-4	3	Clays – Clay to silty clay	CPTu
-6.1	-7.9	1.80	4 (3 - 5)	3 (4-5)	A mixture of Clay, Silt, and Sand	CPTu
-7.9	-8.45	0.55	3-4	3	Clays – Clay to silty clay	CPTu
-8.45	-9.3	0.85	4 (3 - 5)	3 (4-5)	A mixture of Clay, Silt, and Sand	CPTu
-9.3	-9.7	0.40	3-4	3	Clays – Clay to silty clay	CPTu
-9.7	-10.3	0.60	4 (3 - 5)	3 (4-5)	A mixture of Clay, Silt, and Sand	CPTu
-10.3	-14.4	4.10	3-4	3	Clays – Clay to silty clay	CPTu
-14.4	-15	0.60	4 (3 - 5)	3 (4-5)	A mixture of Clay, Silt, and Sand	CPTu
-15	-21.7	6.70	3-4	3	Clays – Clay to silty clay	CPTu
-21.7	-22.9	1.20	4 (3 - 5)	3 (4-5)	A mixture of Clay, Silt, and Sand	CPTu
-22.9	-23.8	0.90	3 to 6	3 to 6	Silty sand to sand silty	CPTu
-23.8	-24.48	0.68	3	3	Sensitive soil, Fine-grained	CPTu
-24.48	-26.1	1.62	-	-	Rock (Sandstone or Rhyolite)	Total Sounding

It should be noted that soil layering presented in Table 5.3 is only based on the data gathered from the field investigation; complimentary data can be collected via tube sampling to clarify the exact soil type through laboratory tests.

As shown in Figure 5.9, according to the national bedrock database from NGU (Geological Survey of Norway), the location of piles is so close to the intersection of sandstone - a clastic sedimentary rock - (the yellow color on the map) and rhyolite - an extrusive igneous rock - (the pink color on the map) [59].

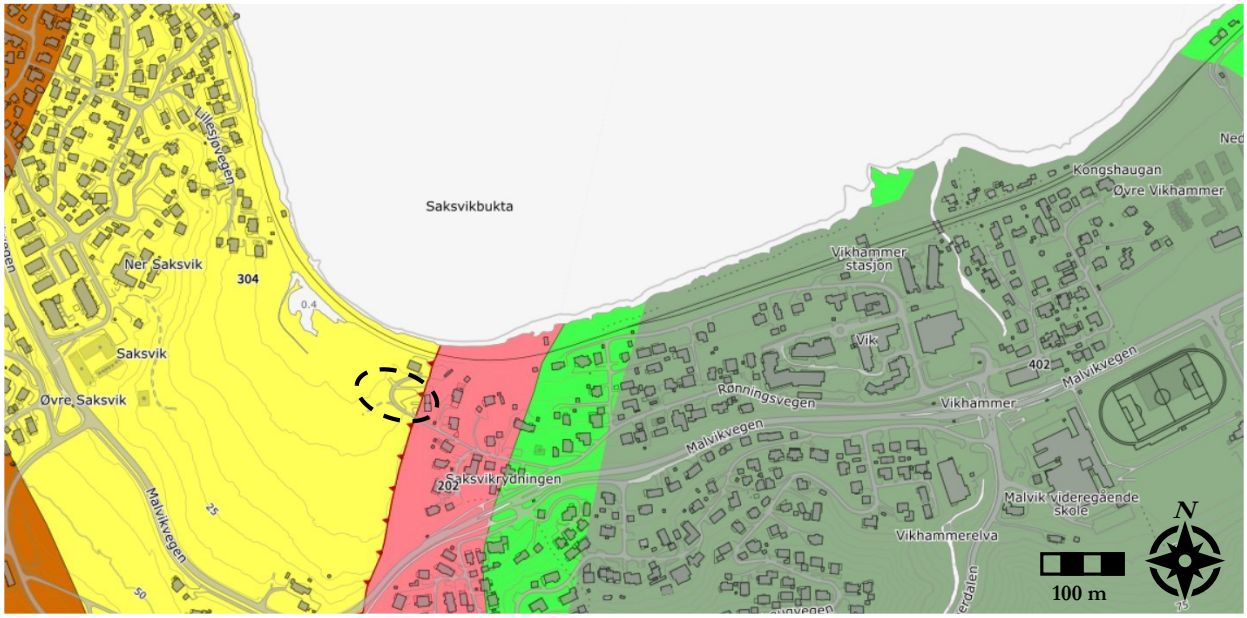

Figure 5.9: Bedrock at the location of piles [59]

5.3 Numerical analysis

According to the thermal research plan outlined for the BEAR project, both piles will be outfitted with the necessary equipment for TRT (Thermal Response Test). Thermistor strings will be installed along the centerline of both piles. It has been suggested to conduct the TRT test on the big pile while concurrently measuring the thermal response at the small pile.

Two test scenarios have been designed for the TRT testing. In the first scenario, piles will be evaluated based on a constant power supply (constant kW), like the usual TRT experiments conducted in energy boreholes. Depending on the available HCF flow rates, tests may be performed with 3, 6, 9, or 12 [kW] of constant input power. The second scenario is to test with consistent input temperatures of 15, 30, and 60 to 70 [°C]. Tests will be conducted on 8-hour heating and 16-hour rest cycle.

According to the prescribed test scheme, numerical simulations of the thermal performance of the BEAR project have been conducted. Since field studies were not completed when this thesis was written, comparing field experiments and numerical simulation was not feasible. Numerical simulation has been performed according to the plan explained in Table 5.4. Each scenario simulates the proposed TRT test for 72 hours.

Table 5.4: Numerical simulation scenarios used in the present study

		Flow rate [lit/min]		
		10	15	20
Constant energy source [kW]	3	✓	✓	-
	12	-	✓	✓
Constant temperature source [℃]	15	✓	✓	-
	65	-	✓	✓

5.3.1 Geometry

Figure 5.10 shows the cylindrical geometry chosen for simulating the BEAR project piles. The model has a diameter equal to 30 [m] and a height of 46 [m]. The top 26 meters of the cylinder height represents the soil layers, and the rest is the bedrock. All the components in the model have dimensions, as stated in Table 5.1. Pile caps (lids) are steel plates with 10 [mm] thickness.

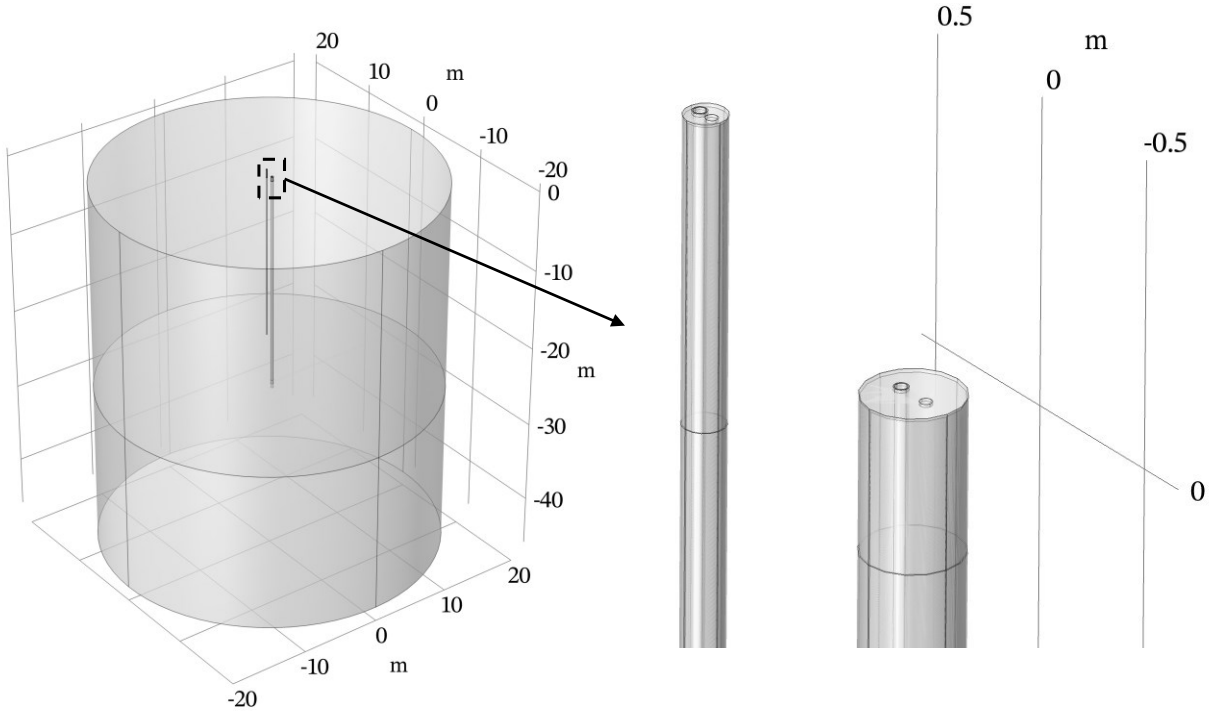

Figure 5.10: BEAR Project 3D FEM model geometry

5.3.2 Mesh building

Mesh elements were built using the physics-controlled sequence with the normal size elements. Based on the described setting, COMSOL Multiphysics has produced a meshing geometry, as shown in Figure 5.11.

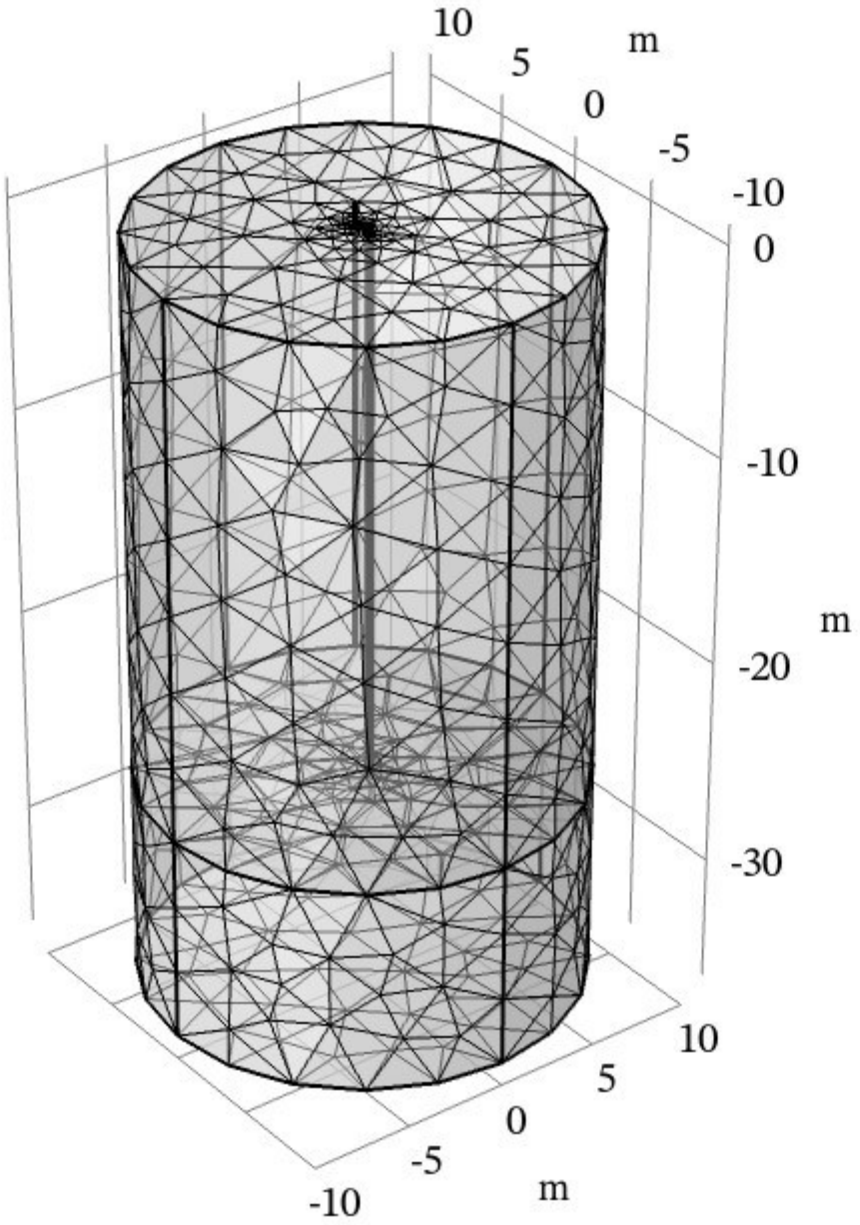

Figure 5.11: Mesh elements of the assigned geometry

5.3.3 Material and thermal parameters

Table 5.5 shows the material properties used in the numerical simulation of the BEAR project. Water is considered the heat carrier fluid with temperature-dependent properties, as described in (Table 4.6).

The soil domain is considered a water-saturated mixture of clay and silt; in the simulation, bedrock material is assumed as sandstone.

Table 5.5: Material characteristics used in numerical simulations

Parameter	Value	Unit	Reference
Soil, Clay/Silt (water-saturated)			
Density, (ρ_{soil})	2100	$[kg/m^3]$	
Heat capacity at constant pressure, $\left(C_{p_{soil}}\right)$	1143	$[J/kg \cdot K]$	[42]
Thermal conductivity, (k_{soil})	1.8	$[W/m \cdot K]$	
Porosity, (ε_{soil})	50	$[\%]$	
Bedrock, Sandstone			
Density, (ρ_{rock})	2450	$[kg/m^3]$	
Heat capacity at constant pressure, $\left(C_{p_{rock}}\right)$	900	$[J/kg \cdot K]$	[42]
Thermal conductivity, (k_{rock})	2.8	$[W/m \cdot K]$	
Porosity, (ε_{rock})	25	$[\%]$	
Steel pile, S355J2H			
Density, (ρ_{steel})	7830	$[kg/m^3]$	
Heat capacity at constant pressure, $\left(C_{p_{steel}}\right)$	470	$[J/kg \cdot K]$	[60]
Thermal conductivity, (k_{steel})	42.7	$[W/m \cdot K]$	
Outlet pipe, polyethylene (PE100)			
Density, (ρ_{PE})	950	$[kg/m^3]$	
Heat capacity at constant pressure, $\left(C_{p_{PE}}\right)$	2400	$[J/kg \cdot K]$	[61]
Thermal conductivity, (k_{PE})	0.45	$[W/m \cdot K]$	
Grout			
Density, (ρ_{grout})	2000	$[kg/m^3]$	
Heat capacity at constant pressure, $\left(C_{p_{grout}}\right)$	1500	$[J/kg \cdot K]$	[62]
Thermal conductivity, (k_{grout})	2.00	$[W/m \cdot K]$	

5.3.4 Initial and boundary conditions

The soil and bedrock domains have an initial temperature equal to 7 [°C]. The ground surface has a convective heat flux Cauchy boundary condition. The ambient air temperature is assumed to be equal to 10 [°C], and the convective heat transfer coefficient between air and soil is calculated using the equation stated in Table 4.12. Other surrounding far-field ground boundaries are all considered to have a stable temperature equal to 7 [°C]. The highest Reynolds number associated with 20 [lit/min] flow is 942, which falls in the laminar flow range. The simulation of the constant power mode has been done according to Equation (5.1).

$$T_{in} = T_{out} + \frac{Q}{\dot{m} c_p} \quad (5.1)$$

Where:

T_{in}: Inflow Temperature [℃]

T_{out}: Outflow Temperature [℃]

Q: Constant applied power [W]

$\dot{m}$: gravimetric flow rate [kg/s]

c_p: specific heat of water [J/kg · ℃]

5.4 Results

To assess the thermal interaction between the piles, heat is injected in the big pile, the temperature of the water at the big pile outlet, the average temperature of the small pile surrounding surface, and water temperature at the top, middle, and bottom of the center line of the small pile were recorded during the simulation.

5.4.1 Heating with constant power

Figure 5.12 and Figure 5.13 show the inflow and outflow temperatures of the big pile at the constant heating power mode.

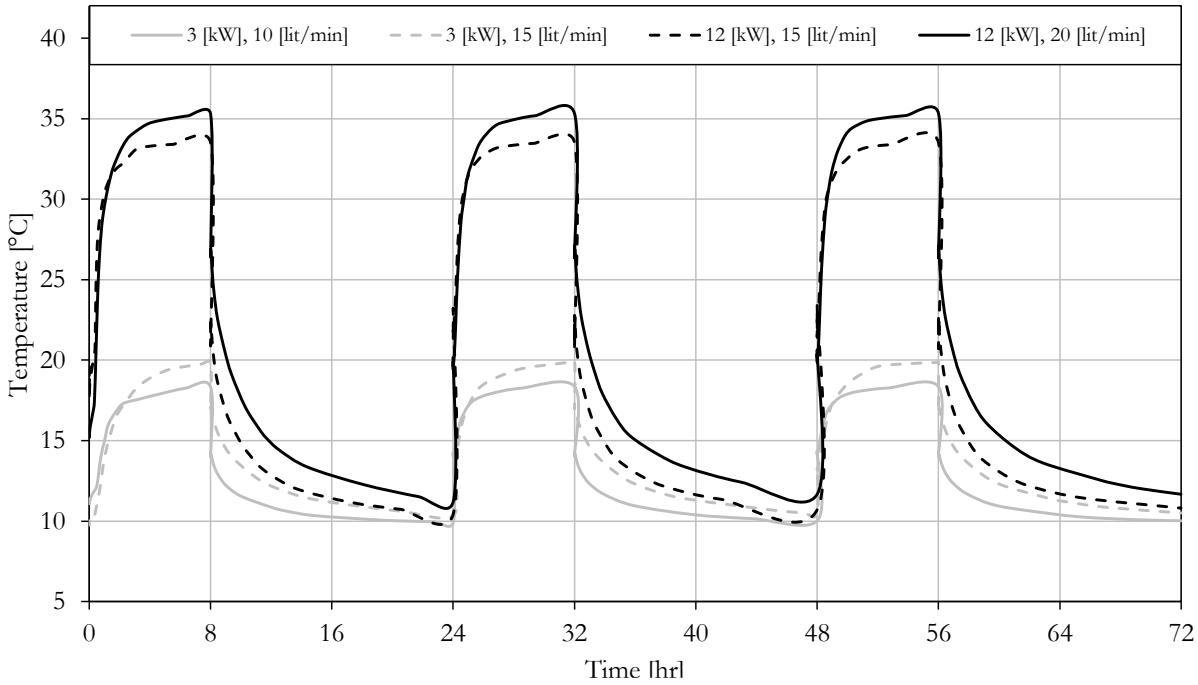

Figure 5.12: Big pile inflow temperatures in constant heating power mode

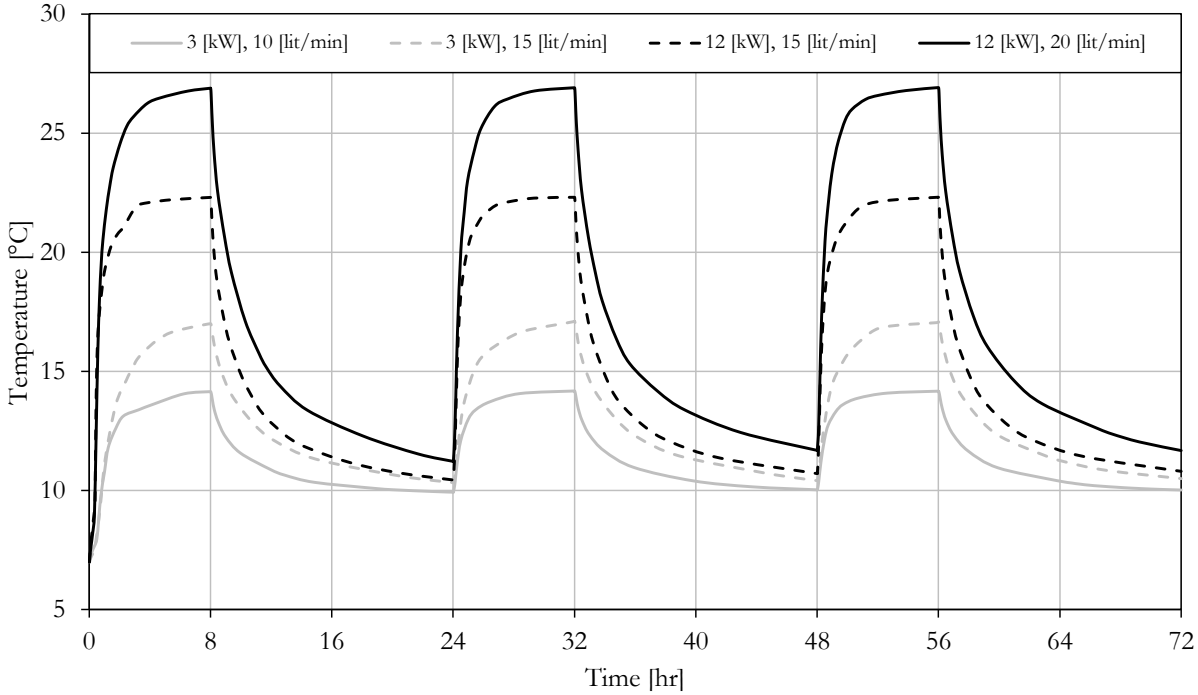

Figure 5.13: Big pile outflow temperatures in constant heating power mode

Figure 5.14 to Figure 5.17 show temperature variation on the surface and the water inside the small pile at different depths.

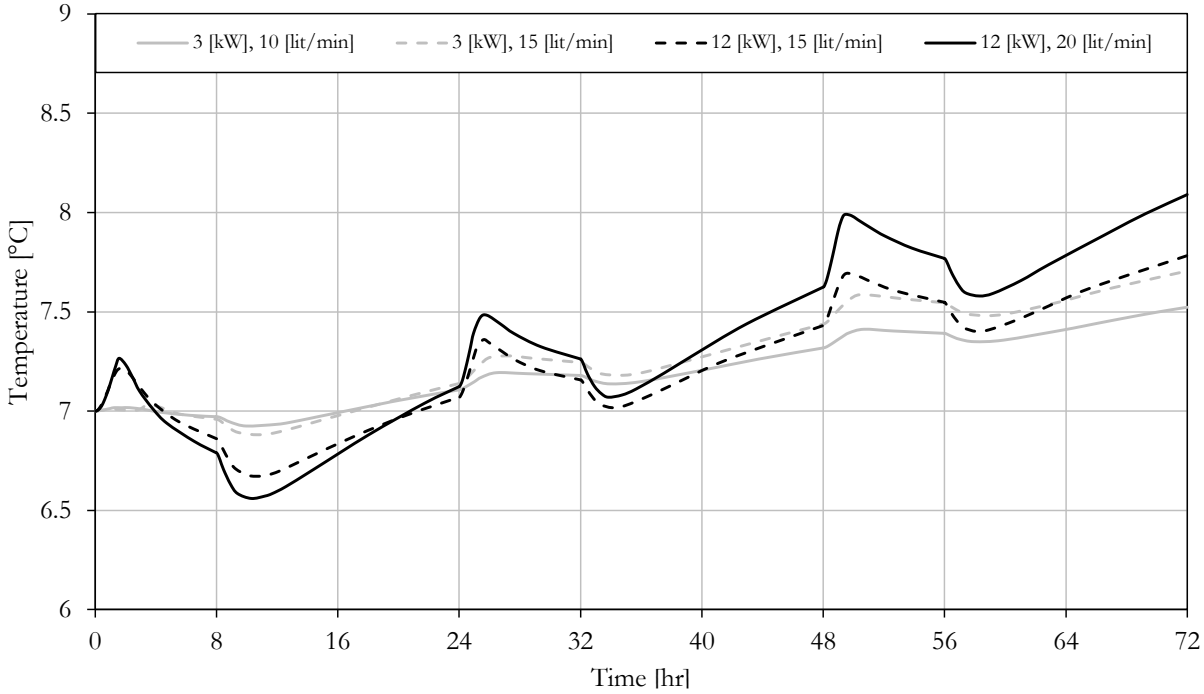

Figure 5.14: Temperature variation on the small pile surface in constant heating power mode

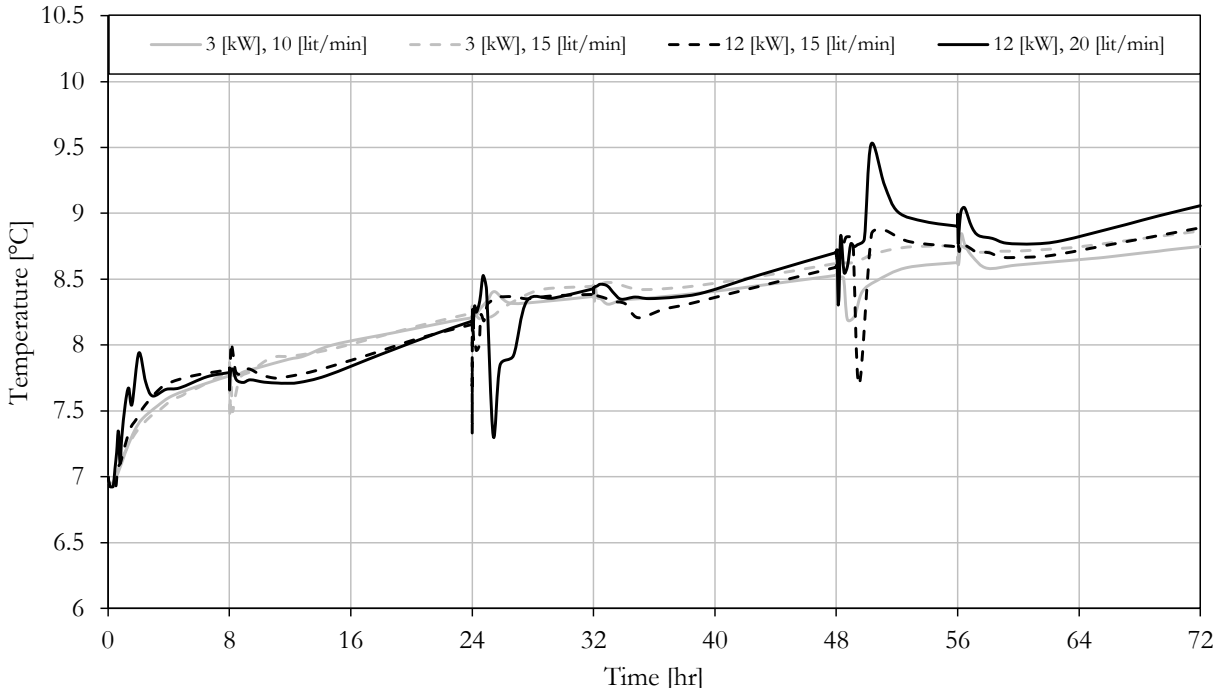

Figure 5.15: Temperature variation of the water inside the small pile at z=0 [m] in constant heating power mode

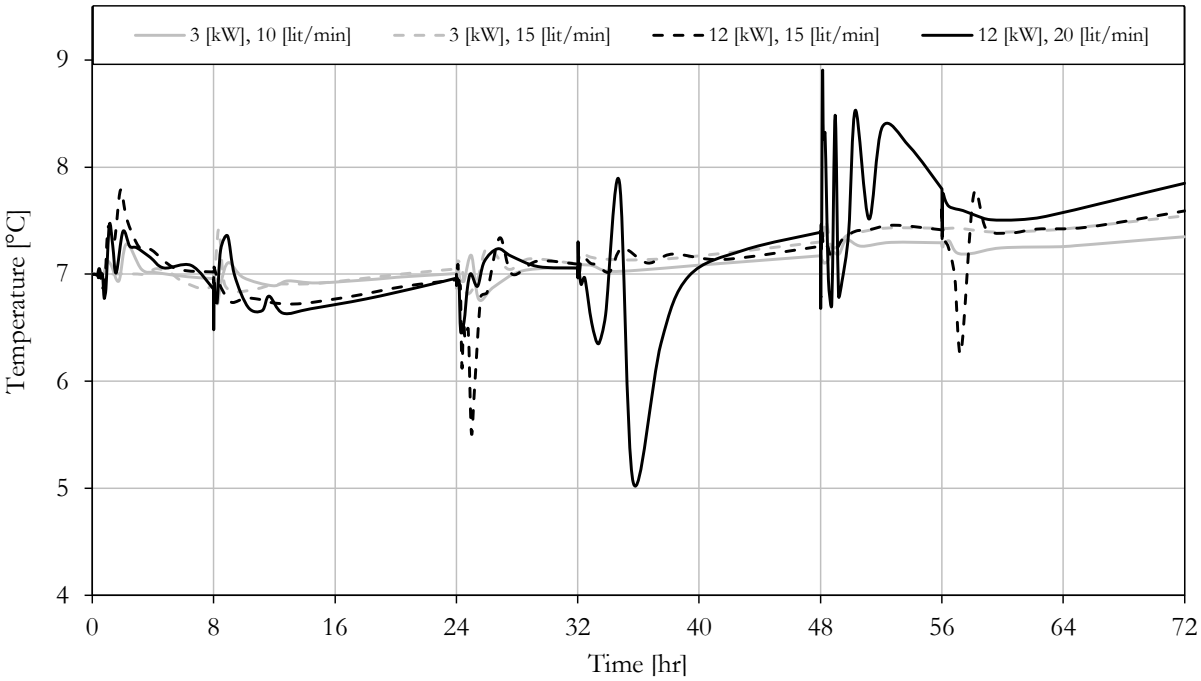

Figure 5.16: Temperature variation of the water inside the small pile at z=-7 [m] in constant heating power mode

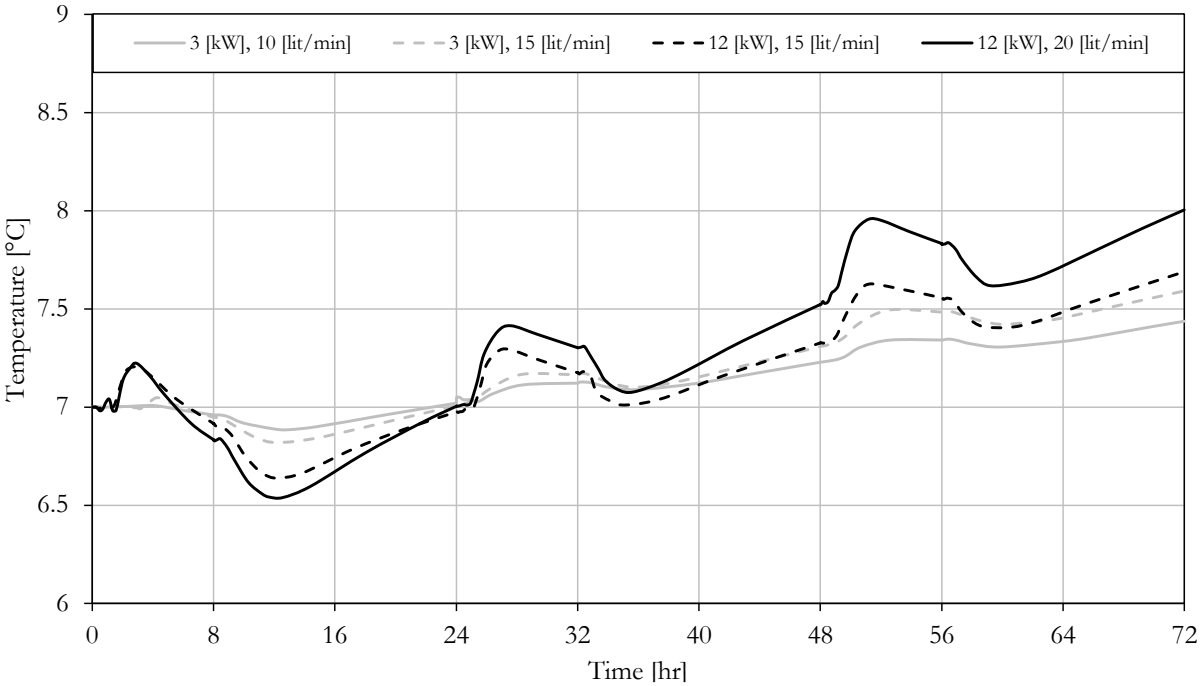

Figure 5.17: Temperature variation of the water inside the small pile at z=-14 [m] in constant heating power mode

Table 5.6 shows the recorded temperatures at the end of the heating mode after 56 hours from the test initiation.

Table 5.6: Recorded temperatures in constant heating power mode at t=56 [hr]

	Injected heat [kW]		3		12	
	Inflow rates [lit/min]		10	15	15	20
Temperature [℃]	Big pile inflow		18.3	19.9	33.5	35.3
	Big pile outflow		14.2	17.1	22.3	26.9
	Small pile surface		7.4	7.5	7.5	7.8
	Water in the small pile	at z=0 [m]	8.6	8.7	8.7	8.9
		at z=-7 [m]	7.3	7.4	7.4	7.8
		at z=-14 [m]	7.3	7.5	7.5	7.8

Figure 5.18 shows the temperature distribution after 56 hours from the test initiation while the heat injected at constant power equal to 3 [kW] and the flow rate of 10 [lit/min]. Figure 5.19 shows the isothermal contours around the piles while the heat injected at constant power equal to 3 [kW] and the flow rate of 10 [lit/min].

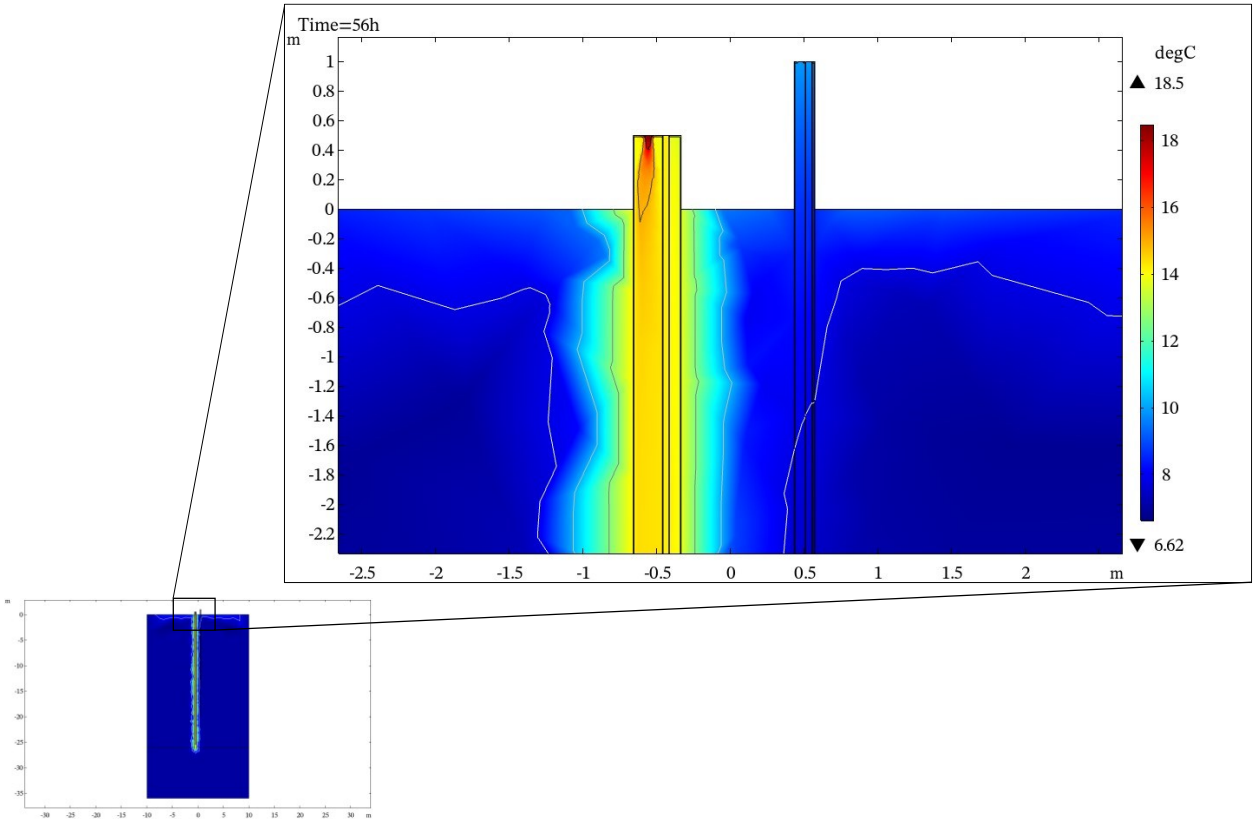

Figure 5.18: Cross section of the model showing temperature distribution in the ground in the constant heating power

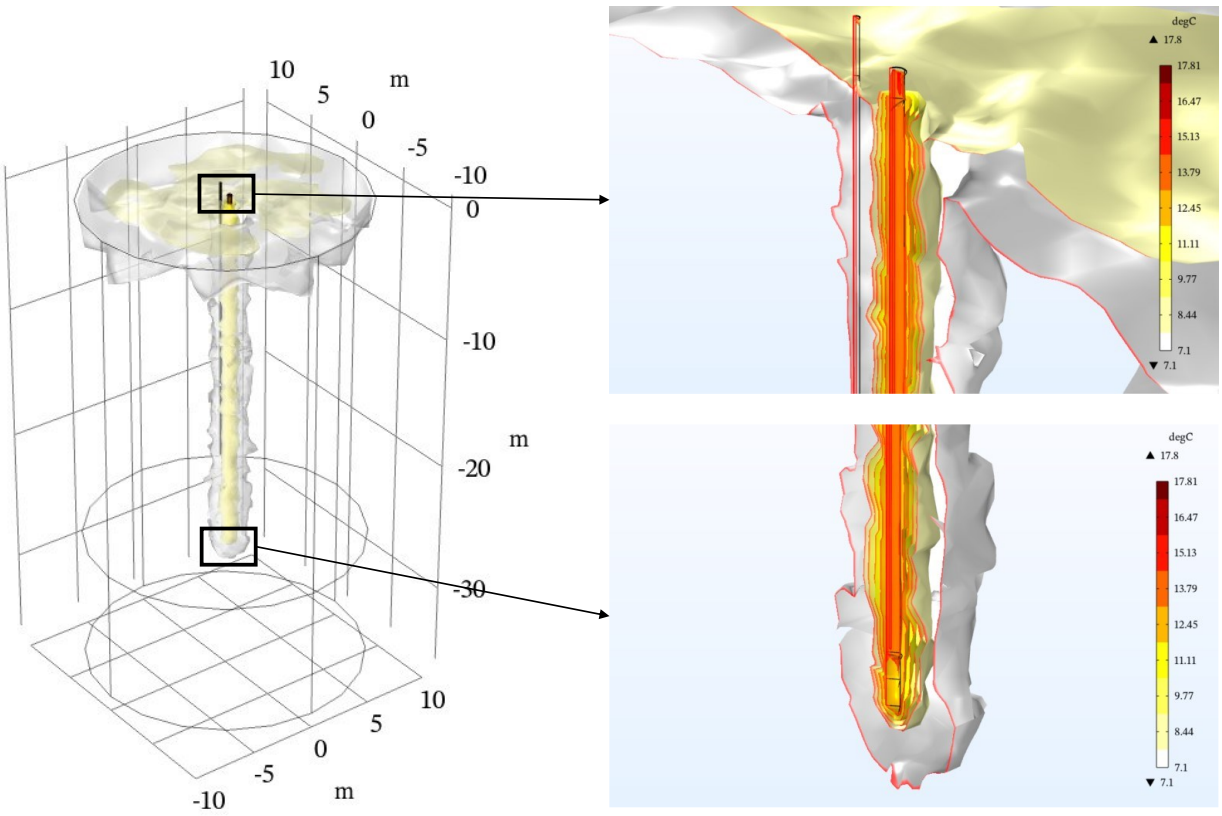

Figure 5.19: Isothermal contours around the piles in the ground in the constant heating power mode

5.4.2 Heating with constant temperature inlet

Figure 5.20 and Figure 5.21 show the inflow and outflow temperatures of the big pile at the constant temperature mode.

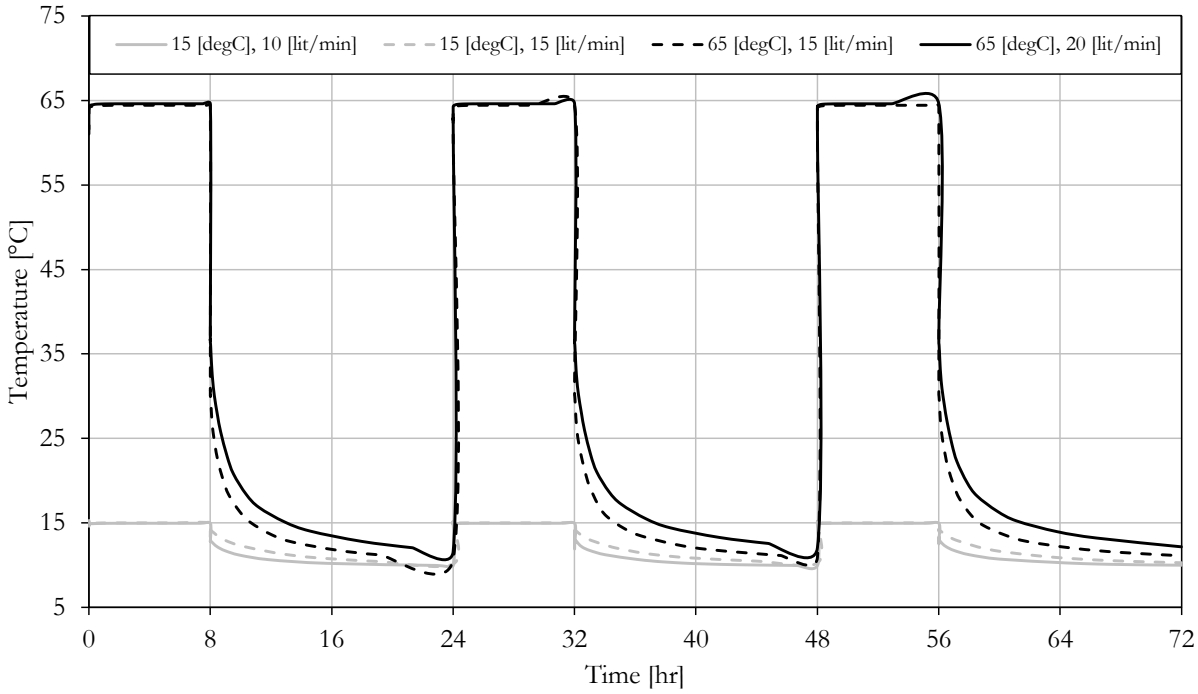

Figure 5.20: Big pile inflow temperatures in the constant temperature mode

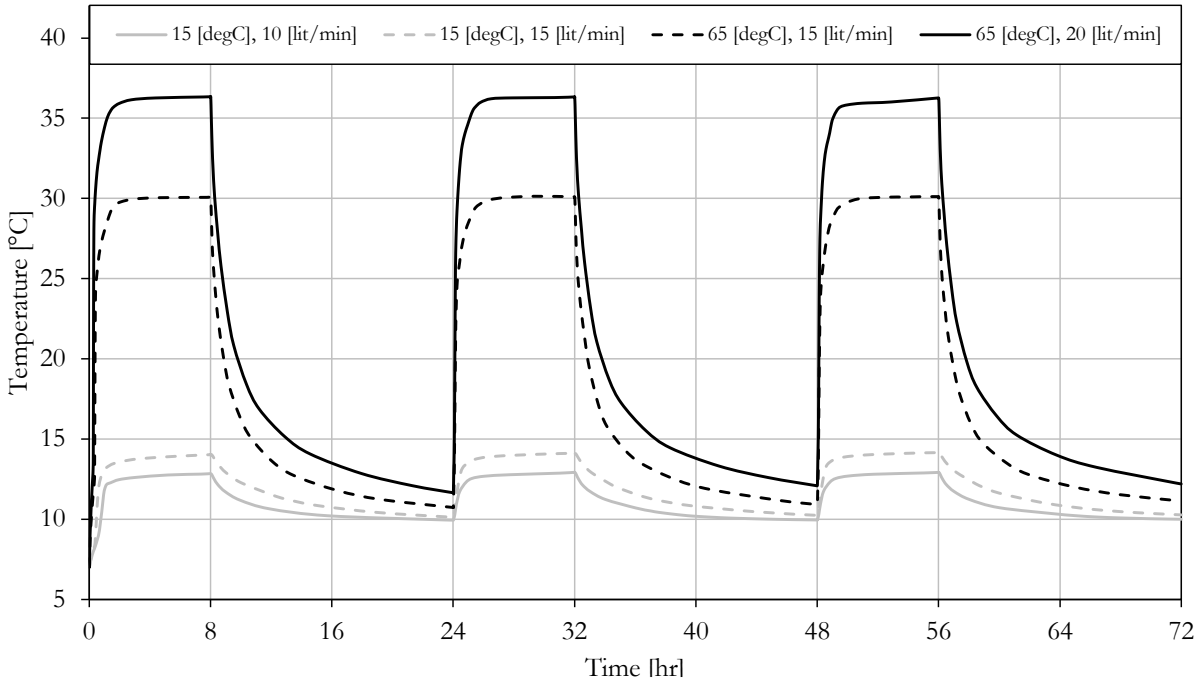

Figure 5.21: Big pile outflow temperatures in the constant temperature mode

Figure 5.22 to Figure 5.25 show temperature variation on the surface and the water inside the small pile at different depths.

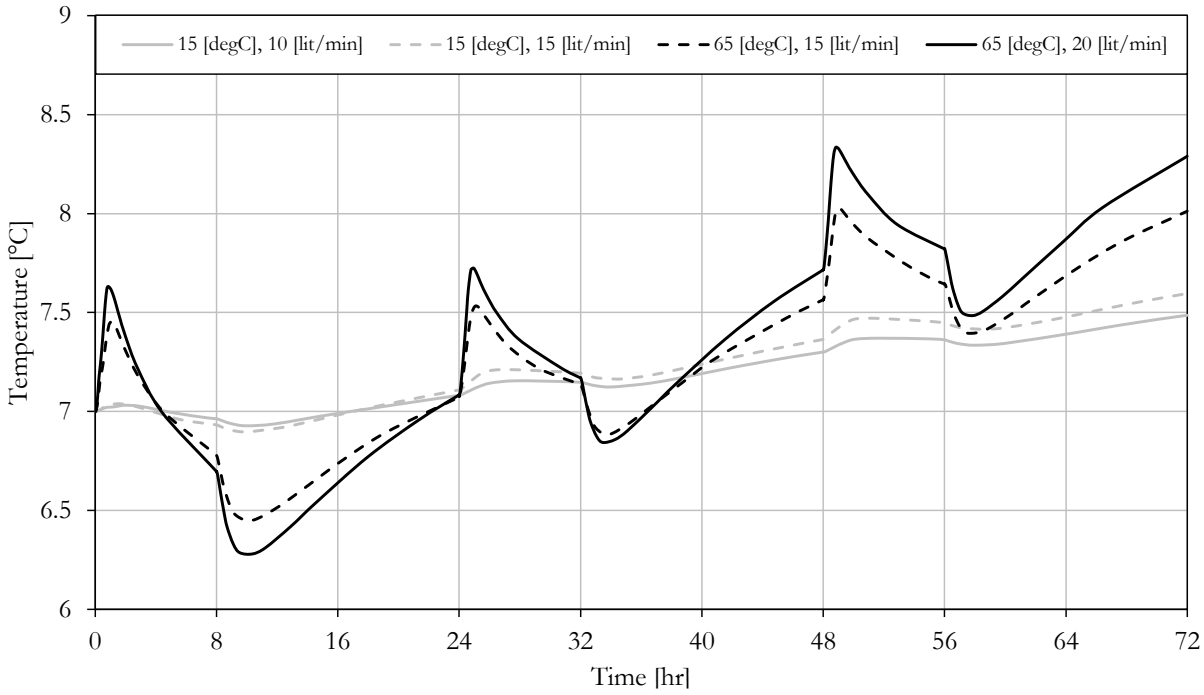

Figure 5.22: Temperature variation on the small pile surface in the constant temperature mode

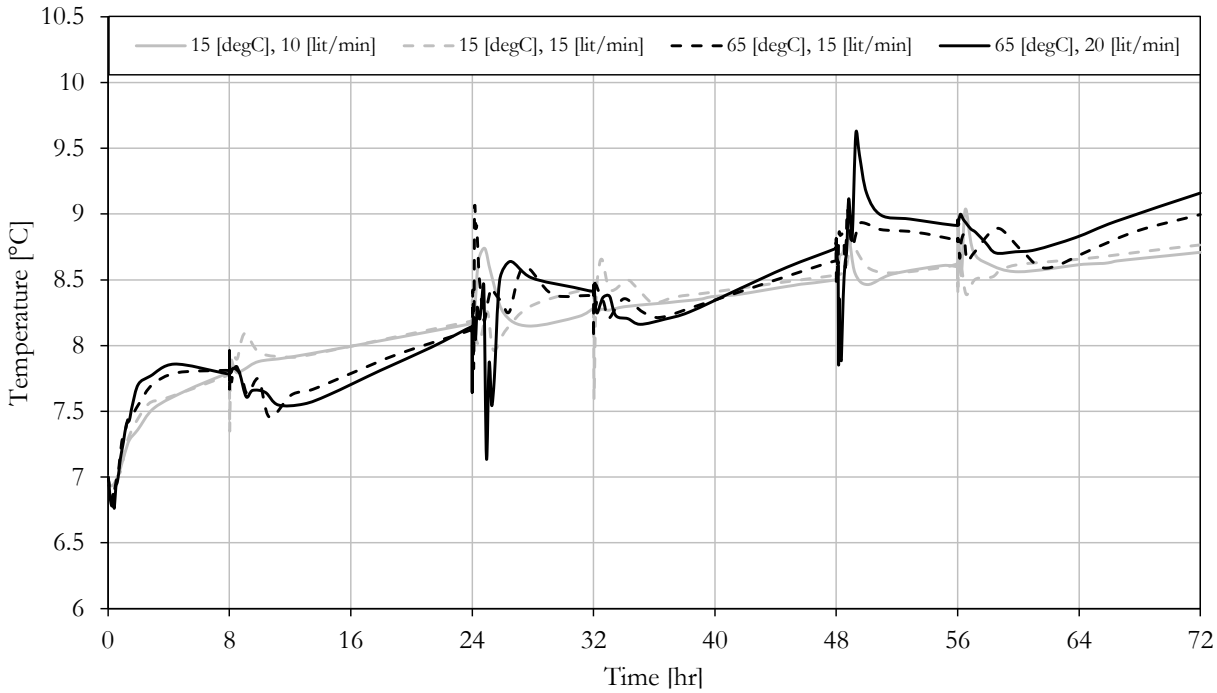

Figure 5.23: Temperature variation of the water inside the small pile at z=0 [m] in the constant temperature mode

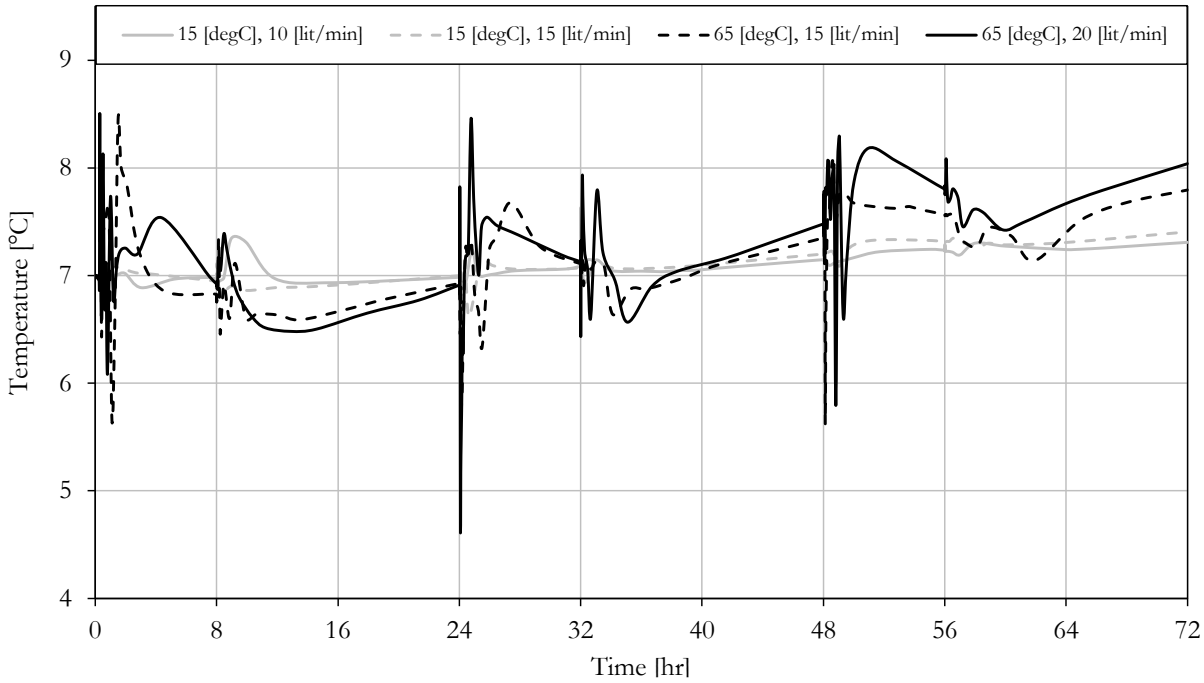

Figure 5.24: Temperature variation of the water inside the small pile at z=-7 [m] in the constant temperature mode

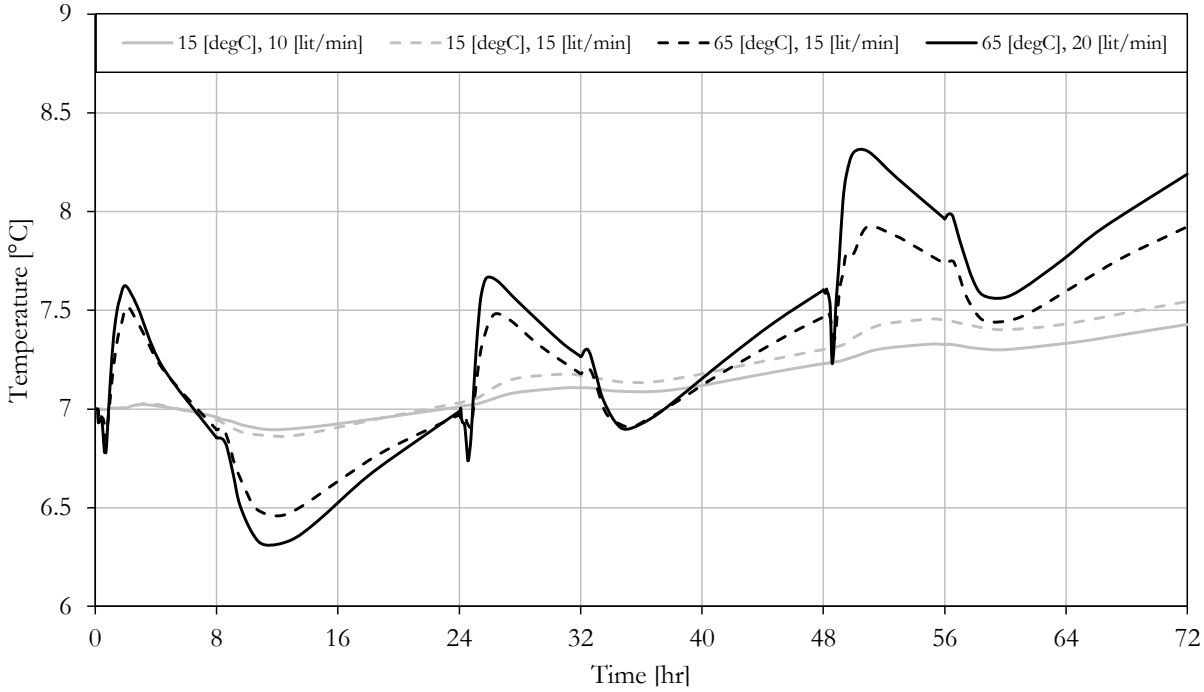

Figure 5.25: Temperature variation of the water inside the small pile at z=-14 [m] in the constant temperature mode

Table 5.7 shows the recorded temperatures at the end of the heating section after 56 hours from the test initiation.

Table 5.7: Recorded temperatures in the constant temperature mode at t=56 [hr]

	Inflow temperature [℃]		15		65	
	Inflow rates [lit/min]		10	15	15	20
Temperature [℃]	Big pile outflow		12.9	14.1	30.1	36.2
	Small pile surface		7.4	7.4	7.6	7.8
	Water in the small pile	at z=0 [m]	8.6	8.7	8.8	8.9
		at z=-7 [m]	7.2	7.3	7.6	7.8
		at z=-14 [m]	7.3	7.4	7.7	8.0

Figure 5.26 shows the temperature distribution after 56 hours from the test initiation while the heat was injected at the constant temperature of 65 [°C] and the flow rate of 15 [lit/min]. Figure 5.27 shows the isothermal contours around the piles while the heat is injected at the constant temperature of 65 [°C] and the flow rate of 15 [lit/min].

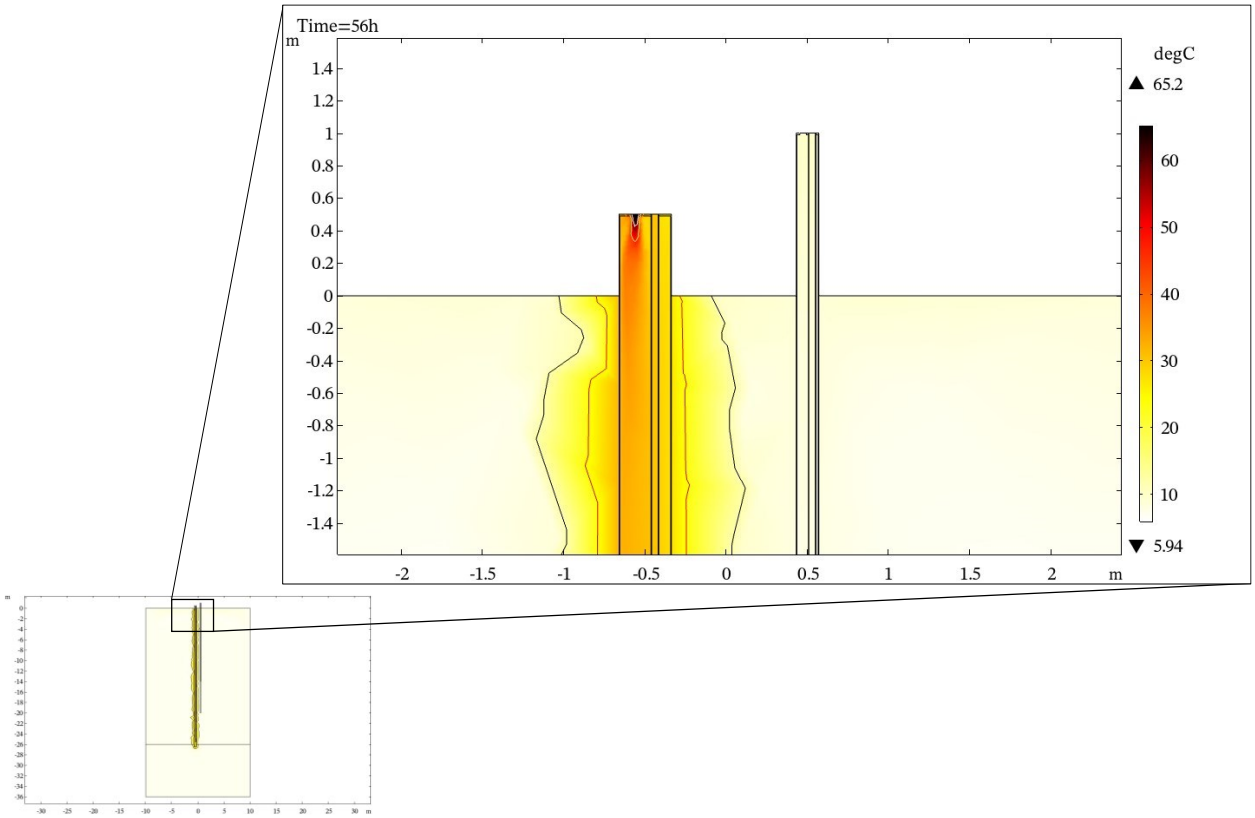

Figure 5.26: Cross section of the model showing temperature distribution in the ground in the constant temperature mode

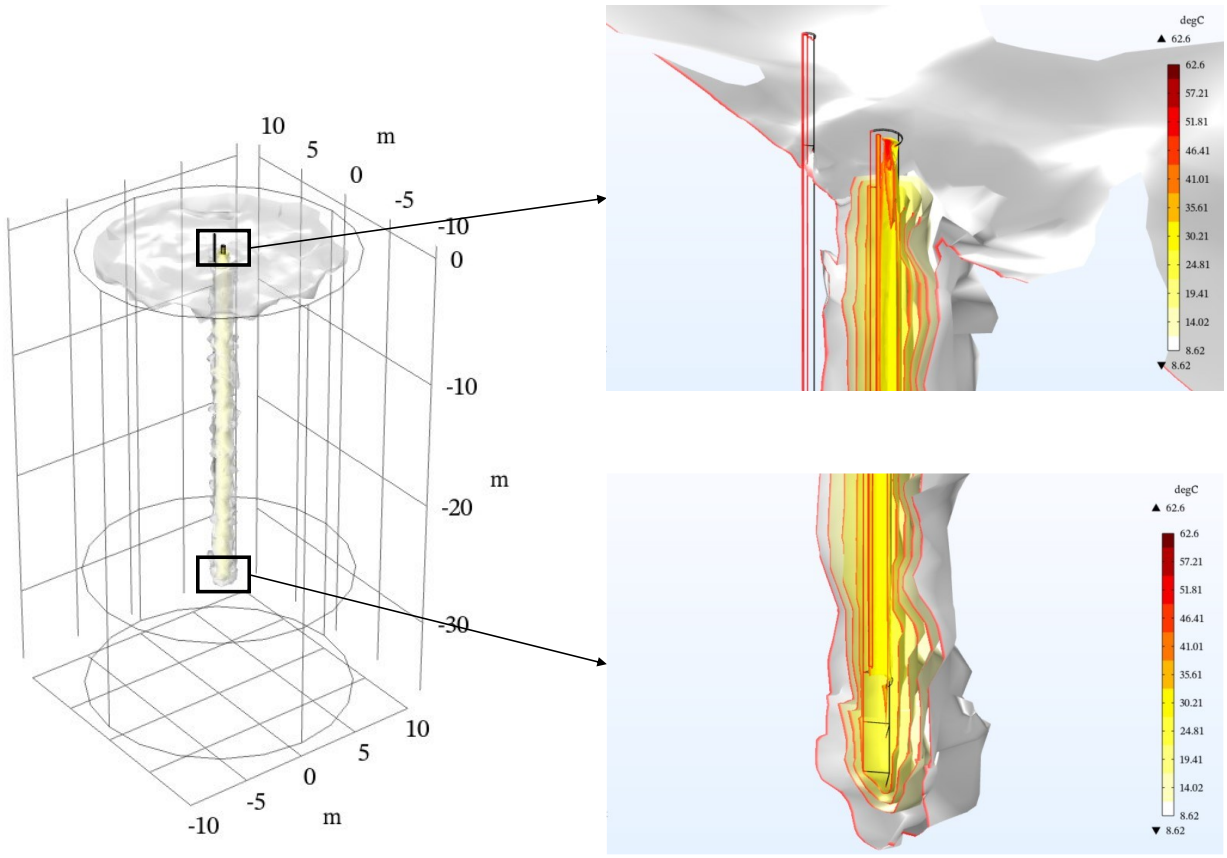

Figure 5.27: Isothermal contours around the piles in the ground in the constant temperature mode

5.5 Discussion

Cross sections of the temperature variation in the ground for both scenarios (Figure 5.17 and Figure 5.24) show that after 72 hours, the heat injection into the big pile influences a zone around the big pile by less than one meter. Thus, one meter from the center of the big pile can be considered a thermally undisturbed area. This zone will be larger by the continuous operation of the heat injection for more extended periods. Due to the higher heat capacity of the water compared to other materials in this simulation, the temperature on the centerline of the small pile is lower compared to the outer surface of the small pile.

The temperature on the outer surface of the small pile has been calculated by averaging the temperature all over its surface for each simulation step. In this simulation, the ambient air temperature is slightly higher than the ground temperature; consequently, in the shallow depths from the surface, the ground temperature is higher than in the other areas, which is also reflected in the recorded temperatures at depth z=0 [m] inside the small pile.

Each test consists of three heating cycles. Each cycle contains 8 hours of heat injection and 16 hours of rest. In the simulation, some heat fluctuations at the start of each heat injection phase and resting phase are observed, which are related to the nature of the numerical simulation and due to sudden large changes imposed in the model.

6 Conclusion and recommendations for further work

6.1 Analytical modeling

Based on the general equation of heat transfer for infinitesimal volume, the most straightforward and reliable relations governing the heat transfer in porous media have been presented. After that, by considering the slenderness of an infinite annular coaxial pile, the three-dimensional heat conduction-convection equations for measuring the temperature distribution in a pile, HCF, pipe, and the surrounding soil are extracted and presented.

6.2 Numerical simulation of the Saga university experiment

A numerical model has been established based on the experimental results of the thermal performance of a coaxial annular steel energy pile carried out at Saga University. This numerical simulation combines fluid flow and heat transfer physics in solid, liquid, and porous media. Comparison between the experimental results and outcomes of the numerical simulation verified that the suggested three-dimensional model works accurately and can apply such a model for investigating the thermal performance of similar piles.

6.3 Numerical simulation of the BEAR project

Based on the numerical simulations verified with data from the Saga experiment, thermal reactions of the steel coaxial piles installed at the BEAR project site have been investigated. The lack of laboratory data limits the real case simulation; however, eight numerical studies of different heating cases with constant heating power or maintaining the constant temperature of the inflowing HCF under cyclic heating schemes for different flow rates have been investigated.

6.4 Recommendations for further work

- **Analytical measurements**: Based on the presented heat transfer equations in a coaxial pile model, it is possible to calculate the temperature distribution around the pile directly to compare with the experimental and numerical results.
- **Soil sampling and laboratory tests:** Numerical simulation of the thermal performance of the piles at the BEAR project site can be done more accurately if the soil sampling was carried out and parameters such as soil type, density, porosity, and moisture content, thermal conductivity, and heat capacity were measured. It can be proposed to take at least 6 samples from depths of 15 to 22 meters and 6 samples from depths of 22 to 24 meters for index testing and thermal properties measurements.

- **Numerical simulation for the long-term:** The short-term thermal performance of the steel piles in the BEAR project site has been evaluated in the current thesis. However, the long-term simulations will better show the potential of harvesting or storing energy from/to the ground in Norway, utilizing coaxial steel piles.

References

[1] R. Al-Khoury, *Computational Modeling of Shallow Geothermal Systems*. Taylor \& Francis Group, 2017.

[2] Jalaluddin, A. Miyara, K. Tsubaki, S. Inoue, and K. Yoshida, "Experimental study of several types of ground heat exchanger using a steel pile foundation," *Renew. Energy*, vol. 36, no. 2, pp. 764–771, Feb. 2011, doi: 10.1016/J.RENENE.2010.08.011.

[3] L. Laloui and A. F. Rotta Loria, *Analysis and Design of Energy Geostructures - Theoretical Essentials and Practical Applications*, vol. 4, no. 3. 2020.

[4] S. Lee, J. G. Speight, and S. K. Loyalka, Eds., *handbook of Alternative fuel technologies*, vol. 9, no. 21. CRC Press, 2007.

[5] H. Shao, P. Hein, A. Sachse, and O. Kolditz, *Geoenergy Modeling II Shallow Geothermal Systems*. Cham, Switzerland: Springer, 2016.

[6] L. Laloui and A. Rotta Loria, *Analysis and Design of Energy Geostructures: Theoretical Essentials and Practical Application*. San Diego: San Diego: Elsevier Science & Technology, 2019.

[7] R. Cataldi, "The Year Zero of Geotherrnics," Sacramento, California, 1999. [Online]. Available: https://www.geothermal-library.org/index.php?mode=pubs&action=view&record=1018266.

[8] J. W. Lund, "geothermal energy, Description, Uses, History, & Pros and Cons ," *Britannica*. 2018, Accessed: Dec. 07, 2021. [Online]. Available: https://www.britannica.com/science/geothermal-energy.

[9] G. Narsilio, I. Johnston, A. Bidarmaghz, O. Mikhayalova, O. Kivi, and R. Aditaya, "Geothermal Energy: Intorducing an emerging technology," *Adv. Civ. Eng. Sustain. Dev.*, no. August, pp. 141–154, 2014.

[10] M. Preene and W. Powrie, "Ground energy systems: From analysis to geotechnical design," *Geotechnique*, vol. 59, no. 3, pp. 261–271, 2009, doi: 10.1680/geot.2009.59.3.261.

[11] "Geothermal Switzerland - Swiss Geothermal Association (SVG)." https://geothermie-schweiz.ch/ (accessed Dec. 08, 2021).

[12] "Geothermal energy - British Geological Survey." https://www.bgs.ac.uk/geology-projects/geothermal-energy/ (accessed Dec. 08, 2021).

[13] "Geothermal energy from abandoned coal mines - Coal Authority." https://www2.groundstability.com/geothermal-energy-from-abandoned-coal-mines/ (accessed Dec. 08, 2021).

[14] A. K. Sani, R. M. Singh, T. Amis, and I. Cavarretta, "A review on the performance of geothermal energy pile foundation, its design process and applications," *Renew. Sustain. Energy Rev.*, vol. 106, pp. 54–78, May 2019, doi: 10.1016/J.RSER.2019.02.008.

[15] K. Midttømme, "T0685_Ground-Source Heat Pumps and Underground Thermal Energy Storage - Energy for the future," no. May 2014, 2008.

[16] F. Loveridge and W. Powrie, "2D thermal resistance of pile heat exchangers,"

Geothermics, vol. 50, pp. 122–135, Apr. 2014, doi: 10.1016/J.GEOTHERMICS.2013.09.015.

[17] H. Brandl, "Energy foundations and other thermo-active ground structures," *Geotechnique*, vol. 56, no. 2, pp. 81–122, Mar. 2006, doi: 10.1680/GEOT.2006.56.2.81.

[18] H. Park, S. R. Lee, S. Yoon, and J. C. Choi, "Evaluation of thermal response and performance of PHC energy pile: Field experiments and numerical simulation," *Appl. Energy*, vol. 103, pp. 12–24, 2013, doi: 10.1016/J.APENERGY.2012.10.012.

[19] K. Nagano *et al.*, "Thermal Characteristics of Steel Foundation Piles As Ground Heat Exchangers," *IEA Heat Pump Conf.*, vol. 8th, 2005.

[20] K. D. Murphy, J. S. McCartney, and K. S. Henry, "Evaluation of thermo-mechanical and thermal behavior of full-scale energy foundations," *Acta Geotech.*, vol. 10, no. 2, pp. 179–195, Apr. 2015, doi: 10.1007/S11440-013-0298-4/FIGURES/16.

[21] Y. Hamada, H. Saitoh, M. Nakamura, H. Kubota, and K. Ochifuji, "Field performance of an energy pile system for space heating," *Energy Build.*, vol. 39, no. 5, pp. 517–524, May 2007, doi: 10.1016/J.ENBUILD.2006.09.006.

[22] L. Laloui, M. Nuth, and L. Vulliet, "Experimental and numerical investigations of the behaviour of a heat exchanger pile," *Int. J. Numer. Anal. Methods Geomech.*, vol. 30, no. 8, pp. 763–781, Jul. 2006, doi: 10.1002/NAG.499.

[23] N. Yavari, A. M. Tang, J. M. Pereira, and G. Hassen, "Experimental study on the mechanical behaviour of a heat exchanger pile using physical modelling," *Acta Geotech.*, vol. 9, no. 3, pp. 385–398, 2014, doi: 10.1007/S11440-014-0310-7.

[24] P. Bourne-Webb, S. Burlon, S. Javed, S. Kürten, and F. Loveridge, "Analysis and design methods for energy geostructures," *Renew. Sustain. Energy Rev.*, vol. 65, pp. 402–419, Nov. 2016, doi: 10.1016/J.RSER.2016.06.046.

[25] P. J. Bourne-Webb, B. Amatya, K. Soga, T. Amis, C. Davidson, and P. Payne, "Energy pile test at Lambeth College, London: geotechnical and thermodynamic aspects of pile response to heat cycles," *Géotechnique*, vol. 59, no. 3, pp. 237–248, Apr. 2009, doi: 10.1680/GEOT.2009.59.3.237.

[26] G. A. Akrouch, M. Sánchez, and J.-L. Briaud, "Effect of the Unsaturated Soil Condition on the Thermal Efficiency of Energy Piles," pp. 1618–1627, Mar. 2015, doi: 10.1061/9780784479087.146.

[27] N. Batini, A. F. Rotta Loria, P. Conti, D. Testi, W. Grassi, and L. Laloui, "Energy and geotechnical behaviour of energy piles for different design solutions," *Appl. Therm. Eng.*, vol. 86, pp. 199–213, Jul. 2015, doi: 10.1016/J.APPLTHERMALENG.2015.04.050.

[28] R. Saggu and T. Chakraborty, "Thermal analysis of energy piles in sand," *Geomech. Geoengin.*, vol. 10, no. 1, pp. 10–29, Jan. 2015, doi: 10.1080/17486025.2014.923586.

[29] L. Laloui and A. di Donna, "Understanding the behaviour of energy geo-structures," *Proc. Inst. Civ. Eng. Civ. Eng.*, vol. 164, no. 4, pp. 184–191, Nov. 2011, doi: 10.1680/CIEN.2011.164.4.184.

[30] C. W. W. Ng, A. Gunawan, C. Shi, Q. J. Ma, and H. L. Liu, "Centrifuge modelling of displacement and replacement energy piles constructed in saturated sand: A comparative study," *Geotech. Lett.*, vol. 6, no. 1, Jan. 2016, doi: 10.1680/JGELE.15.00119.

[31] C. W. W. Ng, C. Shi, A. Gunawan, and L. Laloui, "Centrifuge modelling of energy

piles subjected to heating and cooling cycles in clay," *Proc. Inst. Civ. Eng. Struct. Build.*, vol. 4, pp. 310–316, Oct. 2014, doi: 10.1680/GEOLETT.14.00063.

[32] C. G. Olgun, T. Y. Ozudogru, S. L. Abdelaziz, and A. Senol, "Long-term performance of heat exchanger piles," *Acta Geotech.*, vol. 10, no. 5, pp. 553–569, Oct. 2015, doi: 10.1007/S11440-014-0334-Z.

[33] J. Gao, X. Zhang, J. Liu, K. S. Li, and J. Yang, "Thermal performance and ground temperature of vertical pile-foundation heat exchangers: A case study," *Appl. Therm. Eng.*, vol. 28, no. 17–18, pp. 2295–2304, Dec. 2008.

[34] O. Ghasemi-Fare, "GEOTHERMAL ENERGY HARVESTING THROUGH PILE FOUNDATIONS-ANALYSIS-BASED PREDICTION AND PERFORMANCE ASSESSMENT Omid Ghasemi-Fare," The Pennsylvania State University, 2015.

[35] C. A. Kramer and P. Basu, "Experimental Characterization of Energy Output from a Model Geothermal Pile," pp. 3703–3712, Feb. 2014, doi: 10.1061/9780784413272.359.

[36] K. D. Murphy and J. S. McCartney, "Seasonal Response of Energy Foundations During Building Operation," *Geotech. Geol. Eng.*, vol. 33, no. 2, pp. 343–356, Apr. 2015, doi: 10.1007/S10706-014-9802-3.

[37] T. You and H. Yang, "Feasibility of ground source heat pump using spiral coil energy piles with seepage for hotels in cold regions," *Energy Convers. Manag.*, vol. 205, Feb. 2020, doi: 10.1016/J.ENCONMAN.2020.112466.

[38] P. Cui, X. Li, Y. Man, and Z. Fang, "Heat transfer analysis of pile geothermal heat exchangers with spiral coils," *Appl. Energy*, vol. 88, no. 11, pp. 4113–4119, 2011.

[39] "Difference Between Conduction, Convection and Radiation (with Comparison Chart) - Key Differences." https://keydifferences.com/difference-between-conduction-convection-and-radiation.html (accessed Jun. 23, 2022).

[40] D. R. Pitts and L. E. Sissom, *Schaum's Outline of Heat Transfer*, 2nd ed. New York: McGraw-Hill, 1998.

[41] H. J. G. Diersch, D. Bauer, W. Heidemann, W. Rühaak, and P. Schätzl, "Finite element modeling of borehole heat exchanger systems: Part 1. Fundamentals," *Comput. Geosci.*, vol. 37, no. 8, pp. 1122–1135, Aug. 2011, doi: 10.1016/J.CAGEO.2010.08.003.

[42] G. Dibowski and E. al. Sanner B., "VDI Richtlinie 4640-4 Thermische Nutzung des Untergrundes -Direkte Nutzungen-," 2003. [Online]. Available: https://elib.dlr.de/2754/.

[43] "COMSOL Documentation, Material Library," .

[44] "SUS304 Stainless Steel vs SS304." https://matmatch.com/learn/material/sus304-stainless-steel-ss304 (accessed Jan. 07, 2022).

[45] "Polyvinyl Chloride (PVC)." https://matmatch.com/materials/mbas020-unplasticized-polyvinyl-chloride-upvc- (accessed Jan. 07, 2022).

[46] T. Y. Ozudogru, O. Ghasemi-Fare, C. G. Olgun, and P. Basu, "Numerical Modeling of Vertical Geothermal Heat Exchangers Using Finite Difference and Finite Element Techniques," *Geotech. Geol. Eng.*, vol. 33, no. 2, pp. 291–306, Apr. 2015, doi: 10.1007/S10706-014-9822-Z.

[47] A. J. N. Khalifa, "Natural convective heat transfer coefficient – a review: I. Isolated vertical and horizontal surfaces," *Energy Convers. Manag.*, vol. 42, no. 4, pp. 491–504, Mar. 2001, doi: 10.1016/S0196-8904(00)00042-X.

[48] A. J. N. Khalifa, "Natural convective heat transfer coefficient – a review: II. Surfaces in two- and three-dimensional enclosures," *Energy Convers. Manag.*, vol. 42, no. 4, pp. 505–517, Mar. 2001, doi: 10.1016/S0196-8904(00)00043-1.

[49] *Building components and building elements-Thermal resistance and thermal transmittance-Calculation method*. International Organization for Standardization, 2007.

[50] G. Lixia, G. Lei, Z. Ling, and Y. Zhu, "Thermal Conductivity and Heat Transfer Coeffi cient of Concrete," *J. Wuhan Univ. Technol. Sci. Ed*, 2011, doi: 10.1007/s11595-011-0312-3.

[51] J. C. Roy, T. Boulard, C. Kittas, and S. Wang, "PA—Precision Agriculture: Convective and Ventilation Transfers in Greenhouses, Part 1: the Greenhouse considered as a Perfectly Stirred Tank," *Biosyst. Eng.*, vol. 83, no. 1, pp. 1–20, Sep. 2002, doi: 10.1006/BIOE.2002.0107.

[52] T. YENER, Ş. Ç. YENER, and R. MUTLU, "CONVECTION COEFFICIENT ESTIMATION OF STILL AIR USING AN INFRARED THERMOMETER AND CURVE-FITTING," *J. Eng. Technol. Appl. Sci.*, Aug. 2019, doi: 10.30931/JETAS.598862.

[53] "Nonisothermal Flow." https://www.comsol.com/multiphysics/nonisothermal-flow (accessed Jul. 10, 2022).

[54] "Google Earth." https://earth.google.com/web/@63.43860013,10.62238889,7.7075845a,2535.19752493d,35y,-0h,0t,0r/data=OgMKATA?authuser=0 (accessed Jul. 13, 2022).

[55] NGF, "Veiledning for utførelse av totalsodering," 1994. [Online]. Available: www.ngf.no.

[56] E. Haugen, "A preliminary attempt towards soil classification chart from total sounding," *Proc. 17th Nord. Geotech. Meet.*, 2016.

[57] ASTM D5778-12, "Performing Electronic Friction Cone and Piezocone Penetration Testing of Soils," *Astm Int.*, vol. 04.08, no. January 1996, pp. 1–20, 2012, [Online]. Available: papers2://publication/uuid/0587C20D-6DFD-497E-9B2D-F86ED4D75669.

[58] P. K. Robertson, "Soil classification using the cone penetration test," *https://doi.org/10.1139/t90-014*, vol. 27, no. 1, pp. 151–158, 2011, doi: 10.1139/T90-014.

[59] "Bedrock." https://geo.ngu.no/kart/berggrunn_mobil/?lang=eng (accessed Jul. 14, 2022).

[60] "EN 10025-2 Grade S355J2 normalized or normalized formed (+N) - Low Carbon Steel - Matmatch." https://matmatch.com/materials/minfm94067-en-10025-2-grade-s355j2-normalized-or-normalized-formed-n- (accessed Jul. 15, 2022).

[61] "High Density Polyethylene (HDPE) - High Density Polyethylene (PE-HD) - Matmatch." https://matmatch.com/materials/mbas008-high-density-polyethylene-hdpe- (accessed Jul. 15, 2022).

[62] T. Y. Ozudogru, C. G. Olgun, and A. Senol, "3D numerical modeling of vertical geothermal heat exchangers," *Geothermics*, vol. 51, pp. 312–324, 2014, doi: 10.1016/j.geothermics.2014.02.005.

Appendices

Appendix 1: Specialization project report

Appendix 2: BEAR project CPTu and total sounding recordings

Appendix 3: BEAR project numerical simulation

Appendix 1: Specialization project report

Literature review and feasibility study for energy piles in Norway

Potential of geothermal energy piles in Norway, a review

Saeed Abbasi Hassan Abbadi[1], Habibollah Sadeghi[2], Rao Martand Singh[3*]

1. Master of science student, Department of Civil and Environmental Engineering, Norwegian University of Science and Technology, Trondheim, Norway, Email: saeeda@stud.ntnu.no

2. Ph.D. candidate, Department of Civil and Environmental Engineering, Norwegian University of Science and Technology, Trondheim, Norway, Email: habibollah.sadeghi@ntnu.no

3. Professor, Department of Civil and Environmental Engineering, Norwegian University of Science and Technology, Trondheim, Norway, Email: rao.m.singh@ntnu.no (*Corresponding author)

Abstract

Authorities have identified climate change as one of the most critical socio-economic and environmental challenges that the world has ever faced. All countries, governments, and individuals must find ways to reduce their carbon footprints. One choice is to adopt renewable energy sources, which are becoming more popular and gaining traction worldwide. Being a renewable energy source, Geothermal energy can be particularly efficient in producing thermal energy for building heating and cooling. Geothermal energy piles are a viable approach for lowering the installation costs of ground-source heat pumps and buildings' heating/cooling expenses. This paper reviews the applicability of energy piles in Norway, starting with an introductory description of geostructures and geothermal energy worldwide, followed by the adaptivity of using GSHPs in Norway. Then the application of GSHPs in cold-climate regions such as Norway has been discussed, and some solutions to overcome the issue of thermal imbalance have been presented. By justification of these solutions, geothermal energy from shallow depths can be harnessed efficiently, especially by energy piles.

Keywords: Thermal piles, Geothermal energy piles, Norway, Cold climate

Contents

1. Introduction

Authorities have identified climate change as one of the most significant economic, social, and environmental challenges the world has ever faced [1]. The way humans behave today impacts the way the world would be like in the future. All countries, governments, and individuals need to find methods to reduce their carbon footprints. One alternative option is to use renewable energy resources [2], which are becoming increasingly popular and gaining ground worldwide. The International Energy Agency (IEA) recently produced a report titled "Net Zero by 2050," which provides a roadmap for policymakers to achieve net-zero CO_2 emissions by the year 2050 or sooner [3]. IEA describes this path as "consistent with efforts to limit the long-term increase in average global temperatures to 1.5 °C" compared to preindustrial levels, which is the goal of the Paris Agreement, signed by 197 Parties [4]. A shift away from fossil fuels is required to meet the increasing energy demands while addressing economic, social, and environmental concerns. The portion of renewable energy in the electricity sector has been recommended to climb from 25% in 2015 to 85% in 2050 [5]. Energy resources are divided into two categories: renewable energy and nonrenewable energy.

As a result of the Paris Agreement and the Climate Change Act, Section 4, Norway is legally obligated to transition to a low-emission society by 2050. As of now, the target is to cut greenhouse gas emissions by at least 40% by 2030 [6], with a milestone of 2025, and by 80-90 percent from 1990 levels by 2050. Recent reports from the International Energy Agency (IEA) emphasize the importance of making a rapid transition away from fossil fuels in the energy sector. A solid suggestion is to increase innovation and clean investment in energy-efficient renewable technology [4]. Norway has an electricity supply almost entirely dominated by hydropower regarding energy resources. Norway's power production is roughly equal to its consumption, varying from year to year depending on weather conditions. Norwegians are provided with highly flexible and inexpensive electricity, and Table 1 summarizes the annual electricity production and consumption in Norway as provided by the Norwegian statistical institute [7].

Table 1. Annual production and consumption of electricity in Norway up to August 2021 [7]

Production and consumption of electricity		Percentage	Changes in the last 12 months
Production	Hydropower	92.9	-10.9
	Thermal Power Plants	1.4	-50.0
	Wind Power	5.8	34.6
Consumption	Extraction of crude oil and natural gas	7.3	-16.0
	Power-intensive industries	38.8	9.5
	Ordinary supply	53.9	3.0

Due to the low pricing for electricity, other renewable technologies, such as GSHP systems [8], have not been prioritized in Norway. Hydroelectricity has historically served as the foundation of the Norwegian electricity grid. Around 93 percent of the electricity production is through hydropower resources, which have a significant reservoir capacity of 85 TWh. Due to clean and low-cost hydropower prevalence, Norway's power production is almost free of emissions. At the same time, less than 2 percent of produced electricity is generated in thermal power plants, which use a variety of energy sources, including municipal waste, industrial waste, surplus heat, oil, natural gas, and coal. Many of these thermal power plants are located in large industrial installations that use the electricity generated themselves. Production, therefore, often depends on the electricity needs of industry [9]. In Norway, direct electricity or heat pumps meet over 80% of the country's heating needs, resulting in a nearly carbon-neutral level of energy use in residential and commercial buildings.

The transportation sector is undergoing a decarbonization process. Today, electric vehicles account for 54 percent of all new automobiles, and this percentage is expected to rise to 100 percent by 2025, as decided by the Norwegian parliament [9]. Ferries and boats are also making the switch to electric propulsion. By 2022, over 70 battery-powered ferries would be trafficking Norwegian fjords [10]. Norway has a long history of imposing stringent regulations and restrictions on the construction of airtight and well-insulated building envelopes. The structure of the energy performance requirements was first presented in 2008 and has been in place since then. The standards have been gradually strengthened, with the most recent tightening in 2017, requiring energy performance requirements comparable to those of a passive dwelling [11]. By 2020, the government intended to implement a benchmark for near-zero energy consumption. Parliament also challenged the administration to meet a final savings objective of 10 TWh from existing buildings by 2030, established in 2016. In addition, the government outlawed fossil fuel heating systems from new buildings in 2016 and set measures to prohibit the use of fossil fuels for all space heating which began in 2020. Even though Norway is not a member of the European Union, as a member of the European Economic Area (EEA), Norway shares internal market legislation with the European Union. As a result, It has enacted some European Union directives and regulations about energy [12].

Renewable energy is defined as replenishable and steady energy in nature. Examples of renewable energy sources include but are not limited to wind, biomass, tidal, solar, and geothermal energies [13]. The use of geothermal energy as a renewable energy source can be very efficient in providing thermal energy for the heating and cooling of buildings. Traditionally, these technologies have used boreholes or trenches to build ground heat exchangers (GHEs), which exploit the earth as a heat sink/source by combining the pipework with a circulating heat carrier fluid (HCF). On the other hand, Traditional GHEs have significant capital expenditures due to drilling or the required land area. Fortunately, a relatively new alternative strategy has been developed to circumvent this limitation, which involves incorporating pipe loops into geostructures primarily built for structural purposes such as tunnel linings, pile foundations,

retaining walls, and foundation slabs [14]. One of the most straightforward applications of deep geothermal resources is extracting energy to generate electricity. Additionally, there are other applications for deep geothermal systems, such as solar energy storage, heating, and cooling systems in places like residential and office buildings, farms, animal husbandries, industrial applications, and water treatment systems.

The shallow resources, which are limited to depths of less than 200 m, contain both open-loop and closed-loop systems, depending on the system. In open systems, the water is retrieved from a recognized site and, after exchanging energy, it is injected back into the same zone or a position in the vicinity of the spot where it was extracted. Geothermal energy is commonly employed for cooling and heating systems because of its shallow geological resources.

On the contrary, in closed-loop systems, the water circulates in closed loops located inside the energy piles, energy tunnels, energy slabs, sewage energy systems, energy walls, and energy columns are the most common types of heat exchanger geostructures. It is a vertical borehole excavated close to the energy-consuming structure that serves as the borehole heat exchanger. An array of pipes can be inserted into the borehole, and the exchange of energy is carried out with the help of an intermediary fluid [13]. To reduce the installation costs of ground-source heat pumps (GSHP), geothermal energy piles are a promising solution. This is due to the fact that the heat-exchanging pipes are embedded in the building foundations without incurring high additional costs in addition to the already required expenditure for geo-mechanical requirements. On the other hand, the assessment of the design and performance of the geothermal energy piles is a multidisciplinary and thermo-hydro-mechanical process that must be completed while considering all of the factors mentioned above [15].

2. Geothermal energy systems

There are various types of geothermal system classifications. One of the frequently-used classifications is based on the depth of the geothermal energy sources. Geothermal systems can be categorized as shallow or deep geothermal systems depending on whether they are located at a depth of less than 100 to 150 m or greater [16]. Shallow geothermal systems are designed to work in cold temperatures and low enthalpy. Deep geothermal systems can handle temperatures and enthalpy ranging from mild to high [17].

Generally speaking, geothermal systems are composed of three major components: a heat source, a heat sink, and a heat exchanger (or heat exchangers). Typically, the ground serves as the heat source, and the constructed environment serves as the heat sink, i.e., buildings. On the other hand, the inverse can also occur, in which case the heat source is the constructed environment, and the heat sink is the earth's crust (Figure 1). As it is called, the heat exchanger transmits the heat from the source to the sink. Heat exchangers have gone through long historical development [18]. Following are some early development examples of their type. There is evidence that Native Americans were using geothermal energy for cooking purposes as far back as 10,000 years ago. According to archaeological evidence, the Greeks and the Romans utilized baths heated by hot springs in ancient times, and indications of geothermal space heating may be found as far back as the Roman city of Pompeii in the first century CE. In the beginning, geothermal energy applications were restricted to areas where hot water and steam were readily available [19]. Using the ground as a heat source for electrical power generation, Prince Piero Ginori Conti built the world's first geothermal power plant in Italy in 1904 [17].

One of the most distinguishing characteristics of geothermal systems is utilizing the thermal energy harvested from the ground. It is common to utilize geothermal energy in shallow geothermal systems directly, which means heating and cooling a structure directly with geothermal energy. Deep geothermal energy can be used to generate electricity which is an indirect utilization of energy. Aside from machines or devices that force a heat carrier fluid to flow (exchanging heat between them), machines or devices that adjust (enhance or lower) the energy input transported between the ground and the target environment are also used in such situations.

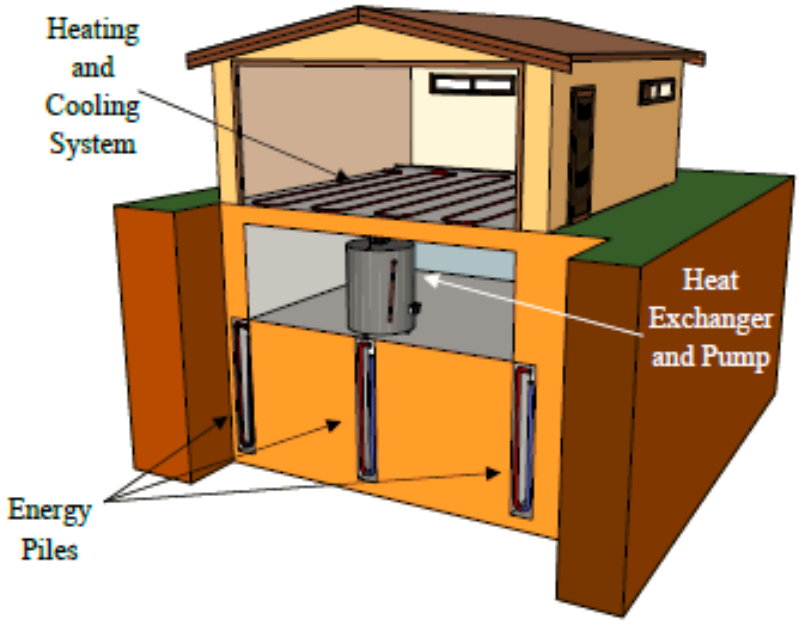

Figure 1. Residential heat pump for summer cooling and winter heating

When an indirect use of geothermal energy is not targeted in deep geothermal systems, it is possible to make direct use of geothermal energy. Instead of machines that modify or control the energy input or output transported between the ground and the target environment, just machines that compel a heat carrier fluid to flow between the ground and the target environment are required in this situation, as opposed to the prior scenario. Shallow geothermal systems that operate at temperatures less than 25°C can provide heat, cooling, and hot water, the temperature available beneath. These systems are environmentally friendly and ideal for small-scale and home use in practically any geographical area. It is possible to use deep geothermal systems to provide heating, hot water, and electricity while taking advantage of temperatures available underground that is greater than 25°C and up to 200°C because the temperatures required for electrical power generation are generally greater than 175°C [20]. Unlike shallow geothermal systems, which are appropriate for medium to large-scale applications, these systems can be implemented in more specific places than shallow geothermal systems. Shallow geothermal systems can be classified as either closed-loop or open-loop systems [20]. Closed-loop systems use a water-based combination that circulates through sealed pipes to transmit heat from the ground to the superstructure or vice versa, depending on the application. While in open-loop systems, the groundwater is taken from or injected into aquifers through wells, used directly in the heat exchange process[21].

Horizontal ground heat exchangers (GHEs) are the shallowest geothermal system, generally located at a depth of less than 10 m [20]. In most cases, these systems comprise closed polyethylene pipes plowed or excavated horizontally into the ground next to the desired building. A flowing

heat carrier fluid in the pipes permits the interchange of heat present in the ground (primarily due to solar radiation), beneficial for heating purposes in residential, agricultural, and aquaculture applications. While it is possible to achieve energy storage goals by drilling deep geothermal baskets can be used as a more compact system than horizontal and vertical geothermal boreholes, and they can be used for the same objectives as horizontal geothermal boreholes. These systems, which usually are buried in the ground at a depth of a few meters, i.e., less than 10 m [22], are composed of closed polyethylene pipes fixed in a spiral geometry through which a heat carrier fluid flows and are typically buried at a depth of several meters. The most significant advantage of horizontal GHEs and geothermal baskets is the application for previously constructed buildings.

Table 2. Characteristics of geothermal systems [22], [17], [20], [23]

system	Depth [m]	Harvested temperature [°C]	Primary circuits	Application	Ecology
Horizontal GHEs	<10	<12	Closed-loop	New or renovated single-family houses or small-scale businesses	Needs 20-30% electricity boost Emitting 5 ton/yr less CO_2
Geothermal baskets					
Foundation piles, tunnels, walls	<50			Larger buildings	
Ground water wells	<200	<17	Open-loop	Single-residential houses	
The array of geothermal boreholes	<100 (500)	<25	Closed-loop	Single-residential houses, Larger buildings	
Mine water energy	<800	<25	Open-loop	Larger private or industrial buildings	Needs electricity for pumping water
Thermal springs	<1000 (3000)	<100	Open-loop	Bathing, local or district heating	
Deep hydrothermal Systems	>3000	<120	Open-loop	Generating electricity, District heating	No CO_2 produced
Petrothermal systems	>5000	<150	Open-loop		

Furthermore, applications that spiral coils are located in surface water reservoirs adjacent to buildings are also feasible. However, such applications require the reservoirs to be located deep enough to avoid conditions detrimental to system operation, such as freezing the reservoir water and the circulating heat carrier fluid in the pipelines. When underground mines are abandoned, the pumps that keep them dry are often switched off, and the mines get filled with water. Geological processes heat this water, and the temperature remains stable year-round. UK coal authorities have calculated that the constantly replenishing water within these mines could potentially be a resource to provide all of the heating requirements for the coalfield areas [24].

Groundwater capture systems use open wells surrounded by groundwater reservoirs (around 200 m deep) [22]. These systems can be used in situations with no hydrological, geological, or environmental constraints to contend with. They are primarily employed for heating water by extracting the thermal energy contained within the underlying water. Singular wells can be utilized for small-family house sizes. Doublet wells are typically required in more significant constructions. It may be necessary to use extraction and injection wells to maintain a balanced underground thermal field, which is necessary for the performance and, in some circumstances, environmental considerations. Unlike the previous applications, vertical geothermal boreholes (single or an array of boreholes) are made out of closed polyethylene pipes buried vertically in the earth beneath or next to buildings at greater depths than the previous ones (from 100 meters to 500 meters) [22], [23]. To improve the heat exchange between the earth and the pipes, a filler material (for example, bentonite) is typically inserted in the borehole. A heat carrier fluid (HCF) circulating in the pipes provides heat exchange for heating, cooling, storing, and producing hot water in a wide range of construction types and environments. Single boreholes can provide enough water to supply tiny residential structures. Borehole fields (an array of several boreholes) are necessary to feed more significant buildings with thermal energy. Higher energy inputs than those transferred through shallower geothermal systems can be attained using vertical geothermal boreholes due to the higher temperature levels of the ground at the specified depths compared to shallower geothermal systems. New geothermal systems, known as energy geostructures, combine the structural support role of any structure in contact with the ground with the heat exchanger role of shallow geothermal systems, resulting in outcomes comparable to or even better than those achieved by the previously described systems.

Thermal springs are often considered part of deep geothermal systems, while they can also be found at depths characteristic of shallow geothermal systems. A relatively deep heated groundwater reservoir in the subsurface surrounds open wells in this type of arrangement, allowing easy access to the water. Thermal energy extracted from subterranean water is primarily utilized for bathing and medical purposes, and these devices were historically popular. Open-well hydrothermal systems draw groundwater from depths where the temperature and thermal energy available are high enough to allow for the implementation of large-scale heating applications to be realized (from a depth up to 3000 m) [22], [17]. Although these systems are typically employed in district heating, they can efficiently heat immense industrial or agricultural structures and even generate electricity. Like hydrothermal systems, petroleum thermal systems draw groundwater using open wells at a greater depth than hydrothermal systems (from a depth of more than 4 to 5 km). The high temperature and thermal energy inherent in the water at these depths can be utilized to produce and provide enormous amounts of electrical energy on a large scale [17], [22].

3. Benefits and limitations of the technology

Various potential obstacles need to be addressed when constructing and using geothermal piles [25]. As a result of the newness of this technology, there are several concerns to consider. First and foremost, there is a significant scarcity of qualified personnel at all stages of the procurement chain. For example, locating qualified drilling operatives with the appropriate level of competence might be challenging, resulting in flooded building sites, failed drilling, broken pipelines, and malfunctioning systems, among other consequences. Insufficient experience and knowledge among consultants and a lack of design standards result in poor specifications and integration of GSHPS into building constructions. Contractors may have the option to supply lower-quality equipment, supplies, and craftsmanship than may be expected due to this situation. Some contractors provide solutions to reduce carbon dioxide emissions, while others optimize their offerings to reduce installation costs. The influence of cyclic heating and cooling on pile performance is a source of considerable concern. Several extensive investigations have explored the effects of this repeated heating and cooling. One example of these studies is the EPFL [26] and another at Lambeth College in London [27]. Both studies looked at the effects of repeated heating and cooling. Thermal testing was carried out on a group of geothermal test piles in Lausanne at various periods throughout the construction of the building. Heating and recovery cycles were conducted on the piles as the building was constructed and increased loads were placed. According to the findings of Mimouni and Laloui in Lausanne, the thermal loads applied to geothermal piles cause extra stresses to be applied to the adjacent structural piles, resulting in a decrease in lateral friction. That geothermal piles can be built to absorb thermal impacts without generating excessive subsidence of the foundations was proved by this study.

There were 146 piles in the Lambeth College project, each with a length of 25 m. During the seven-week timeframe of the study, pile-loading tests were carried out that included temperature cycles and a prolonged period of maintained loading. When the pile was heated, it was discovered that additional concrete stresses, in addition to those caused by static loading, were formed. Thermal cycling, however, did not result in an overly high mobilization of shear stresses at the pile/soil interface, and it was found that the geotechnical capability of the piles was not compromised and that only minor settlements occurred [27].

The possibility of long-term "below ground global warming" or "below ground global cooling" is also a concern, as it is produced by an imbalance in the heating and cooling demands of the structures above. This is especially true as geothermal piles become more common in densely populated areas. Among the possible solutions to this problem are diversifying the types of buildings supplied by geothermal piles in the local region and designing structures in such a manner that the heating and cooling demands are balanced (for example, if there is a high cooling demand, incorporate water heating into the system to balance this). The ground can be artificially helped back to its original temperature if these strategies fail in the long run. For example, dry coolers, which use ambient air to cool down the steam in powerplants, can be modified to cool

down the HCF and can be used to cool the ground, or waste heat can recharge the ground if the heating demand across the year is unbalanced [25].

A serviceability limit state can be reached in various ways, resulting in the failure of a ground energy system. Given that geothermal energy piles are subjected to dynamic thermal loads over an extended period. Geothermal system failures can be classified as (a) short-term failures (i.e., within one annual cycle), or (b) long-term failures (i.e., beyond one annual cycle but during the design life of the building), or (c) Noncompliance with regulatory norms (e.g., abstraction licensing of open-loop systems) [21]. Failure of a ground energy system would express itself in the ground energy system's inability to meet peak heating or cooling loads or collect heat from the ground, or a constant drop of ground temperature, leading to an unbalanced heave of foundation [28]. The failure can be a steady increase or drop in ground temperature and a gradual decline in system efficiency, While the ground energy system is capable of meeting the thermal load requirements of the building [28].

4. Worldwide use of Geothermal Energy piles

Energy geostructures such as piles, walls, tunnels, and slabs, are increasingly being used as the primary unit in the heat exchanger systems, allowing buildings to benefit from the ground's stable temperature for more efficient heating and cooling in recent years. Many projects worldwide have used full-scale energy piles in structures and experiments. These projects include the Euros office center high-rise building in Vienna [29], the Frankfurt main tower, the Dock E at the Zurich airport [30], and many other projects in countries like Japan [30], the United Kingdom [31], China [32], Australia [33], Turkey [34], and the United States [35]. According to the results of these studies, energy piles can be used as long-term geothermal heat exchangers because of their response to soil-structure interaction and heat exchange capabilities, respectively. [36] The primary advantage of energy piles is that they improve the energy efficiency of building heat without requiring extra infrastructure or resources beyond those required for building support [36].

Countries have committed to altering their energy consumption regulations to achieve a comprehensive agreement to reduce greenhouse gas emissions and prevent global warming and climate change. The Paris Agreement, which is part of the United Nations Framework Convention on Climate Change (UNFCCC), is one of the many international accords on mitigating greenhouse gas emissions that have been reached [37]. Additionally, the Kyoto Protocol, which is annexed to the frameworks established by the United Nations, restricts the production of greenhouse gases by the states that have signed on to the agreement with the United Nations [38]. Beyond that, most industrialized countries, including the European Union, Denmark, Japan, South Korea, California, the United States, the United Kingdom, Australia, and Switzerland, have specified main goals, according to the World Bank. Using geothermal energy to heat and cool residential and

commercial buildings has been used in most parts of the world as a clean and sustainable energy source to address partial heating and cooling needs. Shallow geothermal energy can cut carbon dioxide emissions from buildings by up to 50% while reducing a significant amount of nitrogen oxide and sulfur dioxide emissions from conventional buildings. A total of 88 countries have adopted energy piles, which are essentially ground source heat pump systems in general [34].

The heat exchanger tubes are embedded in the building's structural parts to minimize the amount of drilling required. In the early 1980s, the concept of embedding heat exchanger tubes within structural parts was first floated around. Those pipes have been embedded in the foundation slabs, precast and bored piles (pile foundation), and diaphragm walls [39].

Recent decades have seen three prominent end-users characterize final energy consumption in the European Union and industrialized countries such as the United States: the construction sector, the industrial sector, and the transportation sector [17]. In 2020, these three sectors contributed 27.6 percent, 25.2 percent, and 29.6 percent, respectively, to the total final energy consumption of the European Union [40]. A significant portion of the final energy consumption in the building sector in Norway is utilized for space conditioning and household hot water, like in many other affluent nations. In addition to the data mentioned above, the world's final energy consumption and primary energy supply are increasing to keep up with the growing world population and the expansion of economies. Since the beginning of time, the global energy market has been and continues to be dominated by the combustion of fossil fuels, which are nonrenewable primary energy resources. During recent years (since the middle of the twentieth century), fossil fuels have provided at least 60 percent of total final energy consumption and at least 80 percent of total primary energy production [17].

5. Prospective of Geothermal Energy use in Norway

Net-zero society is Norway's goal by 2050. Norway would achieve a fossil-fuel-free energy system by reaching this milestone. Furthermore, it is a power-intensive sector that provides jobs and value, has surpluses of energy that can be exported, and enjoys energy independence. Norway must generate more renewable energy and use it more effectively and efficiently to achieve this goal, releasing more energy into the system. More than half of Norway's electricity consumption is devoted to heating and cooling homes and businesses. It has been shown that using geothermal energy in conjunction with heat pumps can reduce this usage by more than half, and in the long term, it can release up to 40 TWh of energy each year [41].

Norwegian geothermal energy utilization is dominated by the widespread use of geothermal heat pumps, which are used to generate electricity [42]. According to the Norwegian heat pump organization (NOVAP), the number of ground-source heat pump installations peaked at 3900 in 2018. The number of recent annual installations has been around 2400 [42]. These facts are

illustrated in Figure 2. The dramatic decline in installed GSHP over the last two years, beginning in 2019, could be attributed to the Covid-19 epidemic, which has impacted all markets. Another determining factor is the disagreements between OPEC+ members, resulting in a temporary production boost despite decreased demand. In short, these events have fundamentally altered the global energy situation and decreased energy prices. Some believe the falling price of crude oil could slow the rise of renewables in the energy mix [43].

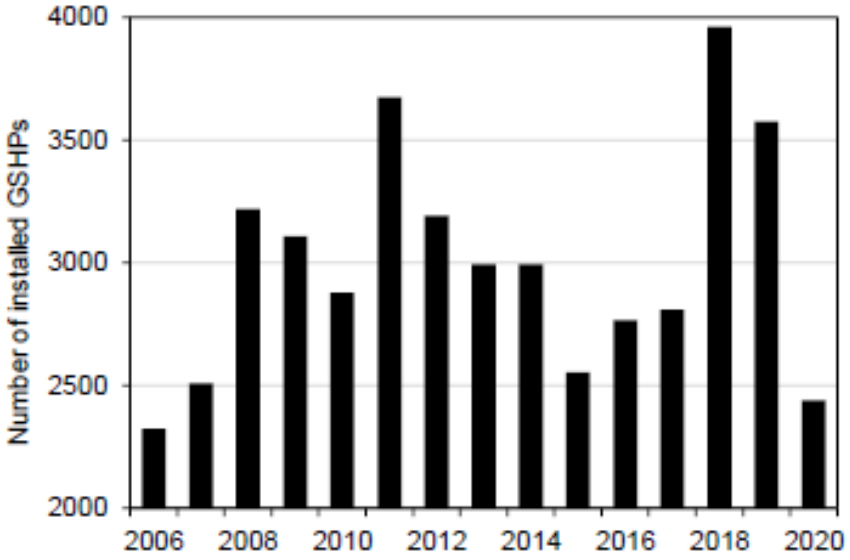

Figure 2. Annual installed GSHPs in Norway [42]

Two 1500-m geothermal wells were built in 2018 at Oslo Avinor airport. The wells were constructed to de-ice the engine test area of the airport during the winter. The heat from the wells is used in an indirect manner [44]. Norwegian geothermal energy is not used to generate power, and there are no geothermal energy installations with wells deeper than 1500 m in operation. Norwegian energy policy, which emphasizes the use of renewable energy sources, is consistent with the country's rising use of geothermal energy. Deep drilling, well technology, reservoir management, corrosion, and scaling reduction are expected to be among the areas where Norwegian industrial and academic competence in off-shore technologies would be most effectively applied in a nascent geothermal industry [45].

Norwegian authorities proposed legislation in June 2017 that would prohibit the use of petroleum (often known as "fossil oil") for the heating of buildings starting in 2020. Mineral oil is prohibited in residential structures, public buildings, and commercial buildings in the primary heating system (baseload) and the supplemental heating system (peak load). The prohibition has been implemented to reduce greenhouse gas emissions. Because hydroelectricity accounts for nearly all of Norway's electricity generation, the country's electricity consumption might have no impact on greenhouse gas emissions. As a result, electrical equipment is primarily responsible for heating dwellings and providing tap water (ovens, heat pumps). District heating and wood stoves

each make a significant contribution, accounting for around 10% of the total. The total emissions from district heating in the non-ETS sector are less than one millimetric ton of carbon dioxide equivalent and are related to trash incineration [6]. Wood or other types of biomass burning for household heating and cooking contributes significantly to atmospheric pollution. Nitrogen oxides (NOx), carbon monoxide (CO), and particulate matter are emitted during wood fuel combustion. Particulate matter is composed of organic substances, such as a high polycyclic aromatic hydrocarbon [46].

According to the Norwegian Water Resources and Energy Directorate (NVE), ground-source heat-based heat pump technology can provide all of Norway's heating and cooling requirements. In 2030, it is estimated that Norway will use 52.7 and about 2 TWh/year of heating and cooling, respectively [47]. It has been shown that using solar heat stored in the soil, water, and bedrock can reduce electricity purchase demands by up to 70% and, in more complex systems, by 75-98 percent [48]. According to the cost analysis, unit costs for ground heating were more cost-effective and lucrative than competing technologies. The profitability of ground heating improves with the size of the plant, and systems that provide both heating and cooling services are desirable.

Geological characteristics, such as a thick loose material layer, increase investment costs but, in most cases, do not influence profitability. The proportion of total investment allocated to boreholes, including transportation to technical rooms, increases as the plant grows. It is clear from the national cost curve that there are primary facilities for extracting heat with unit costs of 46.2 øre/kWh and higher, which demonstrates the enormous potential for ground heat. A total of approximately 31.5 TWh/year is available to households that use small heat pumps, with 22.2 TWh/year at the cost of 70.4 øre/kWh and 9.3 TWh/year at the expense of 83.1 øre/kWh for areas with thin and thick loose material cover, respectively. The price of power has a significant impact on the estimated unit costs. Since the COP (coefficient of performance) for heat pumps (especially GSHPs are high), higher costs for electricity and other competitive energy products have significantly improved the profitability of GSHPs. In addition to predictable running costs, low maintenance requirements, excellent reliability, and the use of locally available, renewable, and emission-free solar heat from bedrock, groundwater, and soil are all key advantages [47].

Pile types used in typical construction projects in Norway include precast or cast-in-situ concrete piles, driven or drilled steel piles, and timber piles. In Norway, precast concrete piles are widely used as end-bearing piles, but they may also be used as friction piles in sand, gravel, and solid clay. Most precast concrete piles are quadratic in shape with diameters of 230×230, 270×270, and 345×345 mm. Precast piles typically have a design capacity of between 1000 and 3000 kN [49]. Typically, energy piles are constructed of cast-in-situ reinforced concrete. They vary from ordinary piles technically only in that pipes are fastened along their reinforcing cage or are embedded inside the filling material [17]. The primary disadvantages of using precast concrete elements as energy piles are the length of the precast segments, which may need to be reduced, and the damage to energy pipelines caused by driving the pile [4].

6. Application of geothermal piles in a cold climate

While geothermal heat pumps and energy piles are among the fastest-growing renewable energy applications worldwide, there are still significant challenges to broader adoption, especially in cold locations like Norway, where winters may be long and harsh. A thermal imbalance under the earth is often generated by an unequal heat extraction/injection from/into the ground. Thermal imbalance is one of the most challenging obstacles to overcome. As energy extracted from the soil surpasses the heat supplied during GSHP operation, the subsurface temperature gradually decreases, failing the GSHPs [50]. Previous scholars proposed strategies for resolving issues that arose due to thermal imbalance [50], [51], [52], and [53]. The following paragraphs discuss some of the most important solutions.

It is possible to use a supplemental heat absorber to increase the performance of the GSHP system in cold climates, which is referred to as the hybrid GSHP (HGSHP) system. It is possible to significantly reduce the quantity of heat extracted from the ground by incorporating a supplemental heat absorber, efficiently balancing the ground thermal loads, thus lowering the system's initial cost and enhancing its operating performance [51]. A solar thermal collector can significantly reduce the size of a ground-source heat pump and installation cost, making GSHP systems more economically viable [54]. Solar heat can either inject heat into the soil to maintain thermal balance or support a portion of the required energy production [50]. Another method for supplying space heating and domestic hot water is using waste heat as an auxiliary heat source. The heat wasted into the atmosphere from different sources such as subway tunnels [55], micro gas turbines [56], or industries [57] are insufficient to supply a portion of residential heating and hot water demands. When the sources mentioned above are integrated with GSHP, they can be effective, efficient, and environmentally and economically beneficial. Another possible source of heat that can be combined with GSHP is small-scale biogas reactors that can intake the food waste of a neighborhood with several inhabitants and produce biomethane to provide heat that can be integrated with GSHP systems [58].

A GHE modification strategy is explicitly recommended to alleviate less severe underground thermal imbalances. The GHE configuration adjustments are the primary focus of this method of implementation. These modifications include extending the length of the borehole and increasing the space between them [59], which is not feasible in most cases because the pile's structural characteristics should be checked before changing the pile's configuration. Moreover, improving the thermal features of the filling materials used in the boreholes and the soil surrounding them is another adjustment that enhances the performance of GHE. The filling material thermal features improvement can be achieved by increasing the grout and soil [60], which accelerates the soil heat recovery process.

7. Conclusion and recommendations

- With the widespread use of geothermal piles in many countries, it has been demonstrated that shallow geothermal energy provides a cost-effective technique of heating and cooling buildings, particularly in areas with cold climates and lengthy winters.
- Norway is located in northern Europe, and because of its high latitude, it has mild to cold weather. Due to a soft sedimentary top layer covering the bedrock in most parts of the country, it is common in Norway to pile the building structures using end-bearing piles stacked to rock.
- Among the piles used for building construction in Norway, quadratic precast piles driven into the ground are the most common. Equipping the driven piles to HCF tubes and their installation makes it challenging.
- In Norway, the yearly heating demand is greater than the annual cooling demand. As a result, the quantity of heat retrieved from the ground during the winter is significantly more than the amount of heat injected into the ground during the summer.
- The difference between extracted and injected heat causes an underground thermal imbalance, which may decrease the efficiency of the GSHP system. In the current paper, some of the long-term impacts of ground thermal imbalance have been addressed, and suggestions on modification of GHE and some supplemental heat absorbers to improve the performance of GHE are reviewed.

8. References

[1] "Climate Change 'Biggest Threat Modern Humans Have Ever Faced', World-Renowned Naturalist Tells Security Council, Calls for Greater Global Cooperation | Meetings Coverage and Press Releases." https://www.un.org/press/en/2021/sc14445.doc.htm (accessed Dec. 06, 2021).

[2] M. De Moel, P. M. Bach, A. Bouazza, R. M. Singh, and J. O. Sun, "Technological advances and applications of geothermal energy pile foundations and their feasibility in Australia," *Renew. Sustain. Energy Rev.*, vol. 14, no. 9, pp. 2683–2696, 2010, doi: 10.1016/j.rser.2010.07.027.

[3] I. Energy Agency, "Net Zero by 2050 - A Roadmap for the Global Energy Sector," 2021. Accessed: Dec. 06, 2021. [Online]. Available: www.iea.org/t&c/.

[4] O. S. Lillevold, "Potential of geothermal energy piles in Norway," 2021.

[5] D. Gielen, F. Boshell, D. Saygin, M. D. Bazilian, N. Wagner, and R. Gorini, "The role of renewable energy in the global energy transformation," *Energy Strateg. Rev.*, vol. 24, pp. 38–50, Apr. 2019, doi: 10.1016/J.ESR.2019.01.006.

[6] Norwegian Ministry of Climate and Environment, "Norway's National Plan related to the Decision of the EEA Joint Committee," 2019.

[7] statistical institute of Norway, "Energy and manufacturing / Energy / Electricity." https://www.ssb.no/energi-og-industri/energi/statistikk/elektrisitet (accessed Oct. 18, 2021).

[8] K. H. Kvalsvik, K. Midttømme, and R. K. Ramstad, "Geothermal Energy Use, Country Update for Norway," in *European Geothermal Congress*, 2019, no. June, pp. 1–8.

[9] "Electricity production - Energifakta Norge." https://energifaktanorge.no/en/norsk-energiforsyning/kraftproduksjon/ (accessed Dec. 06, 2021).

[10] "Electric ferries." https://www.tekna.no/en/news/newsletter-february-2019/electric-ferries/ (accessed Dec. 06, 2021).

[11] *NORSK LOVTIDEND Avd. I Lover og sentrale forskrifter mv. Forskrift om tekniske krav til byggverk (Byggteknisk forskrift)*. 2017.

[12] K. Midttømme, M. Justo Alonso, C. Krafft, K. Kvalsvik, R. Ramstad, and J. Stene, "Geothermal Energy Use in Norway, Country Update for 2015-2019," 2020.

[13] A. Akbari Garakani, E. Motevali Haghighi, A. Rahnavard, M. Beigi, M. Kabiri Tadi, and T. Razmkhah, "A Feasibility Study on Implementing the Energy Piles in Electric Power Industries," *Springer Ser. Geomech. Geoengin.*, vol. 0, no. 217729, pp. 211–217, Sep. 2018, doi: 10.1007/978-3-319-99670-7_27.

[14] N. Makasis, G. A. Narsilio, A. Bidarmaghz, and I. W. Johnston, "The Application of Retaining Walls and Slabs as Energy Structures in Underground Train Stations," *Springer Ser. Geomech. Geoengin.*, vol. 0, no. 217729, pp. 43–50, Sep. 2018, doi: 10.1007/978-3-319-99670-7_6.

[15] P. Conti, E. Schito, and D. Testi, "Thermal Characterization of Energy Pile Dynamics: SEG-2018," 2019, pp. 123–131.

[16] H. Shao, P. Hein, A. Sachse, and O. Kolditz, *Geoenergy Modeling II Shallow Geothermal Systems*. Cham, Switzerland: Springer, 2016.

[17] L. Laloui and A. Rotta Loria, *Analysis and Design of Energy Geostructures: Theoretical Essentials and Practical Application*. San Diego: San Diego: Elsevier Science & Technology, 2019.

[18] R. Cataldi, "The Year Zero of Geothermics," Sacramento, California, 1999. [Online]. Available: https://www.geothermal-library.org/index.php?mode=pubs&action=view&record=1018266.

[19] J. W. Lund, "geothermal energy, Description, Uses, History, & Pros and Cons ," *Britannica*. 2018, Accessed: Dec. 07, 2021. [Online]. Available: https://www.britannica.com/science/geothermal-energy.

[20] G. Narsilio, I. Johnston, A. Bidarmaghz, O. Mikhayalova, O. Kivi, and R. Aditaya, "Geothermal Energy: Intorducing an emerging technology," *Adv. Civ. Eng. Sustain. Dev.*,

no. August, pp. 141–154, 2014.

[21] M. Preene and W. Powrie, "Ground energy systems: From analysis to geotechnical design," *Geotechnique*, vol. 59, no. 3, pp. 261–271, 2009, doi: 10.1680/geot.2009.59.3.261.

[22] "Geothermal Switzerland - Swiss Geothermal Association (SVG)." https://geothermie-schweiz.ch/ (accessed Dec. 08, 2021).

[23] "Geothermal energy - British Geological Survey." https://www.bgs.ac.uk/geology-projects/geothermal-energy/ (accessed Dec. 08, 2021).

[24] "Geothermal energy from abandoned coal mines - Coal Authority." https://www2.groundstability.com/geothermal-energy-from-abandoned-coal-mines/ (accessed Dec. 08, 2021).

[25] "Geothermal pile foundations - Designing Buildings." https://www.designingbuildings.co.uk/wiki/Geothermal_pile_foundations#Geothermal_piles (accessed Nov. 07, 2021).

[26] T. Mimouni and L. Laloui, "Behaviour of a group of energy piles," *Can. Geotech. J.*, vol. 52, no. 12, pp. 1913–1929, May 2015, doi: 10.1139/CGJ-2014-0403.

[27] P. J. Bourne-Webb, B. Amatya, K. Soga, T. Amis, C. Davidson, and P. Payne, "Energy pile test at lambeth college, London: Geotechnical and thermodynamic aspects of pile response to heat cycles," *Geotechnique*, vol. 59, no. 3, pp. 237–248, 2009, doi: 10.1680/GEOT.2009.59.3.237.

[28] H. Brandl, "Energy foundations and other thermo-active ground structures," *Geotechnique*, vol. 56, no. 2, pp. 81–122, Mar. 2006, doi: 10.1680/GEOT.2006.56.2.81.

[29] D. Adam and R. Markiewicz, "Energy from earth-coupled structures, foundations, tunnels and sewers," *Geotechnique*, vol. 59, no. 3, pp. 229–236, 2009, doi: 10.1680/geot.2009.59.3.229.

[30] L. Laloui, M. Nuth, and L. Vulliet, "Experimental and numerical investigations of the behaviour of a heat exchanger pile," *Int. J. Numer. Anal. Methods Geomech.*, vol. 30, no. 8, pp. 763–781, Jul. 2006, doi: 10.1002/NAG.499.

[31] P. J. Bourne-Webb, B. Amatya, K. Soga, T. Amis, C. Davidson, and P. Payne, "Energy pile test at Lambeth College, London: geotechnical and thermodynamic aspects of pile response to heat cycles," *Géotechnique*, vol. 59, no. 3, pp. 237–248, Apr. 2009, doi: 10.1680/GEOT.2009.59.3.237.

[32] J. Gao, X. Zhang, J. Liu, K. Li, and J. Yang, "Numerical and experimental assessment of thermal performance of vertical energy piles: An application," *Appl. Energy*, vol. 85, no. 10, pp. 901–910, Oct. 2008.

[33] G. A. Narsilio and Q. Lu, "Cost Effectiveness of Energy Piles in Residential Dwellings in Australia," *Curr. Trends Civ. Struct. Eng.*, vol. 3, no. 3, Jul. 2019, doi: 10.33552/CTCSE.2019.03.000564.

[34] J. W. Lund and A. N. Toth, "Direct utilization of geothermal energy 2020 worldwide

[48] R. K. Ramstad, "Grunnvarme i Norge - kartlegging av økonomisk potensial," 2011. [Online]. Available: http://webby.nve.no/publikasjoner/oppdragsrapportA/2011/oppdragsrapportA2011_05.pdf .

[49] "GEO foundation & rock drilling AS - GEO foundation & rock drilling AS." https://geofb.no/ (accessed Dec. 25, 2021).

[50] M. Saaly and P. Maghoul, "Thermal imbalance due to application of geothermal energy piles and mitigation strategies for sustainable development in cold regions: a review," *Innov. Infrastruct. Solut.*, vol. 4, no. 1, pp. 1–18, Dec. 2019, doi: 10.1007/S41062-019-0224-1/FIGURES/8.

[51] H. Yang, P. Cui, and Z. Fang, "Vertical-borehole ground-coupled heat pumps: A review of models and systems," *Appl. Energy*, vol. 87, no. 1, pp. 16–27, 2010, doi: 10.1016/j.apenergy.2009.04.038.

[52] Z. Wang, D. Huang, P. Wang, Q. Shen, Q. Zhang, and Y. Sun, "An Analysis of Solar Heating System Assisted by Ground-source Heat Pumps in Office Building," *Procedia Eng.*, vol. 121, pp. 1406–1412, 2015, doi: 10.1016/j.proeng.2015.09.049.

[53] F. M. Rad, A. S. Fung, and W. H. Leong, "Feasibility of combined solar thermal and ground source heat pump systems in cold climate, Canada," *Energy Build.*, vol. 61, pp. 224–232, Jun. 2013, doi: 10.1016/J.ENBUILD.2013.02.036.

[54] A. D.; Chiasson and C. Yavuzturk, "Assessment of the Viability of Hybrid Geothermal Heat Pump Systems with Solar Thermal Collectors," *ASHRAE Trans.*, vol. 109, p. 487, 2003.

[55] Y. Chai, T. Sun, H. Han, F. Cao, and Y. Liu, "Modularly Design for Waste Heat Recovery System in Subway Based on Air Source Heat Pump," *Procedia Eng.*, vol. 205, pp. 273–280, 2017, doi: 10.1016/j.proeng.2017.09.964.

[56] B. Dehghan B., "Performance assessment of ground source heat pump system integrated with micro gas turbine: Waste heat recovery," *Energy Convers. Manag.*, vol. 152, no. June, pp. 328–341, 2017, doi: 10.1016/j.enconman.2017.09.058.

[57] H. Fang, J. Xia, A. Lu, and Y. Jiang, "An operation strategy for using a ground heat exchanger system for industrial waste heat storage and extraction," *Build. Simul.*, vol. 7, no. 2, pp. 197–204, 2014, doi: 10.1007/s12273-013-0140-9.

[58] S. Abbasi, J. Anglevik, V. Ballal, V. Selvik, E. Steinset, and M. Quintanilla, "Small-scale biogas plant in Moholt student village (Unpublished)," Trondheim, 2021.

[59] Y. Shang, M. Dong, and S. Li, "Intermittent experimental study of a vertical ground source heat pump system," 2014, doi: 10.1016/j.apenergy.2014.09.072.

[60] A. D. Chiasson, S. J. Rees, and J. D. Spitler, "Preliminary assessment of the effects of groundwater flow on closed-loop ground-source heat pump systems," *ASHRAE Trans.*, vol. 106, no. January, 2000.

Appendix 2: BEAR project CPTu and total sounding recordings

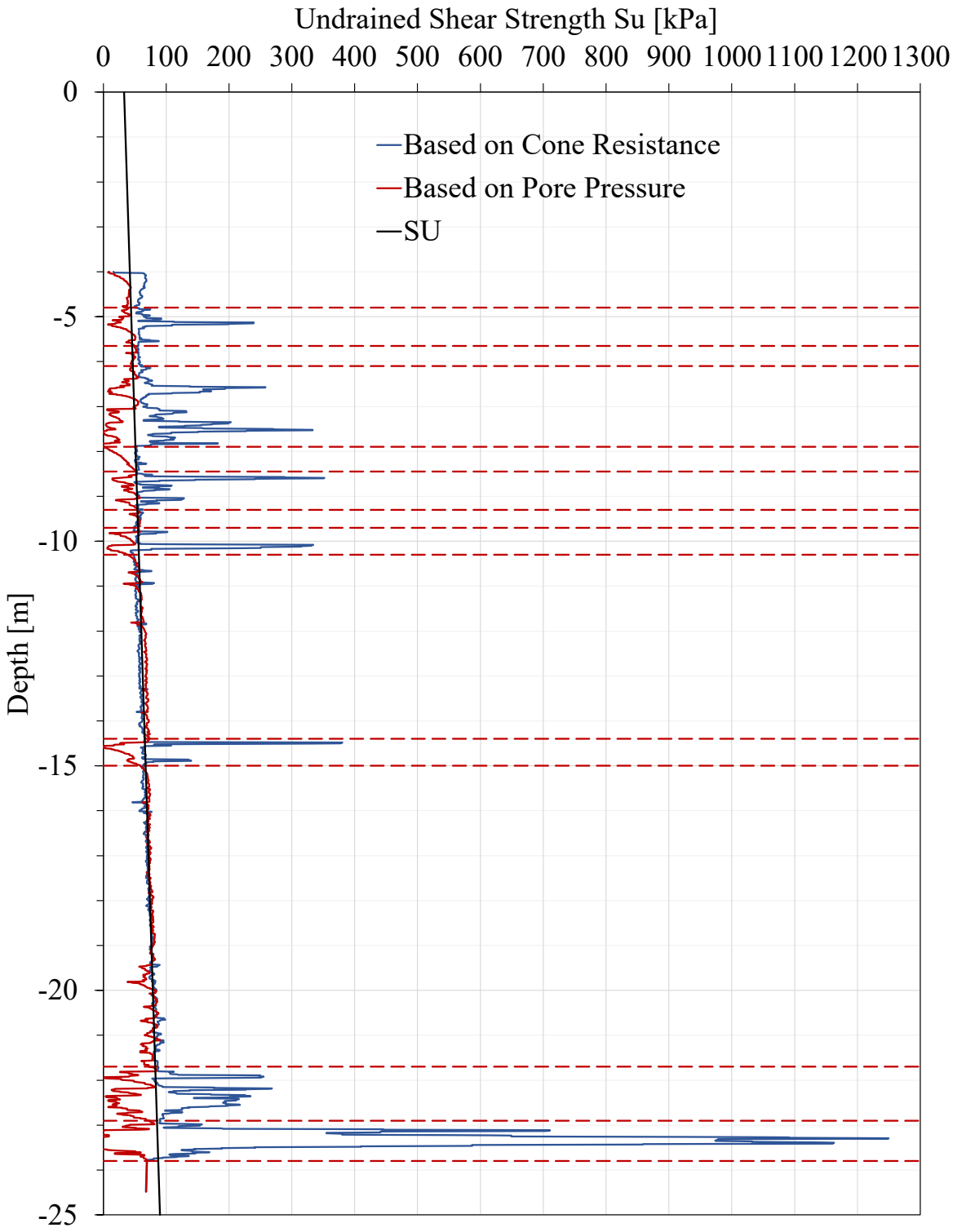

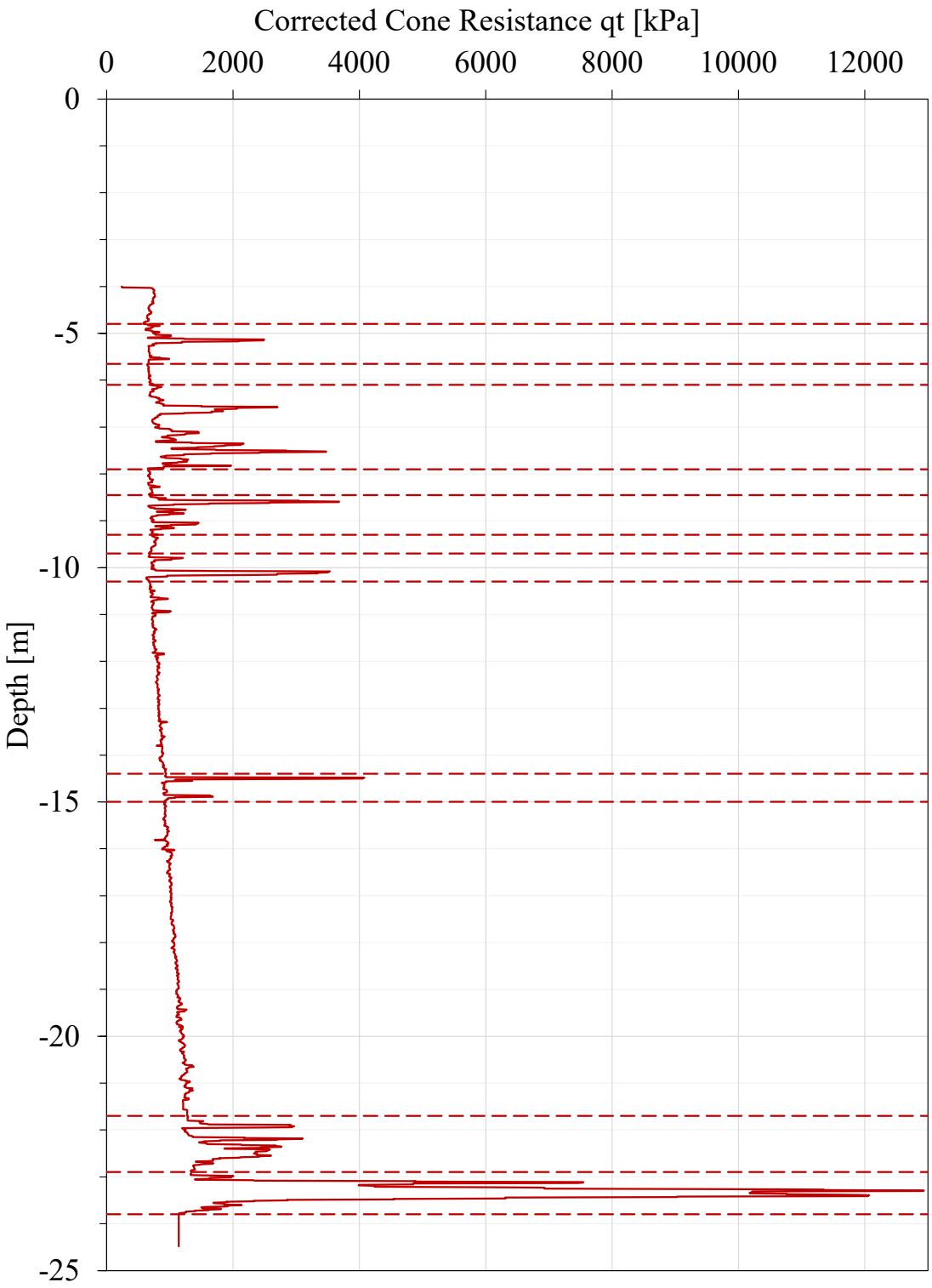
Corrected Cone Resistance qt [kPa]
0
2000
4000
6000
8000
10000
12000
Depth [m]
0
-5
-10
-15
-20
-25

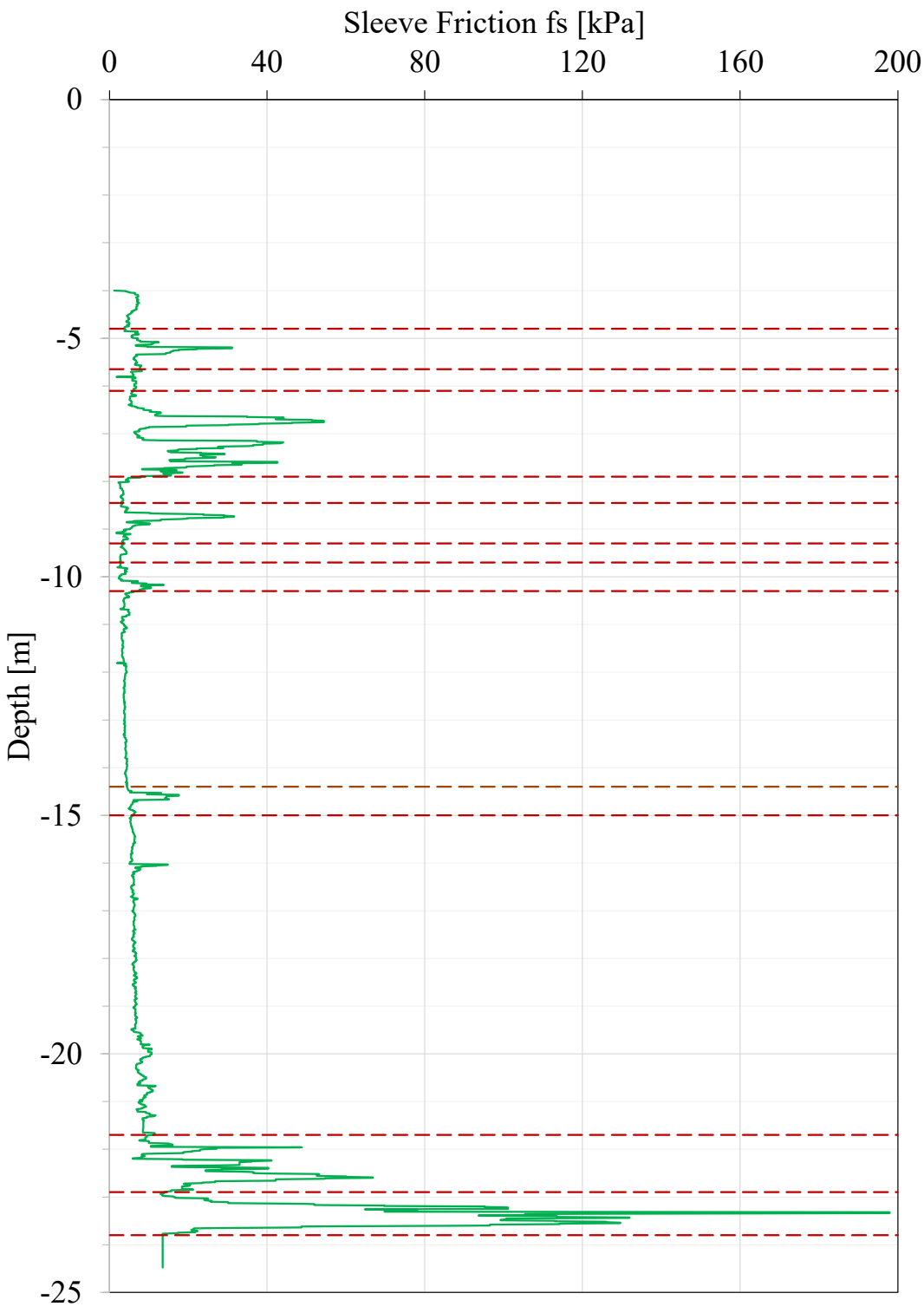
Sleeve Friction fs [kPa]
0
40
80
120
160
200
0
-5
-10
-15
-20
-25
Depth [m]

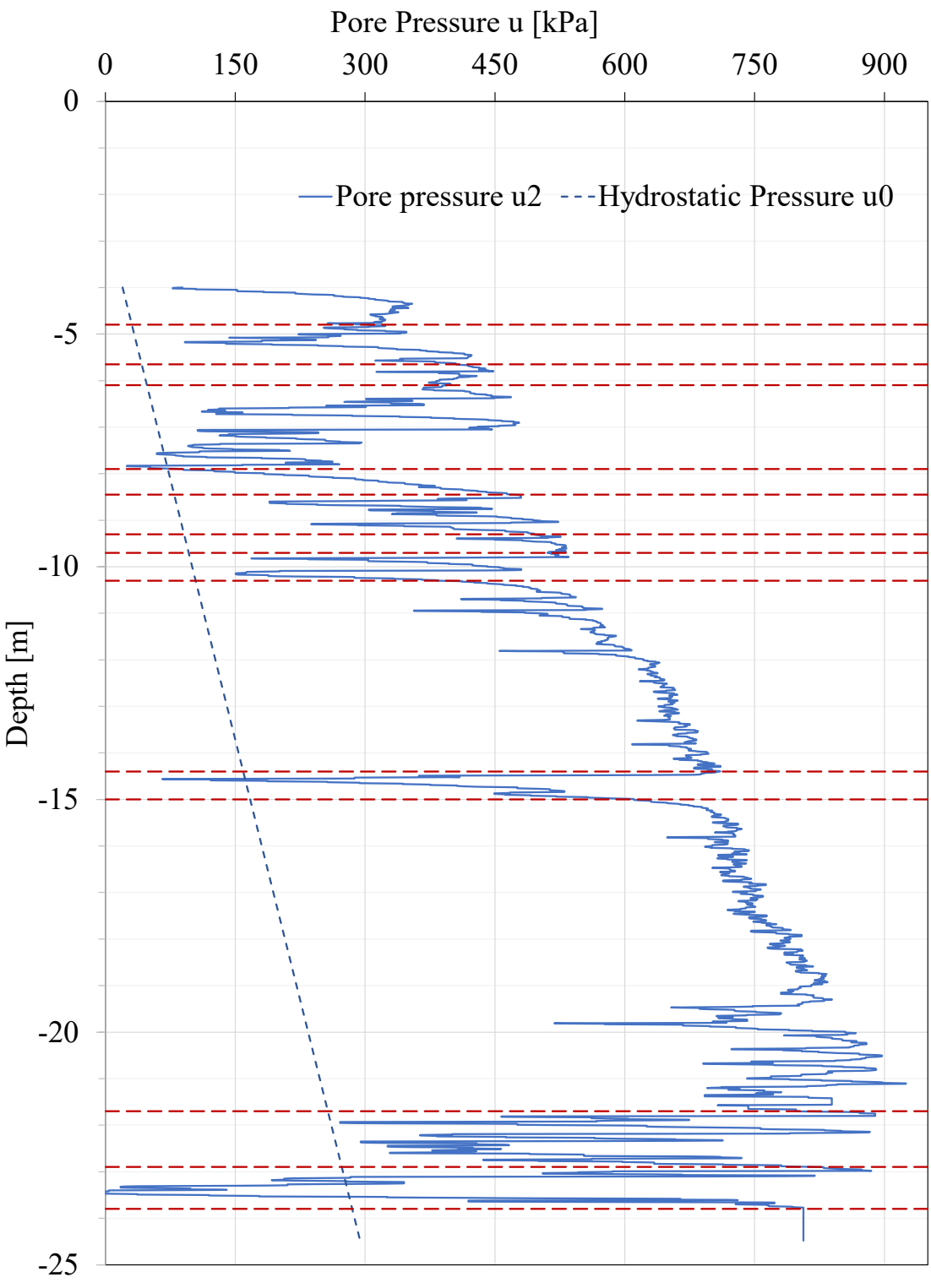
Pore Pressure u [kPa]
0
150
300
450
600
750
900
0
-5
-10
-15
-20
-25
Depth [m]
Pore pressure u2
Hydrostatic Pressure u0

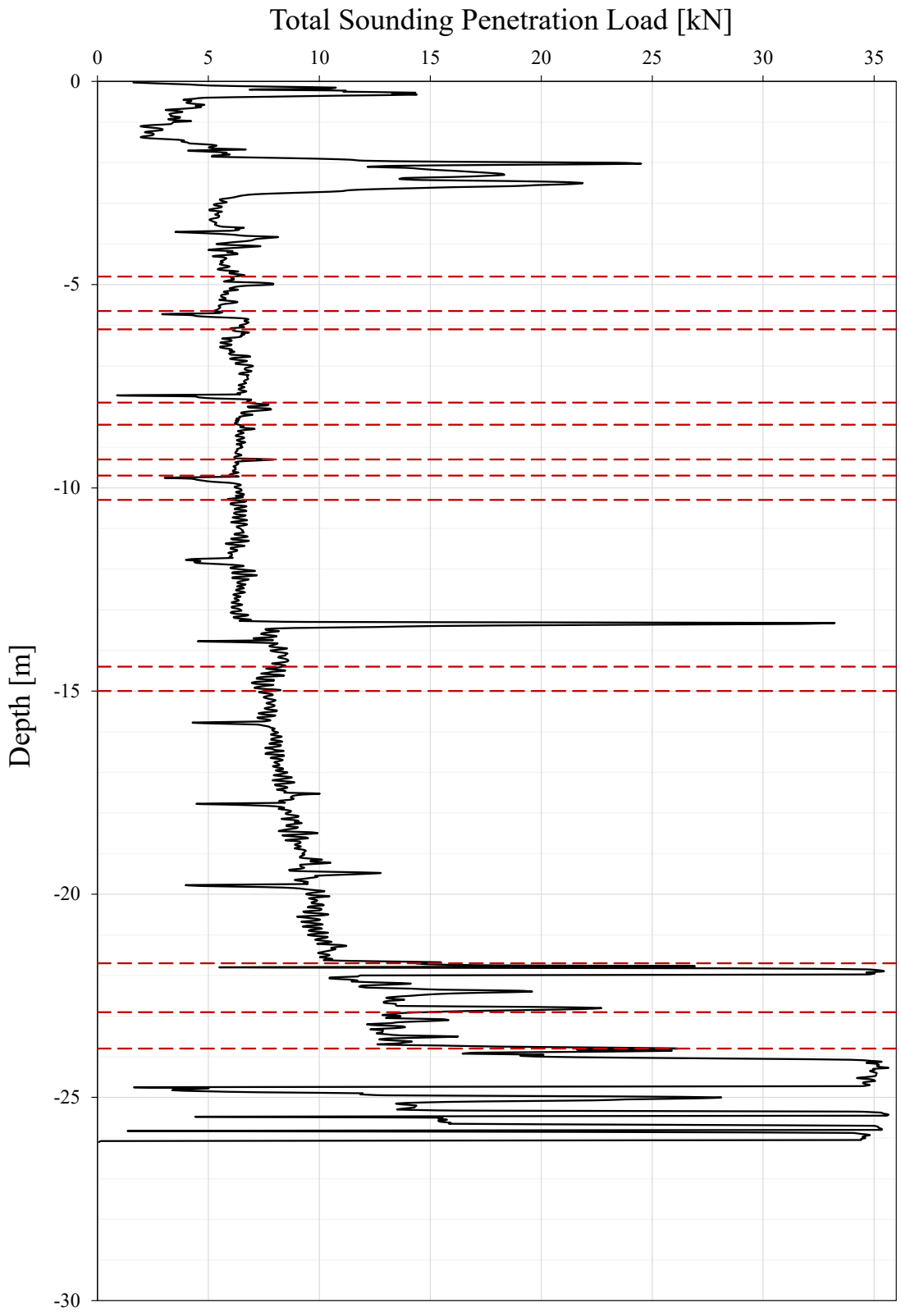
Total Sounding Penetration Load [kN]
0
5
10
15
20
25
30
35
Depth [m]
0
-5
-10
-15
-20
-25
-30

Appendix 3: BEAR project numerical simulation

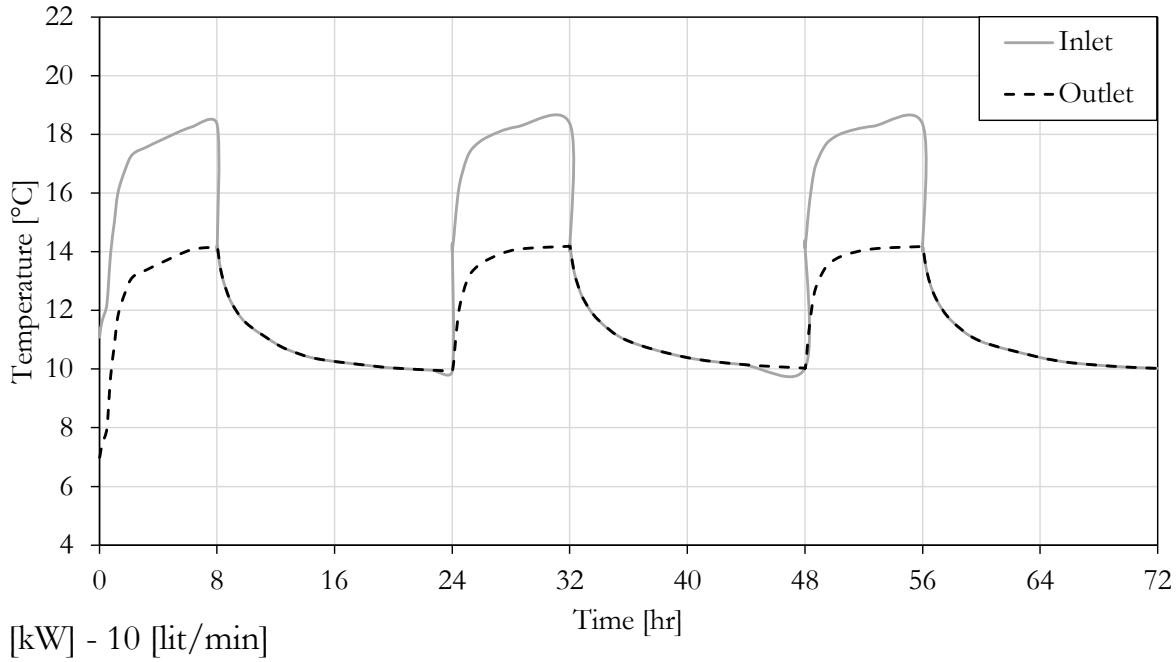

3 [kW] - 10 [lit/min]

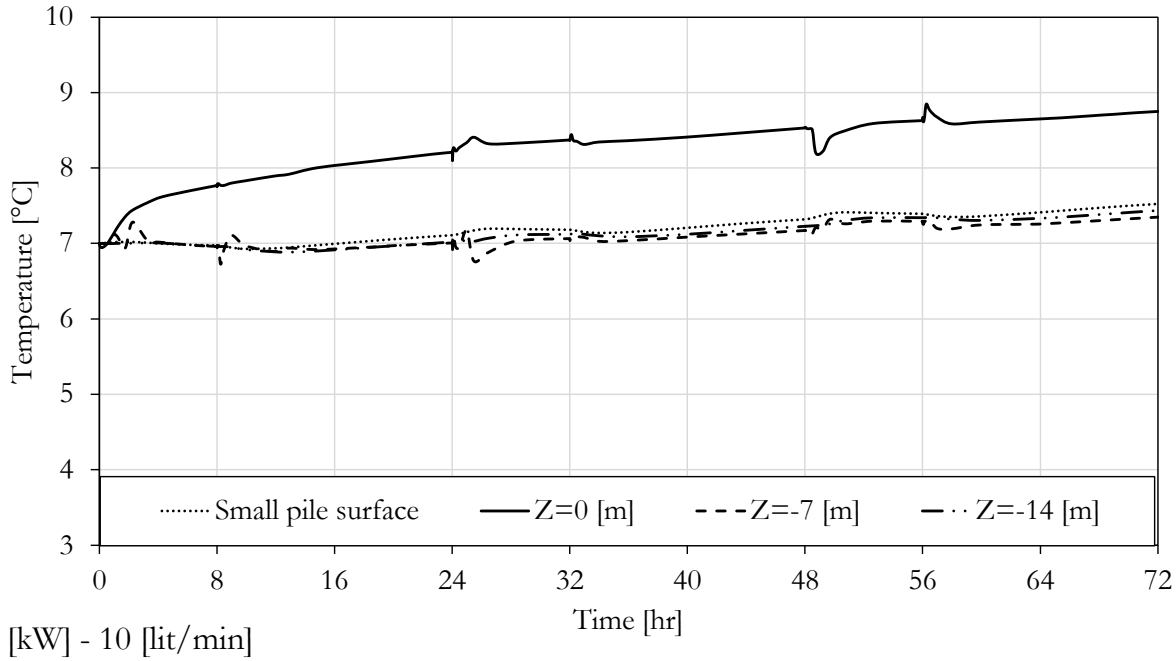

3 [kW] - 10 [lit/min]

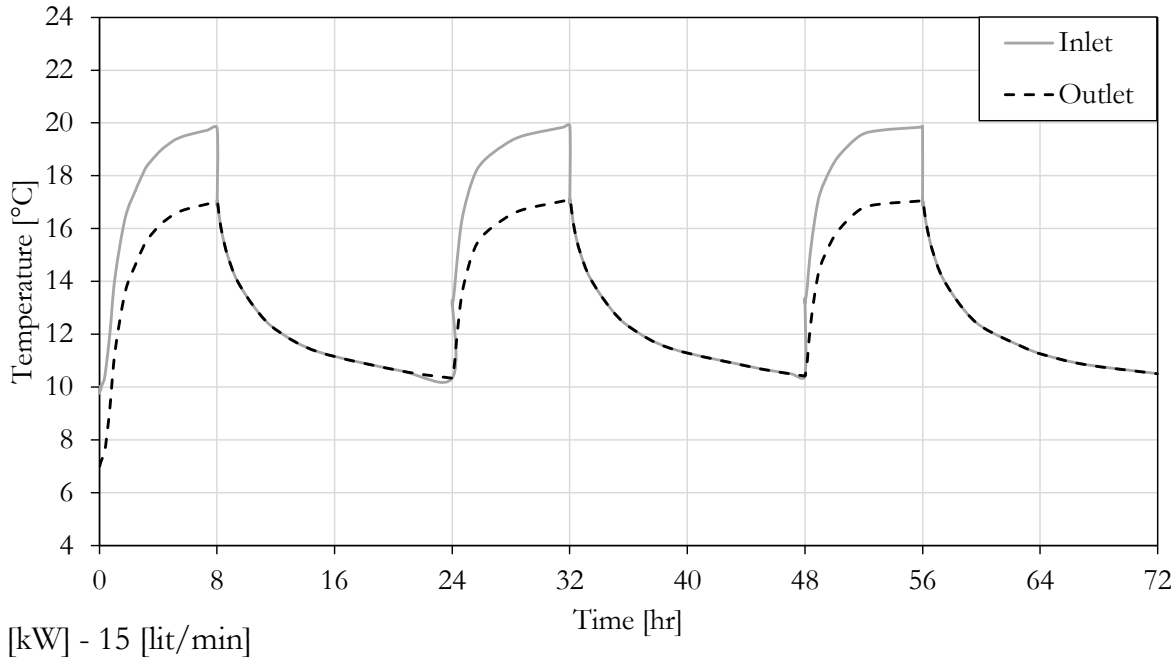

3 [kW] - 15 [lit/min]

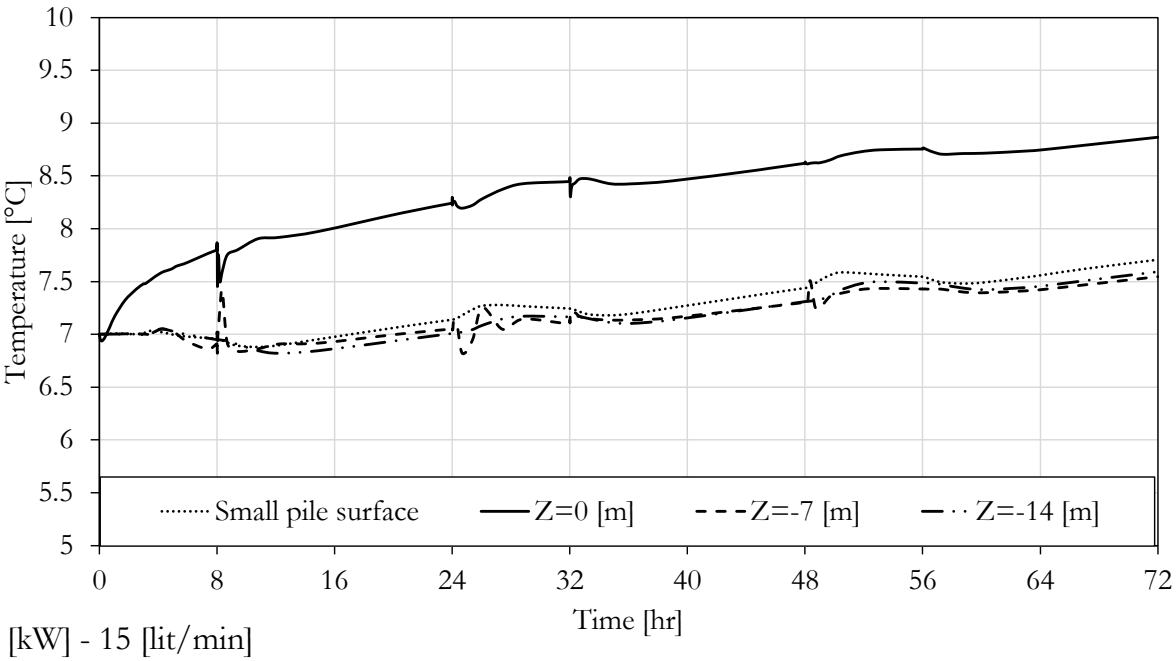

3 [kW] - 15 [lit/min]

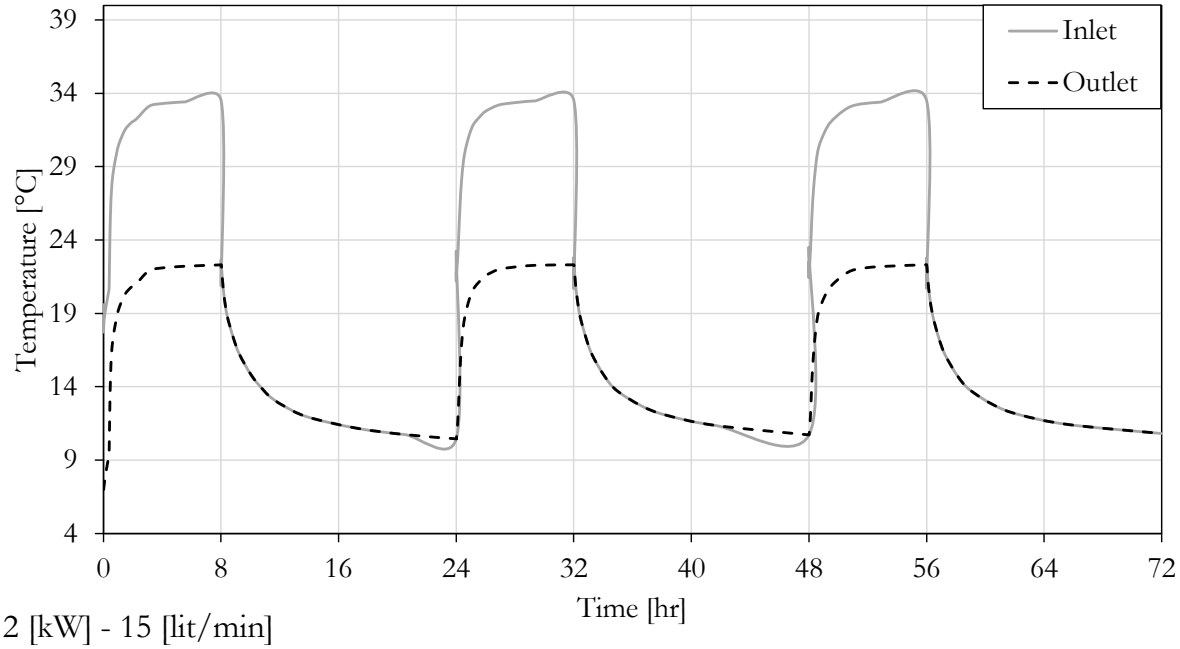

12 [kW] - 15 [lit/min]

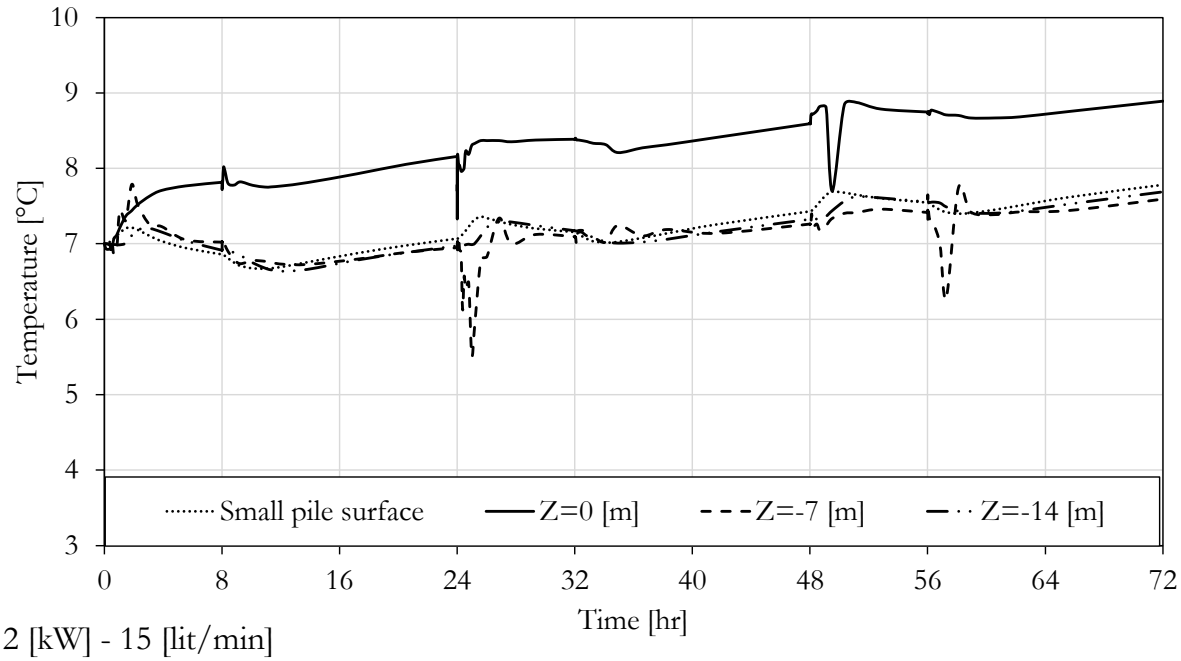

12 [kW] - 15 [lit/min]

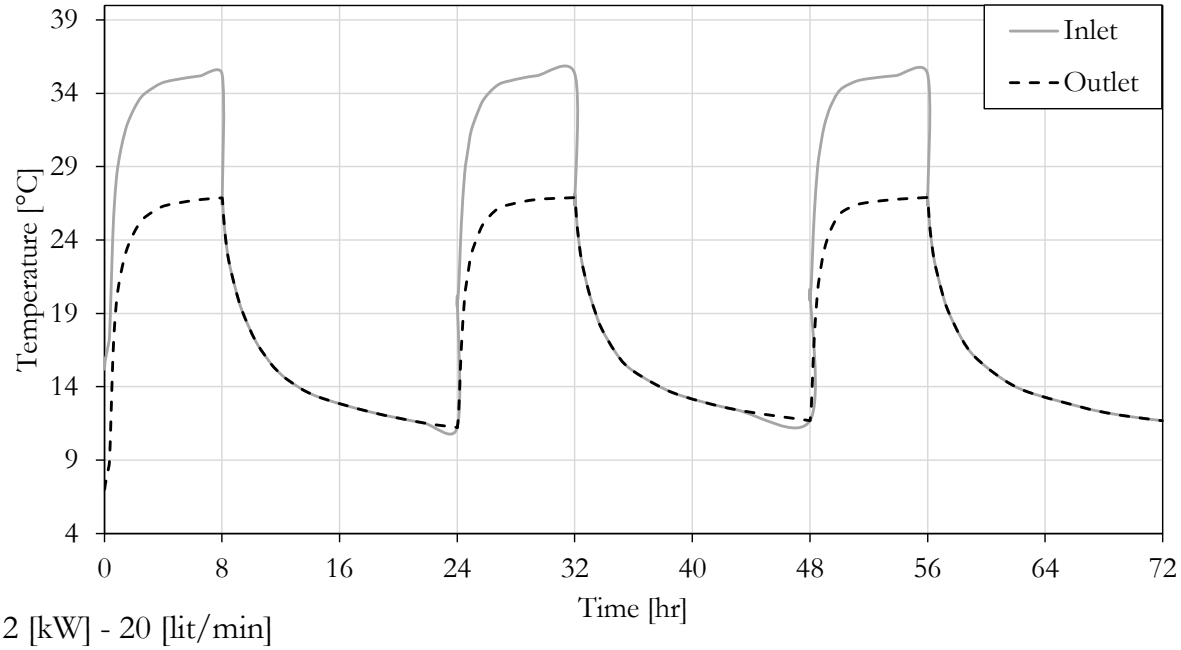

12 [kW] - 20 [lit/min]

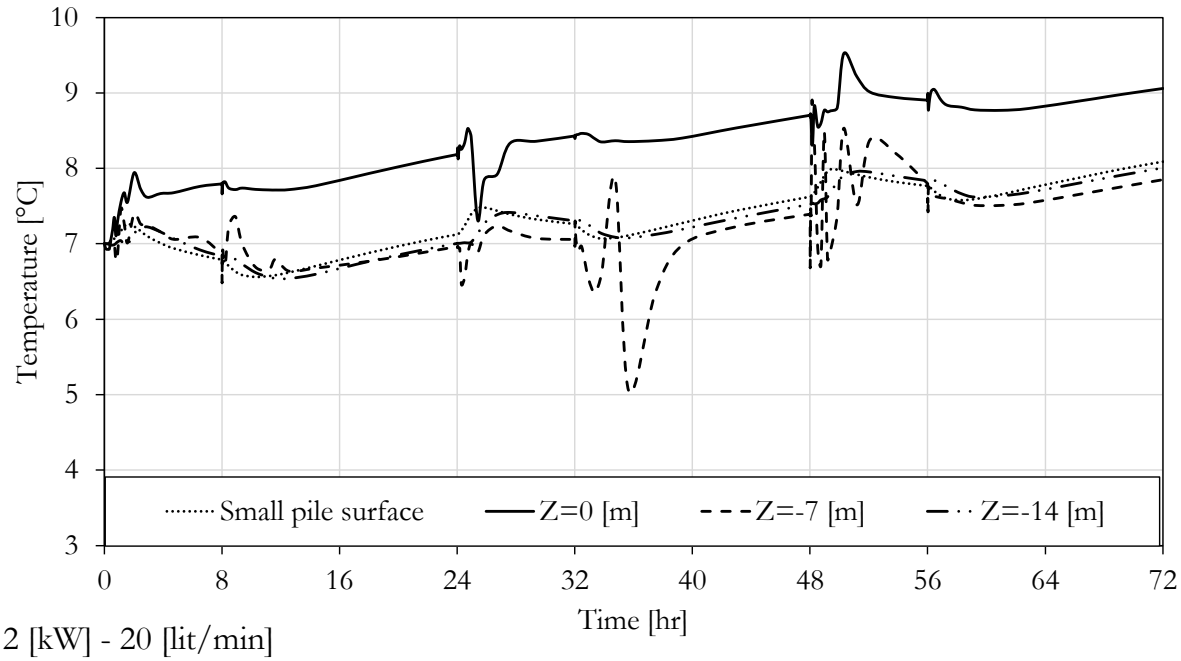

12 [kW] - 20 [lit/min]

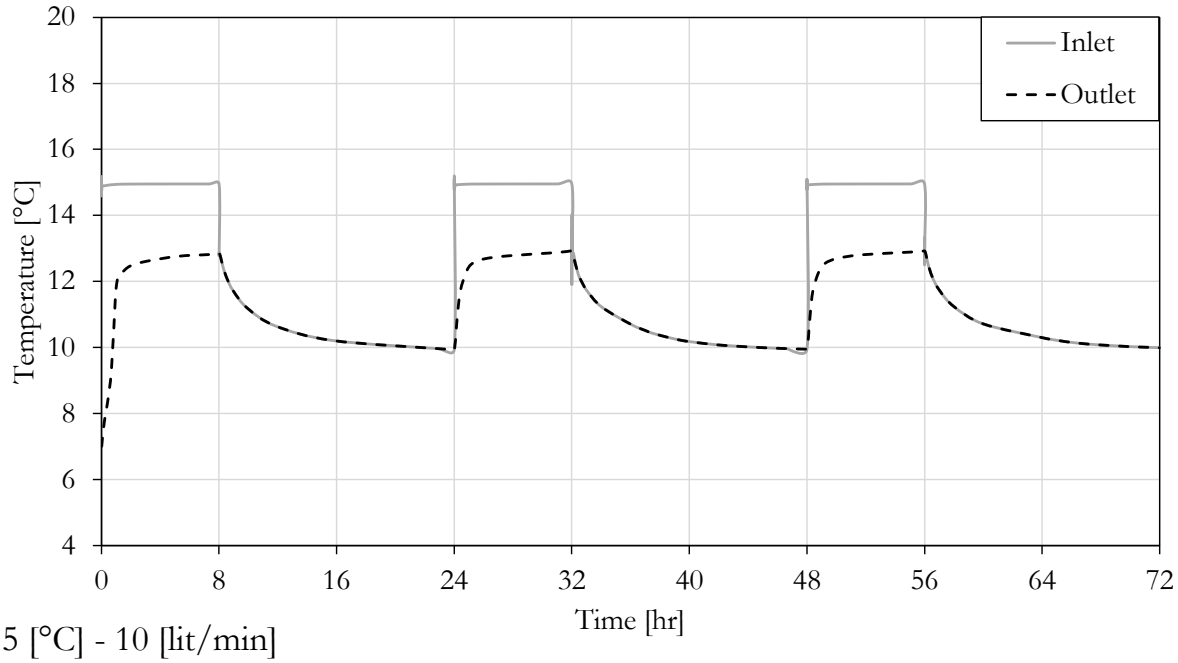

15 [°C] - 10 [lit/min]

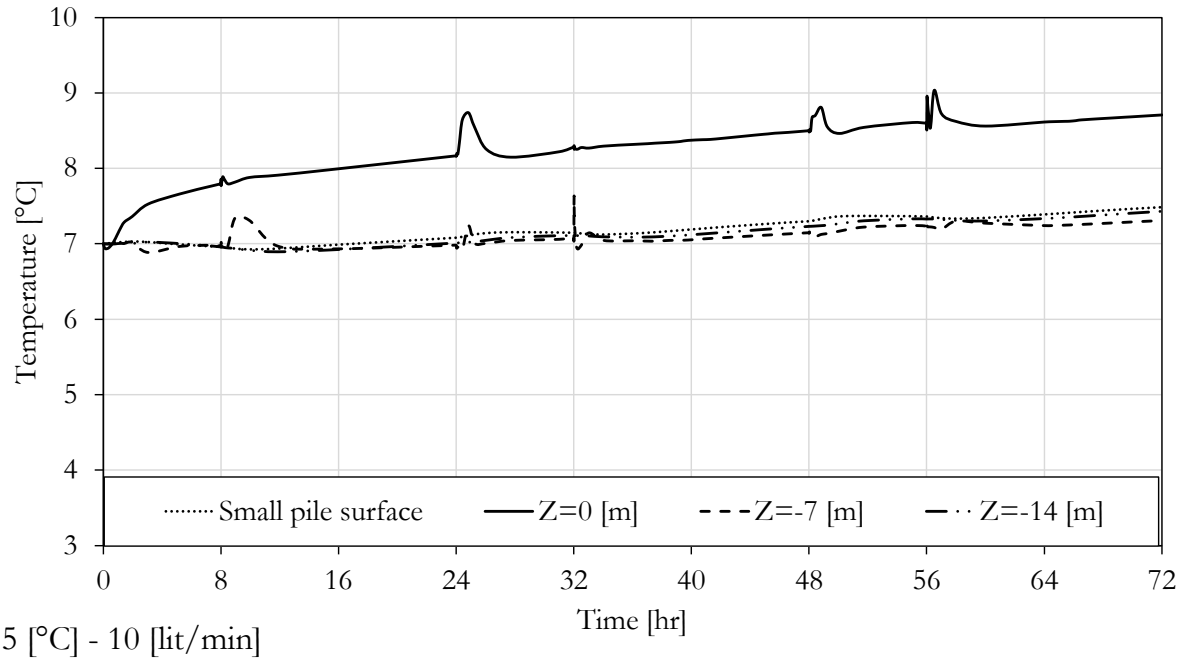

15 [°C] - 10 [lit/min]

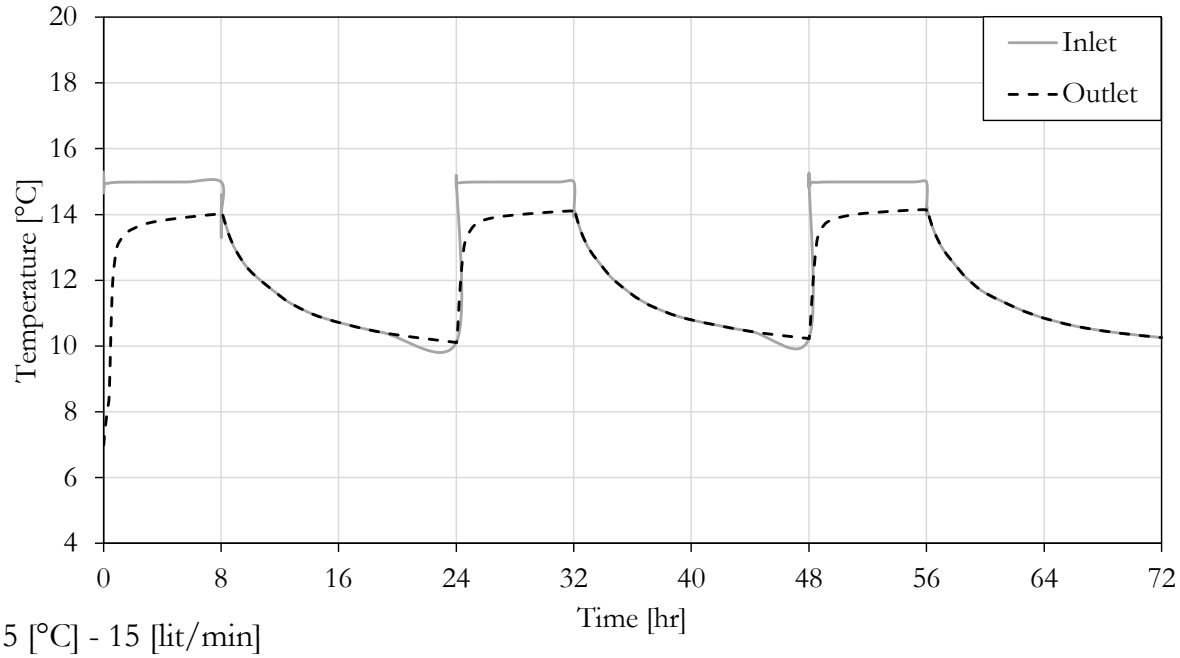

15 [°C] - 15 [lit/min]

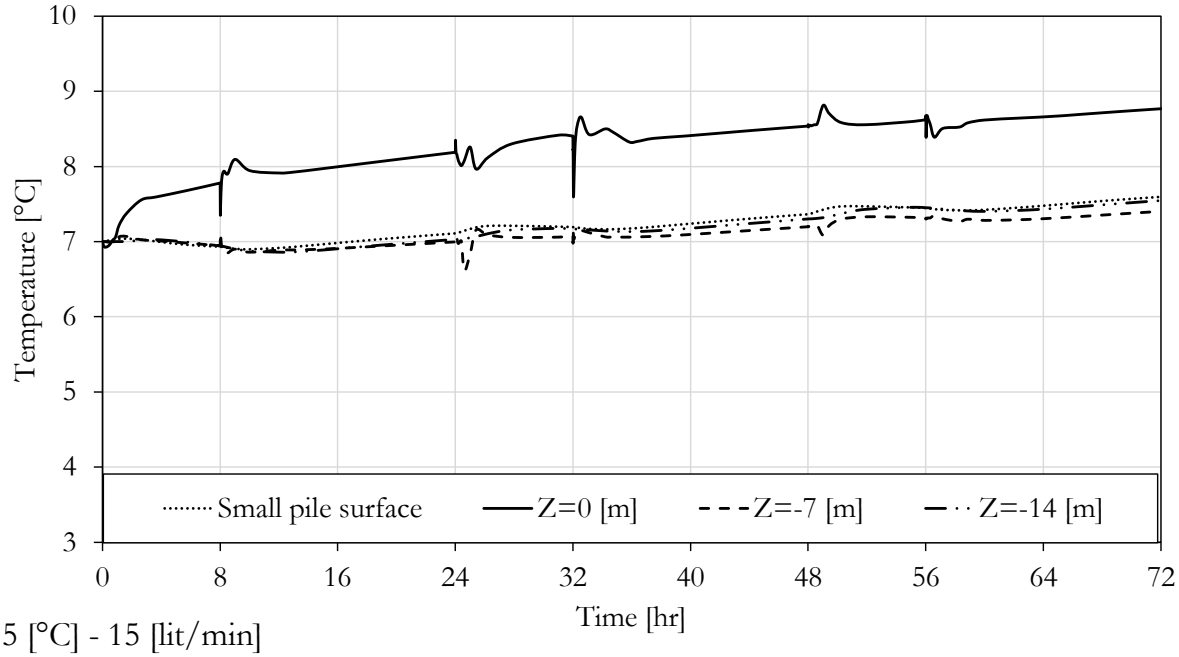

15 [°C] - 15 [lit/min]

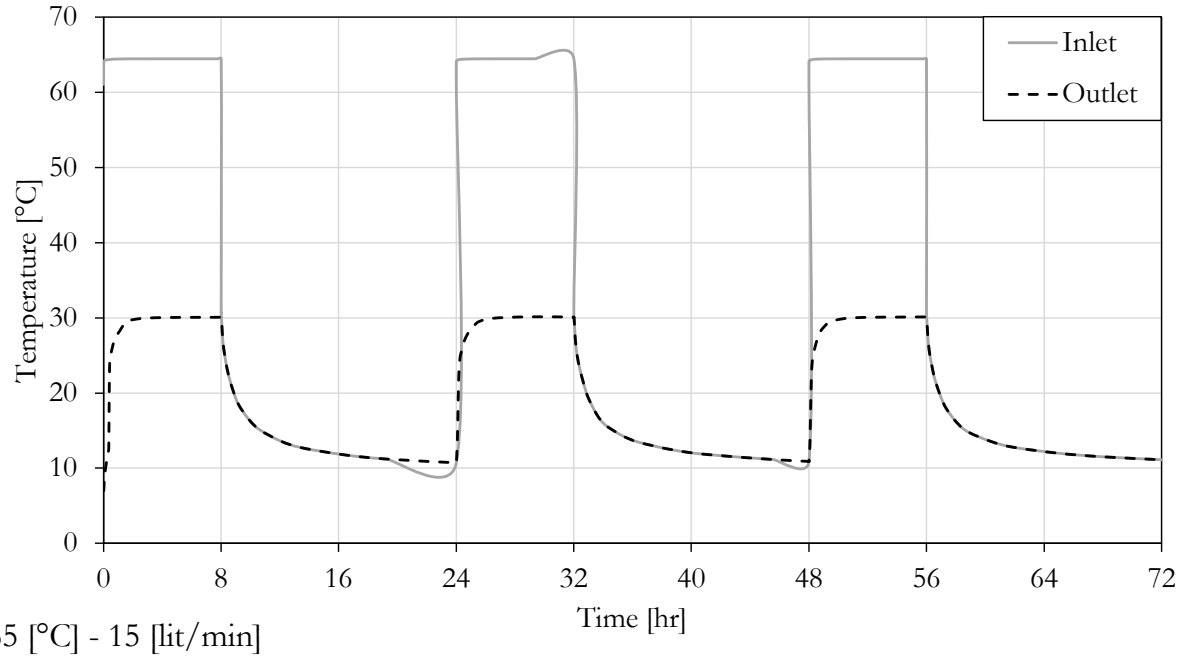

65 [°C] - 15 [lit/min]

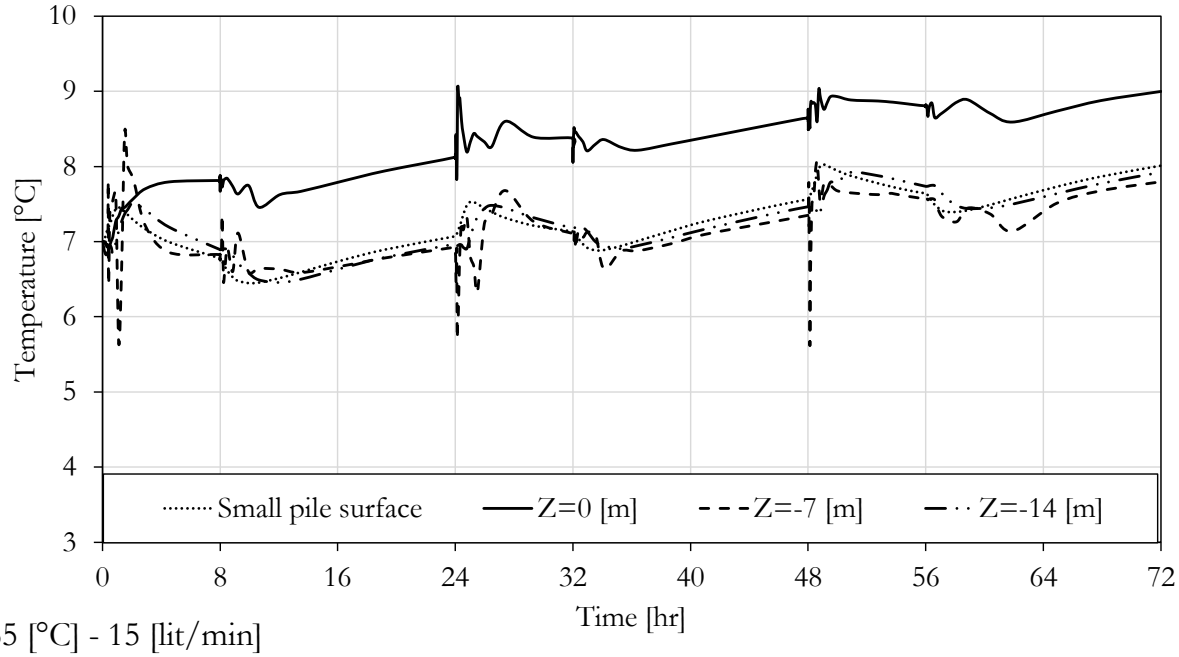

65 [°C] - 15 [lit/min]

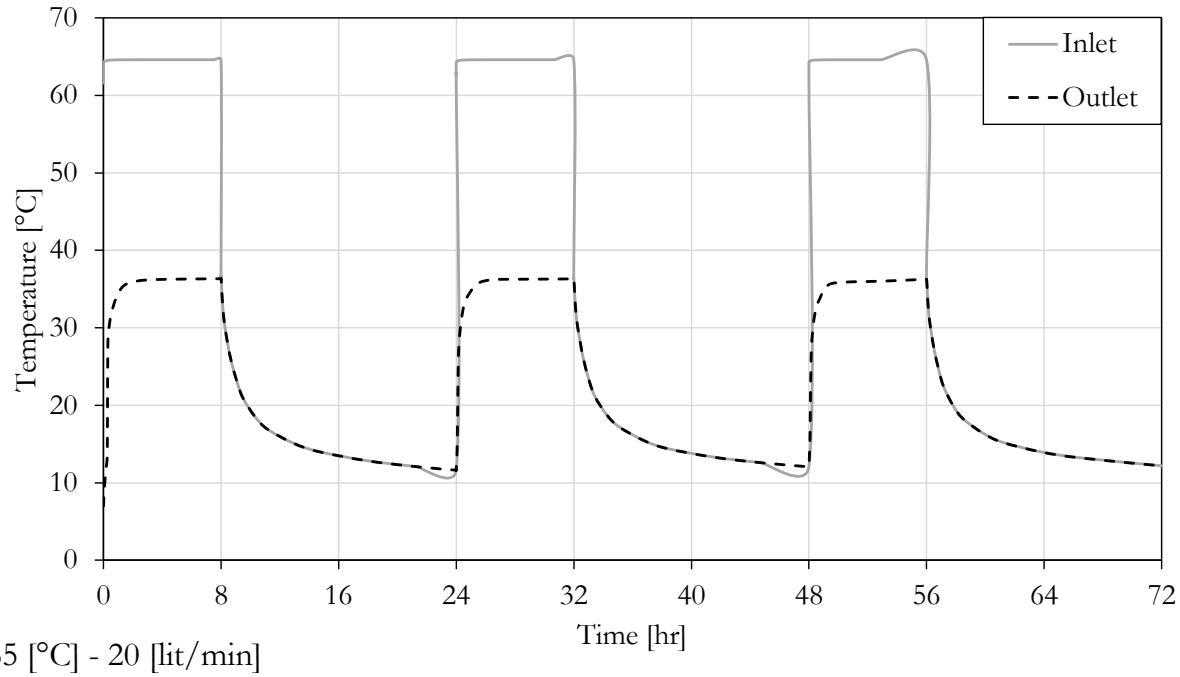

65 [°C] - 20 [lit/min]

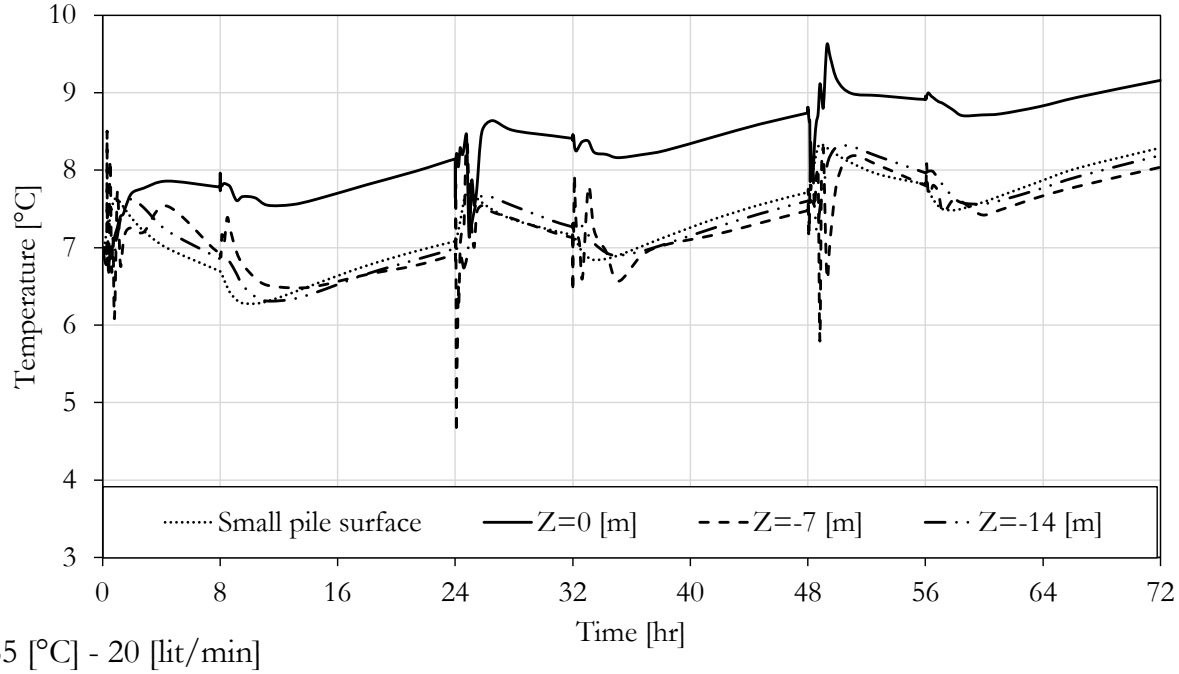

65 [°C] - 20 [lit/min]

Saeed Abbasi Hassan Abbadi

Thermal analysis of steel geothermal energy pile foundation

NTNU
Norwegian University of
Science and Technology